TECHNISCHE UNIVERSITÄT MÜNCHEN

WZW WEIHENSTEPHAN

p27-containing protein complexes regulating gene transcription in adrenomedullary cells

Andrea Kügler

Vollständiger Abdruck der von der Fakultät Wissenschaftszentrum Weihenstephan für Ernährung, Landnutzung und Umwelt der Technischen Universität München zur Erlangung des akademischen Grades eines

Doktors der Naturwissenschaften (Dr.rer.nat.)

genehmigten Dissertation.

Vorsitzende(r): Prof. Dr. Siegfried Scherer

Prüfer der Dissertation: 1. apl. Prof. Dr. Jochen Graw

2. Prof. Dr. Dietmar Zehn

Die Dissertation wurde am 08.11.2017 bei der Technischen Universität München eingereicht und durch die Fakultät Wissenschaftszentrum Weihenstephan für Ernährung, Landnutzung und Umwelt am 26.02.2018 angenommen.

Statutory Declaration:

I declare that I have authored this thesis independently, that I have not used other than the declared sources/resources, and that I have explicitly marked all material which has been quoted either literally or by content from the used sources.

Munich, ……

Andrea Kügler

Eidesstattliche Erklärung

Ich erkläre an Eides statt, dass ich die vorliegende Arbeit selbstständig verfasst, keine anderen als die angegebenen Quellen/Hilfsmittel benutzt, und die den benutzten Quellen wörtlich und inhaltlich entnommene Stellen als solche kenntlich gemacht habe.

München, ……

Andrea Kügler

Table of Content

ABSTRACT

The cyclin-dependent kinase (CDK) inhibitor p27 (*CDKN1B*) mainly functions as cell cycle regulator, which controls the progression from G1 to S phase by binding and inhibiting cyclin-E, -A/CDK2 complexes. In over 50 % of human cancers, p27 levels are reduced, which has been associated with tumor aggressiveness and poor clinical outcome. Moreover, in 8 % of endocrine tumor patients, somatic p27 mutations and genomic deletions could be observed. In our studies, 56 % of human pheochromocytomas (PCC; tumors of the medulla of adrenal glands) were associated with under-expressed p27.

In our lab, we have available a rat model with a phenotypic overlap with MEN1 (multiple endocrine neoplasia) and MEN2 syndromes. These rats named MENX and they develop neuroendocrine tumors, because of a germline frameshift mutation in the gene encoding p27. In addition to parathyroid adenoma, pituitary adenoma and multifocal c-cell hyperplasia, MENX rats also develop bilateral PCCs with complete penetrance. MENX rats display a phenotypic and genotypic overlap with MEN4 patients also bearing mutations in p27. Rat PCCs recapitulate human PCCs regarding *e.g.* blood pressure, catecholamine secretion and histopathological features.

Recently, a novel role of p27 as transcriptional regulator in mouse embryonic fibroblasts (MEFs) was reported. Specifically, in these cells p27 interacts with the transcription factors (TFs) p130, E2F4 and other co-factors to associate with specific promoters of target genes to repress their expression. Although ubiquitously expressed, p27 causes exclusively neuroendocrine tumorigenesis in MEN4 patients and MENX rats. In this context, the molecular processes are unknown. So, we hypothesized a putative function of p27 as transcriptional regulator in neuroendocrine cells; for this study adrenomedullary cells were used as cell model. In contrast to MEF cells, we could show that p27 does not interact with p130 and E2F4 in adrenomedullary cells. Therefore, we suggested an interaction of p27 with other TFs in adrenomedullary cells. To investigate this issue, we performed p27 ChIP-Seq experiments. After we successfully established a suitable anti-p27 antibody and we proved binding of p27 to the chromatin in adrenomedullary cells, the p27 ChIP procedure was optimized to use it finally for rat and human adrenomedullary tissues. Quantitative next generation sequencing identified RUNX1-binding sequences as highly enriched in rat p27

ChIP samples. Indeed, in this study RUNX1 could be identified as novel direct interaction partner of p27 in rat adrenomedullary cells.

Bioinformatic analyses revealed several putative p27/RUNX1 target genes (*e.g. Znf563, Apoc4, Tcf4* and *Gata2*). Expression studies showed *Znf563* to be over-expressed in adrenal cells when p27 or/and RUNX1 are silenced, whereas *Gata2* was under-expressed and *Tcf4* was unchanged. *Apoc4* expression was controversial in different adrenal cell systems. In conclusion, *Znf563* could be elucidated as the most promising p27/RUNX1 target when p27 works as a transcriptional repressor in adrenal cells. Additionally, GATA2 was shown to interact with RUNX1 in these cells.

ZUSAMMENFASSUNG

Die Hauptfunktion des Cyclin-abhängigen Kinase (*CDK*)-Inhibitors p27 (*CDKN1B*) ist die Regulation des Zellzyklus. Durch Bindung und Hemmung von Cyclin E, -A/CDK2-Komplexen kontrolliert p27 den Übergang von der G1- in die S-Phase. In über 50 % aller Krebsarten ist die Expression von p27 reduziert, was mit Aggressivität der Tumoren und schlechter klinischer Prognose einher geht. Desweiteren konnten in 8 % aller Patienten mit neuroendokrinen Tumoren somatische p27-Mutationen und genomische Deletionen festgestellt werden. In Studien unserer Arbeitsgruppe konnten 56 % aller untersuchten humanen Phäochromozytomen (*PCC*; Tumoren der Medulla der Nebennieren) mit runterreguliertem p27-Level assoziiert werden.

In unserem Labor arbeiten wir mir einem Rattenmodel, welches einen überlappenden Phänotyp mit dem MEN1- (multiple endokrine Neoplasie) und MEN2-Syndrom zeigt. Diese MENX-Ratten entwickeln neuroendokrine Tumoren, die von einer Keimbahn-Mutation verursacht werden, die zu einer Leserasterverschiebung des Gens führt, das für p27 kodiert. Neben Nebenschilddrüsenadenomen, Hypophysenadenomen und multifokalen C-Zelltumoren entwickeln die MENX-Ratten auch bilaterale Phäochromozytome; letzteres mit vollständiger Penetranz. MENX-Ratten sind ein Modell für MEN4-Patienten, die phänotypisch und genotypisch mit dem Rattenmodell übereinstimmen, indem sie, aufgrund von p27-Mutationen, bzgl. Blutdruck, Katecholamin-Sekretion und histopathologischen Aspekten, ähnliche Symptome aufweisen.

Kürzlich wurde eine neue Funktion von p27 als transkriptioneller Regulator in murinen embryonalen Fibroblasten (MEFs) beschrieben. p27 bindet in diesen Zellen mit den Transkriptionsfaktoren p130, E2F4 und anderen Co-Faktoren, um an spezifische Promotoren von p27-Zielgenen zu binden. In MEN4-Patienten und MENX-Ratten verursachen p27-Mutationen ausschließlich die Entwicklung neuroendokriner Tumoren, obwohl p27 ubiquitär im Organismus exprimiert wird. Die verursachenden molekularen Prozesse sind dazu noch unbekannt. Daher vermuteten wir eine potenzielle Funktion von p27, als Transkriptions-Regulator in neuroendokrinen Zellen. Zur Bearbeitung dieser Hypothese wurden in dieser Arbeit adrenomedulläre Zellen, repräsentativ für neuroendokrine Zellen, verwendet. Im Gegensatz zu MEFs konnten wir zeigen, dass p27 in adrenomedullären Zellen nicht mit p130

und E2F4 interagiert. Daher nahmen wir an, dass p27 in diesen Zellen mit anderen Transkriptionsfaktoren an die DNS binden kann. Um diese potenziellen Interaktionspartner von p27 zu identifizieren, führten wir p27-ChIP-Seq-Experimente durch. Nachdem wir einen geeigneten p27-Antikörper etabliert und die tatsächliche Bindung von p27 an die DNS adrenomedullärer Zellen bestätigen konnten, wurde das p27-ChIP-Protokoll für adrenomedulläre Gewebe von Mensch und Ratte optimiert. Unter anderem konnten per *quantitative next generation sequencing* angereicherte spezifische Sequenzen für den Transkriptionsfaktor Runx1 identifiziert werden. RUNX1 konnte in dieser Arbeit erstmals als Interaktionspartner von p27 in adrenomedullären Zellen von Ratten identifiziert werden.

Bioinformatische Analysen ermittelten potenzielle p27/RUNX1-Zielgene, wie *Znf563*, *Apoc4*, *Tcf4* und *Gata2*, deren Expression wir in Nebennierenzellen mit runterreguliertem p27 und/oder RUNX1 untersuchten. Aufgrund gehemmter p27/RUNX1-Expression war *Znf563* überexprimiert, während *Gata2* runterreguliert war. Die Expression von *Tcf4* war unverändert und die Expression von *Apoc4* war in verschiedenen Nebennierenzell-Modellen kontrovers. Wenn p27, wie oben beschrieben, als transkriptioneller Repressor agiert, konnte *Znf563* als vielversprechenstes p27/RUNX1-Zielgen ermittelt werden, da seine Expression nach p27/RUNX1-Inhibierung erhöht war. Zusätzlich konnten wir GATA2 als Interaktionspartner von RUNX1 identifizieren.

ABBREVIATIONS

°C	degree Celsius
%	percent
α	anti
µ	micro- (10^{-6})
ACTH	adrenocorticotropic hormones
AKT	AKT serine/threonine kinase
ALL	acute lymphoblastic leukemia
AML	acute myeloid leukemia
APOC4	apolipoprotein C4
APS	ammonium persulfate
Ascl1	Achaete-Scute Family BHLH Transcription Factor 1
Av	average
Az	Aktenzeichen
bp	base pair
B2m	β_2 microglobulin
BCA	Bicinchoninic acid
BEDF	BED-type zinc finger putative TF
bidest.	bidestillatus
BMP	bone morphogenetic protein
BMPR	bone morphogenetic protein receptor
BSA	bovine serum albumin
c	centi- (10^{-2})
CBF	core-binding factor
CDK	cycline-dependent kinase
cDNA	complemetary deoxyribonucleic acid
CEBP	CCAAT/enhancer binding protein
CGI	CpG island
ChIP	chromatin immunoprecipitation
Chr	chromosome
CML	chronic myelogenous leukemia
CO_2	carbon dioxide
cor	adrenal cortex
CRF	corticotropin-releasing factor
CRM	exportin
CT	computer tomography
CTCF	CCCTC-binding factor
CXCR4	C-X-C motif chemokine receptor 4
DAB	3,3'-diaminobenzidine
Da	Dalton
DAPI	4',6-diamidino-2-phenylindole
DBD	DNA-binding domain
ddH_2O	bidestilled water
DMEM	Dulbecco's Modified Eagle's Medium
DMSO	dimethyl sulfoxide
DNA	deoxyribonucleic acid
dNTP	deoxyribonucleotide
DTPA	diethylenetriaminepentaacetic acid
DTT	dithiothreitol
E2F4	E2F transcription factor 4
EBF	Early B-cell factor
ECL	enzymatic chemiluminescence
E. coli	Escherichia coli
EDTA	ethylenediaminetetraacetic acid
e.g.	exempli gratia (for example)
ERK	extracellular-signal regulated kinase
FBS	fetal bovine serum
FC	fold change
FFPE	formalin-fixed, paraffin-embedded
FH	fumarate hydratase
FITC	fluorescein isothiocyanate

g	relative centrifugal force
GAL	Galanin and GMAP Prepropeptide
GATA	GATA binding protein
GCF	GC-rich sequence DNA-binding factor
GFP	green fluorescent protein
GO	gene ontology
H_2O_2	hydrogen peroxide
H&E	hematoxylin and eosin
h	hours
HAT	histone acetylase
HBSS	Hanks' Balanced Salt Solution
HDAC	Histone deacetylase
HFSC	hair follicle stem cells
HIF	hypoxia inducible factor
HOXC4	Homeobox C4
HPA	hypothalamic-pituitary-adrenal-axis
HRP	horseradish peroxidase
HS	horse serum
HSC	hematopoietic stem cells
i.e.	id est
IF	Immunofluorescence
IgG	Immunoglobulin G
igv	integrative genome viewer
IHC	Immunohistochemistry
IP	Immunoprecipitation
k	kilo- (10^3)
KIF	kinesin family member
KPC	Kip ubiquitination-promoting complex
l	litre
LB	Luria-Bertani medium
LGR	Leucine rich repeat containing G protein-coupled receptor
m	metre/milli- (10^{-3})
MAX	MYC-associated factor X
MAZF	MYC-associated zinc finger protein
MDS	myeloblastic leukemia
med	adrenal medulla
MEF	mouse embryonic fibroblast
MEN	multiple endocrine neoplasia syndrome
MENX	multiple endocrine neoplasia-like
$MgCl_2$	magnesium clorid
Mi-2	chromodomain-helicase-DNA-binding protein
MIBG	metaiodobenzylguanidine
min	minute
mio	million
MNase	micrococcal nuclease
mo	months
MOZ	monocytic leukemic zinc finger
MRI	magnet resonance imaging
mRNA	messenger RNA
Mtgr1	myeloid translocation gene -regulated protein
mut	mutant
n	nano- (10^{-9})
NaCl	sodium chloride
NAD(P)H	nicotinamide adenine dinucleotide phosphate
NaOH	sodium hydroxide
NDPK	NME nucleoside diphosphate kinase
NEUROD1	Neuronal differentiation 1
NF-H	Neurofilament-H
NGS	next generation sequencing
NP-40	nonyl phenoxypolyethoxyl-ethanol
NRHc	negative regulatory region for heterodimerization

NuRD	Nucleosome remodeling and deacetylase
OD	optical density
Olf1	Olfactory factor-1
OMIM	online mendelian inheritance in man
p130	Retinoblastoma-associated protein
PBS	phosphate buffered saline
PCA	principal component analysis
PCC	Pheochromocytoma
PCR	polymerase chain reaction
PCNA	proliferating cell nuclear antigen
PET	positron emission tomography
PFA	paraformaldehyde
pH	minus the decimal logarithm of the hydrogen ion activity in a solution
PHOX2A	Paired like homeobox 2A
PI3K	Phosphatidylinositol-4,5-bisphosphate 3-kinase
PLA	proximity ligation assay
PLAG	PLAG like zinc finger
PNMT	penylethanolamine-N-methyltransferase
PPGL	paraganglioma
PTM	post-translational modifications
qRT-PCR	quantitative revers transkriptase polymerase chain reaction
RASSF	Ras association domain family member
RB	Retinoblastoma
REF	rat embryonic fibroblast
REP	repression domain
RET	Ret Proto-Oncogene
Rho	Rhodopsin
RIN	RNA integrity number
RIPA	radioimmunoprecipitation assay
RNA	ribonucleic acid
rpm	revolutions per minute
RPMI	Roswell Park Memorial Institute
RT	room temperature
RUNX1	runt-related transcription factor 1
scr	scrambled
SDH	succinate dehydrogenase subunit
SDS	sodium dodecyl sulfate
SDS-PAGE	sodium dodecyl sulfate poly-acrylamide gel electrophoresis
sec	second
SEMA6A	Semaphorin 6A
Seq	sequencing
SIN3	SIN3 transcription regulatory family
siRNA	small interfering ribonucleic acid
SKP	S-phase kinaseassociated protein
SMAD	Mothers Against Decapentaplegic, Drosophila, Homolog
SOX4	SRY-box 4
SP1	specificity protein
SSC	squamous cell carcinoma
SSD	signal sensing domain STAT signal transducer and activator of transcription
SUV	standardized uptake value
TAD	trans-activating domain
TBE	Tris/boric acid/EDTA
TBP	TATA binding protein
TBS-T	Tris buffered saline with Tween 20
TCF4	transcription factor 4
TE	Tris-EDTA
TEMED	N,N,N',N'-tetramethylethane-1,2-iamine
TF	transcription factor
TGFβ	transforming growth factor beta
TMEM	transmembrane protein

Tris	2-amino-2-hydroxymethyl-propane-1,3-diol	vs	versus
TVA	Tierversuchsantrag	W	watt
UV	ultraviolet	w/v	weight per volume
u	units	WHO	world health organization
UTR	untranslated region	WST	water soluble tetrazolium 1
V	volt	WT	wildtype
v/v	volume per volume	ZNF	zinc finger protein
VHL	Von Hippel–Lindau tumor suppressor gene		

LIST OF FIGURES

LIST OF TABLES

1 INTRODUCTION

1.1 Pheochromocytoma (PCC)

1.1.1 The adrenal glands

The adrenal glands (*Glandula adrenalis*) are endocrine organs located on the top of both kidneys. Each gland is composed of the outer cortex and the inner medulla and lies within the *renal fascia* surrounded by an adipose capsule (Figure 1). The cortex consists of three zones: the *zona glomerulosa*, the *zona fasciculata* and the *zona reticularis* and produces three main steroid hormone types. Mineralcorticoids, such as aldosterone, are produced in the *zona glomerulosa* and regulate blood pressure and electrolyte balance (Dodic *et al*., 1999) (Figure 1). Cortisol and corticosterone are glucocorticoids, which are made in the *zona fasciculata* and function as regulators of metabolism and immune system suppression (Even *et al*., 2012) (Figure 1). The *zona reticularis* synthesizes androgens, such as dehydroepiandrosterone, for functional sex hormones, which are continuatively converted in the gonads (Kreuz *et al*., 1972) (Figure 1). The adrenal medulla (*Medulla glandulae suprarenalis*) is a completely different entity. It consists of chromaffin cells, which are neuroendocrine cells of neural crest origin derived from sympathoadrenal progenitor cells. These progenitor cells differentiate to reach the specific characteristics of mature hormone-producing cells and populate the adrenal medulla and extra-adrenal sympathetic paraganglia (PPGL) (Cochard *et al*., 1978; Huber, 2006).

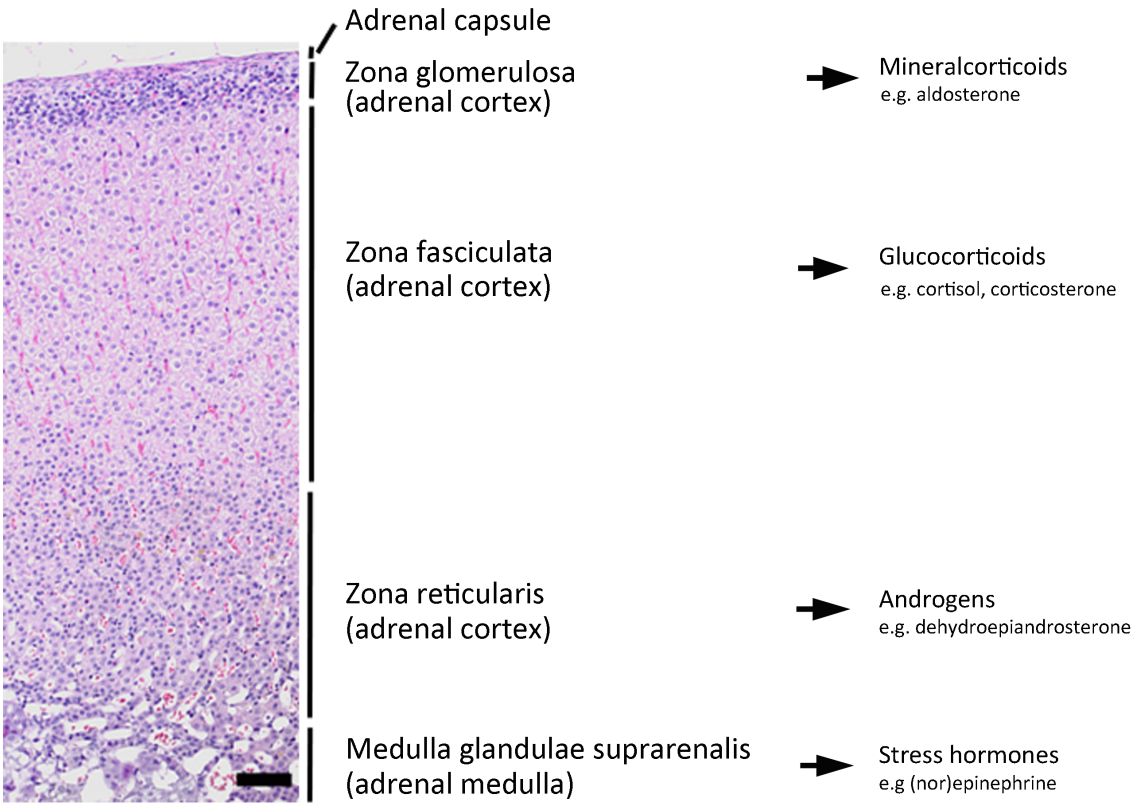

Figure 1: Structure of the adrenal glands. The microscopic picture shows a part of a H&E stained adrenal gland from a wild-type (WT) rat. The glands are composed of an outer cortex and an inner medulla surrounded by a connective tissue capsule. The cortex can be subdivided into additional zones, all of which produce different types of hormones. [scale bar: 50µm]

Chromaffin cells produce the hormones epinephrine/adrenaline (80 %) and norepinephrine/noradrenaline (20 %) with minimal amounts of dopamine, which are then secreted into the bloodstream due to direct stimulation by acetylcholine release from sympathetic nerves (Ernsberger *et al*., 1995) (Figure 1). The hormonal release by the chromaffin cells is regulated by preganglionic nerve fibers from the sympathetic nervous system or as feedback of adrenocortical cortisol secretion (Kantorovich *et al*., 2000; Perlman and Chalfie, 1977). Cortisol-induced catecholamine synthesis promotes an increased expression of the enzyme phenylethanolamine-N-methyltransferase (PNMT) in chromaffin cells, which catalyzes the transformation of noradrenaline to adrenaline as the last step of catecholamine biosynthesis. The dual role of adrenomedullary catecholamines as both, hormones and neurotransmitters in adrenergic neurons of the *medulla oblongata* (Abumi *et al*., 1996), leads to the control of several biological functions in the body, such as blood pressure (Gombos *et al*., 1962), heart rate (Breuer *et al*., 1993) and sweating (Allen and Roddie, 1972).

The medullary chatecholamines derive from the amino acid tyrosine (Spector *et al*., 1965) and are responsible for the fight and flight response - an increase in cardiac output and vascular resistance throughout the body in stress situations (Ranabir and Reetu, 2011). Animals respond to stress by activating a wide array of behavioral and physiological responses. A central role in stress response plays the hypothalamic-pituitary-adrenal (HPA) axis. The HPA axis is principally regulated by the Corticotropin-releasing factor (CRF), which is released into hypophysial portal vessels that access the anterior pituitary gland upon stress stimuli. CRF binds to its repceptor on pituitary corticotropes, which induces the release of the adrenocorticotropic hormone (ACTH) into the blood system. Once circulating, ACTH targets the adrenal cortex, where it stimulates the glucocorticoid synthesis and secretion from the adrenal cortex (*Zona fasciculata*) (Rivier and Vale, 1983; Vale *et al*., 1981). Adrenal glucocorticoids are the downstream effectors of the HPA axis and regulate physiological changes through ubiquitously distributed intracellular receptors (Bamberger *et al*., 1996; Munck *et al*., 1984). Following exposure to stress, elevated levels of circulating glucocorticoids inhibit HPA activity at the level of the hypothalamus and pituitary via a glucocorticoid negative feedback loop (Keller-Wood and Dallman, 1984).

1.1.2 Clinical manifestation of PCC

PCC are tumors of the sympathetic nervous system, which develop from chromaffin cells in the medulla of the adrenal glands (Karagiannis *et al*., 2007; Knudsen *et al*., 1985; Pratt, 1951). They derived their name from the dark brown color (phaiós, dusky; chrôma, color), which most chromaffin tumors assume when treated with potassium dichromate. These tumors can also develop in sympathetic and parasympathetic ganglia and are termed extra-adrenal PCC or PPGL (van Baars *et al*., 1981). Unaffected adrenomedullary cells produce 80 % of adrenaline and 20 % of noradrenaline (Ernsberger *et al*., 1995). According to the classification of the World Health Organization (WHO) in 2004, PCC cells (including extra-adrenal PPGL) express both catecholamines, but in contrast to normal cells usually produce more noradrenaline than adrenaline - a feature that characterizes them as noradrenergic PCC (Warren and Chute, 1972). Adrenergic PCC exist too, which produce mainly adrenaline; but they are more rare (Lehnert 1998). Tumors of the paraganglia, which do not derive from

chromaffin cells, are mainly situated in the head and neck and rarely produce significant amounts of catecholamines (van Duinen *et al*., 2010; Thompson, 2006).

Clinical manifestations of PCC and PPGL are mostly due to the increased secretion of noradrenaline by the tumor. This leads to symptoms such as hypertension, headaches, sweating or clammy skin, palpitations, anxiety, and diaphoresis (Bravo and Tagle, 2003; Manger and Gifford, 1980; Zuber *et al*., 2011). Effects of long-standing and severe hypertension lead to damage of end organs especially heart, kidney, eyes, and central nervous system (Baguet *et al*., 2004; Kudva and Young, 1997). Diabetes or deranged glucose metabolism may be present in up to 30–50 % of PCC patients (Baguet *et al*., 2004; Pogorzelski *et al*., 2014).

1.1.3 Genetics of PCC

About 40 % of PCC are hereditary (Neumann *et al*. 2002, Gimenez-Roqueplo *et al*. 2012). These patients can have germline mutations in one of the following PCC susceptibility genes: the proto-oncogene *RET* (Machens *et al*., 2005), the von Hippel-Lindau tumor suppressor *VHL* (Zbar *et al*., 1996), the succinate dehydrogenase complex (SDH) flavoprotein subunit A *SDHA* (Burnichon *et al*., 2010), *SDHB* (Astuti *et al*., 2001a), *SDHC* (Niemann and Müller, 2000), *SDHD* (Baysal *et al*., 2000) and the SDH assambly factor *SDHAF2* (Hao *et al*., 2009), the Neurofibromin *NF1* (Wallace *et al*., 1990), the transmembrane protein *TMEM127* (Qin *et al*., 2010), the MYC-associated factor *Max* (Comino-Méndez *et al*., 2011) and the fumarate hydratase *FH* (Castro-Vega *et al*., 2014) (Figure 2). Several autosomal dominant cancer syndromes are associated with adrenal or extra-adrenal PCC: MEN2 (Schimke and Hartmann, 1965), von Hippel-Lindau syndrome (Neumann and Wiestler, 1991) or neurofibromatosis type 1 (Borberg, 1951). 60 % of PCC occur sporadically and approximately 7.5 % of them harbor somatic mutations in one of the susceptibility genes mentioned above: *e.g.* 4.4 % *VHL*, 1.6 % *SDHD*, and 1.5 % *SDHB* (Korpershoek *et al*., 2006). Furthermore, some tumor suppressor genes have been identified as downregulated in around 30 % of sporadic tumors through promoter region hyper-methylation, such as the Ras-associated domain family member *RASSF1A* (Astuti *et al*., 2001b) and *CDKN2A,* encoding the tumor suppressor p16 (Muscarella *et al*., 2008). Moreover, the tumor suppressor gene *CDKN1B* (encoding the protein p27) was identified as inactivated in 56 % of sporadic PCC cases (Pellegata *et al*.,

2007) and its expression and function was further investigated and described by studies within this dissertation.

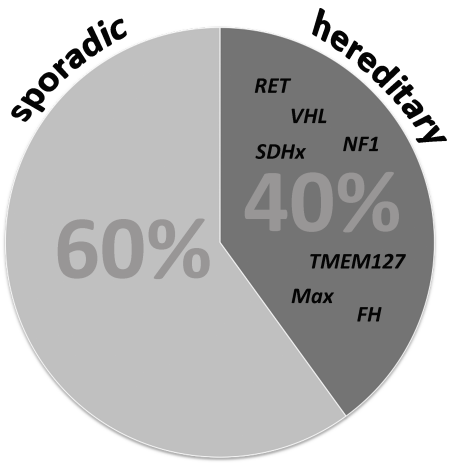

Figure 2: Distribution of the occurrence of hereditary and sporadic cases in PCC patients. 60 % of cases occur sporadic, whereas 40 % occur hereditary with mutations in *RET* (5 % of cases), *VHL* (13 % of cases), *SDHx* [includes: *SDHA*, *SDHB, SDHC, SDHD, SDHAF2*] (16 % of cases), *NF1* (4 % of cases), *TMEM127, Max* or *FH* (Baysal *et al*., 2000; Burnichon *et al*., 2010; Castro-Vega *et al*., 2014; Comino-Méndez *et al*., 2011; Hao *et al*., 2009; Niemann and Müller, 2000; Qin *et al*., 2010; Wallace *et al*., 1990; Zbar *et al*., 1996).

Genome-wide expression studies of PCC/PPGL have suggested a division of the tumors into two clusters based on their transcriptional profiles. Cluster 1 tumors are characterized by mutations in the genes *VHL, SDHx* (*SDHA*, *SDHB*, *SDHC*, *SDHD*, *SDHAF2*), the hypoxia inducible factor *HIF2α* and *FH* (Castro-Vega *et al*., 2015) (Figure 3). These genes are mainly involved in the hypoxic pathway and are affected in about 30 % of PCC/PPGL (Eisenhofer *et al*., 2004a; López-Jiménez *et al*., 2010). The cluster 2 tumors (around 70 % of PCC/PPGL) harbor mutations in the PCC susceptibility genes *NF1*, *RET*, the kinesin family member *KIF1B*, and *TMEM127* (Gimenez-Roqueplo *et al*., 2012; Vicha *et al*., 2013) (Figure 3). Cluster 2 tumors are characterized by activation of kinase signaling and protein translation (Burnichon *et al*., 2011; Dahia, 2014).

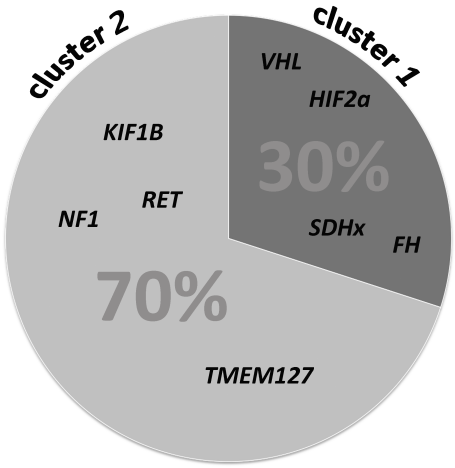

Figure 3: Distribution of PCC cases in the two classification clusters. Cluster 1 PCC are characterized by mutations in *VHL, HIF2a, SHDx* [*SDHA, SDHB, SDHC, SDHD, SDHAF2*] or *FH* and occur in 30 % of cases. 70 % of PCC cases can be classified in cluster 2 PCC, which have mutations in *KIF1B, RET, NF1* or *TMEM127* (Castro-Vega *et al*., 2015; Eisenhofer *et al*., 2004a; Gimenez-Roqueplo *et al*., 2012; López-Jiménez *et al*., 2010; Vicha *et al*., 2013).

1.1.4 Prevalence, prognosis and therapy of PCC

The morbidity of PCC is about 13-29 %, while that of PPGL from extra-adrenal sites is about 43 % (Kaloostian *et al*., 2014). Benign PCC are curable by surgical resection, whereas about 5-26 % are clinically malignant (Edström Elder *et al*., 2003; Eisenhofer *et al*., 2004b; Gimenez-Roqueplo *et al*., 2003; Goldstein *et al.*, 1999). The malignancy rate varies according to the definition of malignancy applied, i.e. presence of metastases, invasion of neighboring organs, or invasion of organ capsules (Eisenhofer *et al.*, 2004b). PCC can metastasize by both lymphatic and haematogenous pathways and can infiltrate into liver, lymph nodes, lung and bones (Cascon *et al*., 2004). The 5-year survival rate for malignant PCC is approximately 40 % due to difficult detection and inefficient diagnostic methodology (Eisenhofer *et al*., 2004a; Hescot *et al*., 2013; Nomura *et al*., 2009). Female patients show a higher overall incidence of PCC than male patients (Cheung *et al*., 1988; Geoghegan *et al*., 1998), but malignant PCC occur more frequently in males (van Heerden *et al*., 1982). The prevalence of PCC is not precisely known. A study from 1980 to 1992 showed an average annual incidence rate of 2.06 per million in the Spanish population in Southern Galicia (Fernández-Calvet and García-Mayor, 1994). The main age of patients at diagnosis was at 21–65 years (Fernández-Calvet and García-Mayor, 1994).

Biochemical tests are required to confirm the diagnosis of PCC. A rise in plasma and urinary

metanephrines is indicative of an increased production of catecholamines by the tumor (Kudva *et al*., 2003; Lenders *et al*., 2002). In addition, imaging studies are important for tumor localization and in diagnosing multiple primary tumors and/or metastatic lesions in PCC patients (Ramachandran and Rewari, 2017). Computed tomography (CT), contrast enhanced CT, and magnetic resonance imaging (MRI) are now routinely complemented by functional imaging using various radiotracers such as ^{123}I-metaiodobenzylguanidine (^{123}I-MIBG) and ^{111}In-DTPA-pentetreotide (Jalil *et al*., 1998; Pacak *et al*., 2004). Recently, the MIBG analog ^{18}F-LMI1195 was found to visualize PCC in MENX rats (Gaertner *et al*., 2013) (Figure 4).

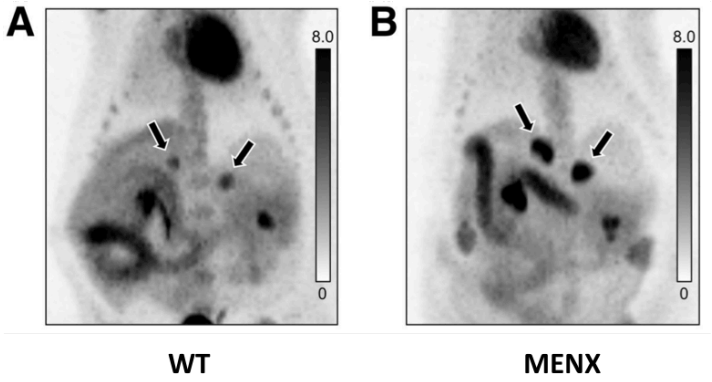

Figure 4: Visualization of the MIBG PET tracer analog ^{18}F-LMI1195 PET in adrenal glands. (A) The image was taken 45 min after injection in WT rats, where moderate tracer accumulation was observed. **(B)** In PCC of p27-mutant MENX rats, an intense tracer accumulation was reported. [Scale bars represent SUV] [This research was originally published in *JNM*. Gaertner *et al*. Title. *J Nucl Med.* 2013; 12: pp:2111-2117. © by the Society of Nuclear Medicine and Molecular Imaging, Inc.]

1.2 Multiple endocrine neoplasia (MEN) syndromes

1.2.1 MEN1

Multiple endocrine neoplasias (MEN) are autosomal dominant syndromes characterized by tumors involving more than one neuroendocrine-derived tissue. The autosomal dominant MEN1 syndrome (OMIM #131100) occur with high penetrance due to a germline mutation in the tumor suppressor gene *MEN1* (Chandrasekharappa *et al*., 1997; Zarnegar *et al*., 2002). *MEN1* is located on Chr. 11q13.1 and encodes the protein Menin that has many functions.

Menin works as transcriptional regulator and binds to several promoters including the *TERT* promoter, thereby repressing telomerase expression (Lin and Elledge, 2003). Additionally,

Menin is known to be involved in cell proliferation, apoptosis, and genome stabilization (Heppner *et al*., 2001; Hughes *et al*., 2004; Jin *et al*., 2003; Kaji *et al*., 2001). Fourteen of 15 patients (93.3 %) suffering from the MEN1 syndrome carry *MEN1* mutations (Mayr *et al*., 1997). Patients suffering from MEN1 develop multiple parathyroid adenomas, pancreatic islet cell neoplasia and anterior pituitary adenomas (Carty *et al*., 1998; Vergès *et al*., 2002) (Table 1). Clinical symptoms appear usually between the ages of 30 and 40 years, whereas an early onset in childhood is rare (Marx *et al*., 1998). MEN1 occurs in approximately one in 30 000 individuals. Males and females are equally affected and no predilection for specific populations is known (Lairmore *et al*., 2004).

1.2.2 MEN2

Another known MEN syndrome is the MEN type 2 syndrome (MEN2) characterized by mutations in the proto-oncogene *RET* (Mulligan *et al*., 1993). *RET* is localized on Chr. 10q11.21 and codes for a receptor tyrosine kinase involved in numerous cellular mechanisms including cell proliferation, neuronal navigation, cell migration, and cell differentiation as well as regulation of cell death/survival balance (Cabrera *et al*., 2011; Cockburn *et al*., 2010; Garcia-Lavandeira *et al*., 2010). More than 90 % of patients affected by MEN2 carry germline point mutations in *RET* (Santoro *et al*., 2002).

Two MEN2 subtypes are characterized by the development of medullary thyroid carcinoma as well as PCC and parathyroid hyperplasias in 50 % and 15-30 % of cases, respectively (MEN2A, OMIM #171400) or by PCC in approximately 50 % of the cases and more seldom by ganglioneuromatosis of the intestine, thickening of the corneal nerves and *marfanoid habitus* (MEN2B, OMIM #162300) (Hansford and Mulligan, 2000; Koch, 2005) (Table 1). MEN2 is inherited with a prevalence of one to 5 000 (Niccoli-Sire and Conte-Devolx, 2007).

1.2.3 MEN4 and MENX

Occasionally, patients showing clinical symptoms compatible with MEN1 had no mutations in the *MEN1* gene. This led to the hypothesis that another predisposing gene for multiple neuroendocrine tumors might be involved. Further examination of these patients identified *CDKN1B* as the causative gene, encoding the cell cycle regulator $p27^{Kip1}$ (p27) (Pellegata *et*

al., 2006). Subsequently, additional patients with *CDKN1B* mutations were identified who presented multiple endocrine tumors. These mutations affect localisation, stability and protein-binding abilities of p27 (Marinoni and Pellegata, 2011). Based on these findings, a novel MEN syndrome - named MEN4 (OMIM #610755) - was defined. The tumor spectrum of MEN4 is not clearly defined due to limited number of patients, but their most common phenotypic features are parathyroid and pituitary adenomas (Georgitsi, 2010; Lee and Pellegata, 2013).

Table 1: Summary of common clinical manifestations of human MEN syndromes. Despite of different mutations occurring in the different MEN syndromes (*MEN1* in MEN1, *RET* in MEN2, *CDKN1B* in MEN4), they share common clinical features such as pituitary adenoma, parathyroid adenoma, medullary thyroid carcinoma or PCC. The grey boxes indicate the lesions occuring in patients suffering from certain MEN syndromes. White boxes indicate that this tumor type is not developed in the displayed MEN syndrome.

	MEN1	**MEN2A**	**MEN2B**	**MEN4**
pituitary adenoma				
parathyroid adenoma				
medullary thyroid carcinoma				
PCC				

A MEN syndrome due to a homozygous tandem duplication of eight nucleotides in exon 2 of the *Cdkn1b* gene, causing a frameshift mutation, developed spontaneously in a Sprague-Dawley rat strain (Figure 5) (Pellegata *et al.,* 2006). The mutant *Cdkn1b* allele encodes a highly unstable p27 protein, which is expressed as reduced levels or lost in the tissues of affected animals. The syndrome was called MENX. Affected rats develop bilateral PCC, PPGL, multifocal pituitary adenoma, multifocal thyroid C-cell hyperplasia and endocrine pancreas hyperplasia (Fritz *et al*., 2002). Therefore, MENX shows phenotypic overlap with the human MEN syndromes. Additional genotypic overlap is given with the MEN4 syndrome, which is caused by mutations in *CDKN1B*. Additionally, affected animals develop bilateral juvenile cataracts in the first weeks of age (Fritz *et al.*, 2002). Before the characterization of the genotype of MENX rats was figured out (Pellegata *et al*., 2006), the previous breeding criteria was the development of cataracts only in homozygous mutant rats.

Figure 5: *Cdkn1b* mutation found in MENX rats. Shown is the alignment of annotated WT p27 sequence with the MENX mutant p27. The mutant p27 is 21 amino acids longer than the WT protein due to the 8 bp insertion at the indicated position. (Pellegata *et al*., 2006) [Copyright (© 2006) National Academy of Sciences]

1.2.4 PCC in MENX

MENX rats develop endogenous bilateral PCC with complete penetrance (Figure 6). Hyperplasia of adrenal medullary cells is evident at two months of age and then progresses to PCC by siw to eight months of age (Molatore *et al*., 2010; Pellegata *et al*., 2006). The tumors in MENX rats do not express PNMT indicating that they are noradrenergic. Transcriptome profiling of adrenal tumors and tissue from WT rats was conducted (Molatore *et al*., 2010). This study revealed 183 genes overexpressed (more than two-fold) in medullary hyperplasia and PCC tissue samples of homozygous MENX rats *versus* unaffected adrenal. Overrepresented genes belonged to the gene ontology (GO) category "nervous system development" and included *Mash1* (*Ascl1*), *Bmp7*, *Phox2a*, *Neurod1*, *Gal*, *Cxcr4*, *Cdkn2a*, *Cdkn2c*, *Gata2*, *Sema6a*, *Tcf4* and *Sox4*. All these genes are implicated in the differentiation of neural crest cells into the precursor cells of the sympathoadrenal cell lineage from which adrenal medullary cells are derived (Molatore *et al*., 2010). Further studies characterized an over-activation of the Bmp-Smad pathway in the rat tumors, including an overexpression of *Bmp7* and of known targets *Sox9*, *Gata2* and *Hoxc4* (Leinhäuser *et al*., 2015). In addition, the well characterized oncogenic PI3K/AKT pathway was shown to be over-activated in MENX PCC because of overexpression of the secretin receptor (Lee *et al*., 2011, 2012).

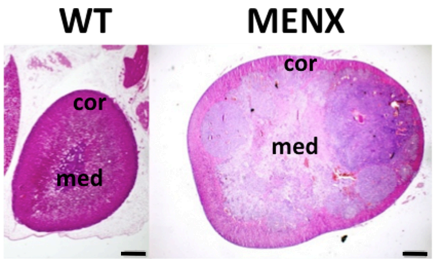

Figure 6: PCC in MENX rats. H&E stainings revealed that PCC develop in the medullary part of the adrenal glands of MENX mutant rats. In comparison with adrenal glands of WT rats, the adrenal cortex is extremly compressed due to the expansive growth of the adrenal medulla. [scale bar: 200 µm; cor: cortex, med: medulla]

1.3 Transcription Factors

1.3.1 Cellular Function of TFs

In the vertebrate genome, 6-10 % of all protein-coding genes encode for sequence-specific DNA-binding transcription factors (TF) (Maston *et al*., 2006). General or basal TFs have an activator or repressor function to control gene expression of their target genes by regulating the recruitment of RNA-polymerases, which perform the transcription from DNA to messenger RNA (mRNA). In every individual cell, a unique subset of specific TFs activates gene expression and regulates cell differentiation (Lee *et al*., 2000; Nikolov and Burley, 1997; Roeder, 1996). In addition to TFs, several additional proteins (co-factors) contribute to this regulation although they do not possess DNA-binding capacities (Brivanlou and Darnell, 2002). The named pre-initiation complex contains general TFs, RNA polymerases, and the multiple-protein complex known as mediator as shown in the example of ribosomal RNA genes (Figure 7). This complex constitutes the basic transcriptional apparatus that first binds to the promoter of a target gene and starts gene transcription (Bywater *et al*., 2013; Pierce and Kumamoto, 2012). General eukaryotic TFs, which initiate RNA polymerase II activity, are TFIIA, TFIIB, TFIID, TFIIE, TFIIF, TFIIH (Lee *et al*., 2000; Orphanides *et al*., 1996). Nucleosome remodeling enzymes make the DNA accessible and histone modifying enzymes - together with other non-DNA-binding proteins - change the local chromatin state to increase or reduce the rate of transcription (Kadonaga, 2004; Lee *et al*., 2014; Maston *et al*., 2006; Spitz and Furlong, 2012). To regulate their target genes specifically, TFs bind sequence-specific cis-regulatory elements, which are DNA sequences of several hundred basepairs (bp) in length that contain binding sites for multiple specific TFs (Lelli *et al*., 2012; Spitz and Furlong, 2012). Cis-regulatory elements were initially considered to be located mainly in the vicinity of a

genes transcription start site (Lee *et al*., 2014; Lenhard *et al*., 2012). These findings were made in bacteria. During the last decade studies in eukaryotic cells could investigate the ability of TFs to bind to thousands of sites in the genome. Interestingly, most TF binding sites were found to be located in intergenic regions that can be hundreds of kilobases away from the nearest gene (He *et al*., 2011; Junion *et al*., 2012; Wang *et al*., 2012).

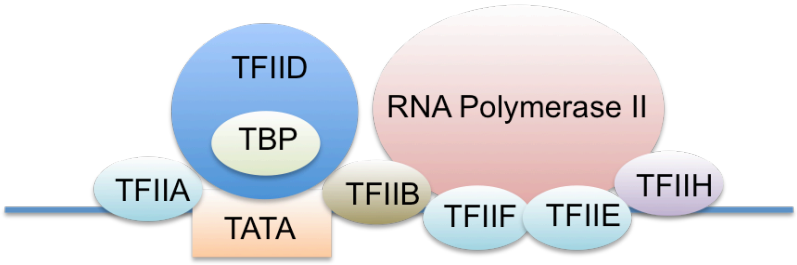

Figure 7: Assembly of the RNA polymerase II pre-initiation complex at ribosomal RNA gene promoters. The assembly begins with the binding of upstream binding factors to the upstream control elements and core element of the rDNA promoter. TBP initiates the pre-initiation complex assembly by binding to the TATA box of promoters. TFIIA and TFIIB interact with TBP (in complex with TFIID) and reinforce its binding to DNA. In turn, TFIIB recruits RNA Polymerase II, TFIIE and TFIIF, thus positioning RNA Polymerase II over the transcription start site. TFIIH mediates 'melting' of the transcription start site to form the open complex.

1.3.2 TF Recognition and Co-Factors

TFs are modular in structure and contain the following domains: a DNA-binding domain (DBD), a trans-activating domain (TAD) and an optional signal sensing domain (SSD) (Latchman, 1997). The DBD usually recognizes a short degenerated DNA sequence of 6-12 bp of length - the response element (Krieger *et al*., 2003).

Different families of TFs exist, which bind DNA through different structural motifs, *e.g.* helix-loop-helix (Littlewood and Evan, 1995), leucin-zipper (Vinson *et al*., 2002), helix-turn-helix (Wintjens *et al*., 1996) or zinc fingers (Laity *et al*., 2001). The sequence-specificity of TFs is often variable and allows a number of similar sequences to be recognized. Therefore, the base homology between the TF binding sites and the TF is not always hundred percent. In addition, some of the electrostatic and van der waals forces between TF binding sites and TF may be weaker than others. Thus, TFs do not bind just one sequence but are capable of binding a subset of closely related sequences, each with a different strength of interaction (Garvie and Wolberger, 2001; Luscombe and Thornton, 2002; Stanford *et al*., 2000). Furthermore, together with cofactors, more than one TF can bind to one TF binding site at

the same time. Mostly, TFs bind cofactors via protein-interaction domains that are separate from the DBD (Thomas, 2006; Xu *et al*., 1999a). Upon the formation of these complexes, TFs can change their recognition sequences (Gil *et al*., 2001; Narlikar *et al*., 2002). Such mechanisms ensure the recognition of certain binding sites only if more than one specific TF is present. This allows a more variable and specific DNA-binding of TFs within the genome ultimately leading to a highly regulated *ad versatile* gene transcription.

1.4 *Cdkn1b* / p27

As introduced in 1.2.3, the *Cdkn1b* gene encodes the cyclin-dependent kinase (CDK) inhibitor $p27^{Kip1}$ (p27) (Polyak *et al*., 1994). p27 is a key player in the regulation of the cell cycle progression from G1 to S phase (Wander *et al*., 2011). As shown in Figure 8, p27 binds to the cyclinE/CDK2 complex, causing the inhibition of the kinase activity of CDK2. Upon mitotic stimulation, p27 gets released from the cyclinE/CDK2 and cyclinA/CDK2 complexes. The conformational changes of these complexes lead to the activation of CDK2 (Larrea *et al*., 2009). The targets of the CDK2 kinase are members of the retinoblastoma (pRb) family, which upon phosphorylation, release E2F transcription factors. These factors then induce the transcription of genes responsible for the progression into the S phase (Figure 8). Beside its function in cell-cycle progression, emerging evidence suggests that p27 can regulate other cellular functions, including cell differentiation, migration and apoptosis (Besson *et al*., 2004; Blagosklonny, 2002; Collard, 2004; Philipp-Staheli *et al*., 2001). Furthermore, recent reports revealed a dual role of p27, behaving as an inhibitor or activator of cyclin D/CDK4/6 and cyclin E/CDK2 depending on specific tyrosine phosphorylations (Blain, 2008; Chu *et al*., 2007; Grimmler *et al*., 2007; James *et al*., 2008). In non-dividing cells, p27 is localized in the nucleus until mitogenic stimuli initiate the translocation of p27 into the cytoplasm where it gets degraded by ubiquitine proteases (Shirane *et al*., 1999). Proteasome-mediated p27 degradation follows two pathways. On the one hand, p27 can be degraded in the cytoplasm by the ubiquitinylation-promoting complex KPC1/KPC2 (Kamura *et al*., 2004). p27 gets phosphorylated at the Ser10 residue followed by the export from the cell nucleus into the cytoplasm of cells (Ishida *et al*., 2002). On the other hand, p27 degradation can occur in the cell nucleus by the ubiquitin ligase SKP2, which requires the p27 phosphorylation at the Thr187 residue by cyclin E/A/CDK2 complexes (Carrano *et al*., 1999).

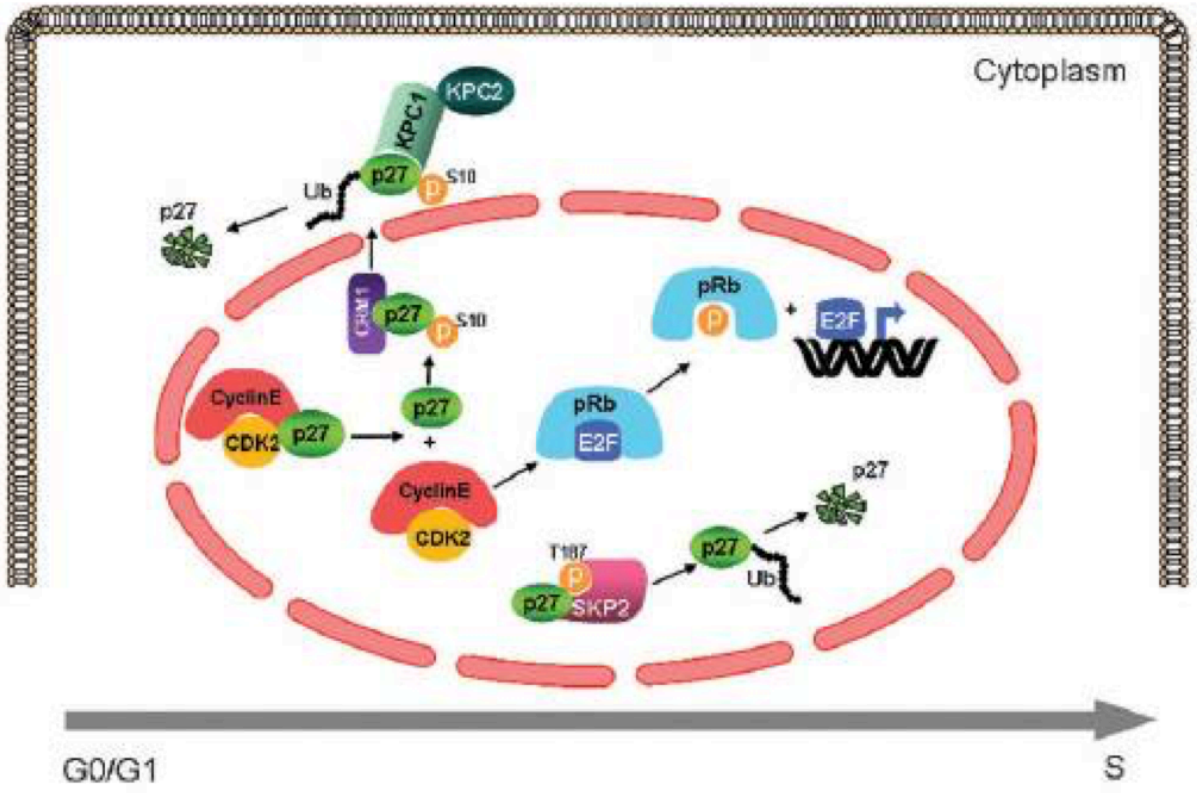

Figure 8: Graphic representation of the nuclear and cytoplasmic interactions of p27. Upon mitotic stimulation, p27 is released from cyclinE/CDK2 complexes and this dissociation from p27 activates CDK2, which phosphorylates pRb. pRb releases the TF E2F, which induces the expression of genes required for the G1 to S phase progression. After the dissociation of p27 from the cyclinE/CDK2 complex in early G1, a portion of p27 is phosphorylated on Ser10 and exported into the cytoplasm through the interaction with CRM1 (exportin). Once in the cytoplasm, p27 is ubiquitinylated by the KPC1/KPC2 complex, which phosphorylates the protein at the Thr187 residue, thereby creating a recognition site for the SKP2 ligase, which promotes ubiquitinylation-mediates degradation of p27 by the proteasome in S phase [PELLEGATA, Natalia S..MENX and MEN4. *Clinics* [online]. 2012, vol.67, suppl.1, pp.13-18. ISSN 1807-5932. http://dx.doi.org/10.6061/clinics/2012(Sup01)04.]

Besides proteasomal degradation, p27 also has some CDK-independent activities specific for its localization in the cytoplasm: p27 participates in actin rearrangement and cell motility through the modulation of RhoA activity (Besson *et al*., 2004; McAllister *et al*., 2003) and p27 interacts with the microtubule-associated stathmin to regulate cell morphology, motility and cell migration (Baldassarre *et al*., 2005; Besson *et al*., 2007). In contrast, p27 has some CDK-independent functions, which takes place in cell nuclei as well. It has been postulated, that modulated p27 levels in mouse muscle cells (C2C12) induce or prevent myogenic differentiation in a Cdk-independent manner (Muñoz-Alonso *et al*., 2005). Furthermore, p27 can stabilize the neurogenin-2 protein by its N-terminal half, which leads to a CDK-independent differentiation of neural progenitors in the cortex (Nguyen *et al*., 2007). In

addition, p27 was shown to induce the expression of erythroid markers in human myelogenous leukemia cells (K562) without any influence of CDK proteins (Acosta *et al*., 2008).

The role of p27 in tumorigenesis was first studied in mice. $p27^{-/-}$ mice displayed in *in vivo* studies an increase in body size and the development of multiple organ (thymus, spleen, pituitary, adrenal glands and gonads) hyperplasias, which indicates the role of p27 in tumorigenesis (Fero *et al*., 1996; Kiyokawa *et al*., 1996; Nakayama *et al*., 1996). In human cancers, reduced p27 levels or mislocalization of the protein in the cytoplasm of the tumor cells are associated with tumor aggressiveness and poor clinical outcome (Slingerland and Pagano, 2000; Viglietto *et al*., 2002).

More interesting - for the topic of this dissertation - is a study published in 2012, where p27 was shown to be able to associate with promoter sequences of the chromatin in mouse embryonic fibroblasts (MEFs) to regulate gene transcription (Pippa *et al*., 2012). In this study p27 was shown to interact with the E2F transcription factor 4 (E2F4), the retinoblastoma-like protein p130 and co-repressors such as histone deacetylases (HDACs) and the transcriptional regulatory protein mSIN3a to bind DNA (Figure 9). E2F4 and p130 were already known to build a transcriptional repressor complex (Mayol *et al*., 1996). The large multiprotein SIN3/HDAC complex had already been identified in several studies before (Ayer, 1999; Dannenberg *et al*., 2005; Knoepfler and Eisenman, 1999; Silverstein and Ekwall, 2005). Pippa *et al*. (2012) observed that p27, which associates with specific promoters of genes involved in important cellular functions, such as processing and splicing of RNA, mitochondrial organization and respiration, translation and cell cycle.

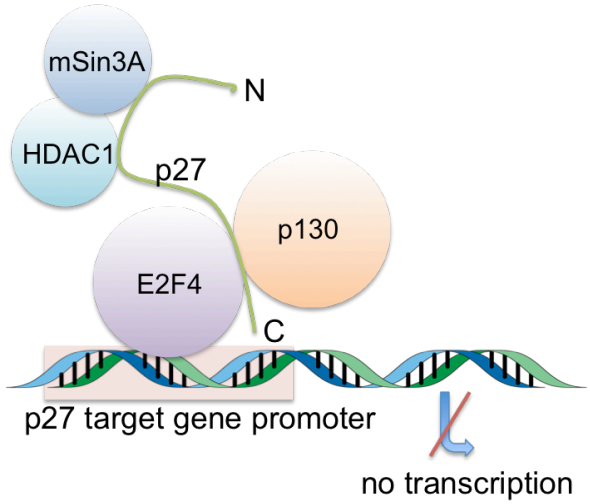

Figure 9: Model illustrating the participation of p27 on the organization of p130/E2F4 repressor complexes. p130 first drives E2F4 to the promoters of p27 target genes, then p27 is subsequently loaded by directly interacting via its carboxyl-domain with both p130 and E2F4. Finally, p27 recruits the co-repressors HDAC1 and mSIN3A on these promoters.

1.5 Hypothesis and Aims

The *Cdkn1b* gene encodes the p27 cell cycle regulator which binds and inhibits cyclin-CDK complexes. In adult tissues, p27 is ubiquitously expressed and plays a crucial role in maintaining tissue homeostasis by preventing differentiated cells from re-entering the cell cycle. *Cdkn1b* was also demonstrated to be a tumor susceptibility gene for multiple endocrine neoplasia tumors in both rats (MENX syndrome) and in human patients (MEN4 syndrome). MENX is caused by a germline frameshift mutation in *Cdkn1b* that renders the encoded mutant p27 protein very unstable. Among other neuroendocrine tumors, MENX rats develop bilateral pheochromocytoma with complete penetrance.

In addition to its role as a cyclin-CDK inhibitor, p27 also performs cyclin-CDK-independent functions. Recently, it was reported that p27 indirectly regulates gene transcription in mouse fibroblasts (MEFs) by associating with TFs and inhibiting gene transcription at specific promoters. p27 co-localizes with p130, E2F4 and co-repressors such as HDACs and mSIN3A and binds to specific promoter regions. The genes regulated by this complex are involved in important cellular functions such as RNA processing and splicing, mitochondrial organization and respiration, translation and cell cycle.

We hypothesize that defective p27 may promote tumor formation because of aberrant gene expression regulation. Specifically in adrenomedullary tissues, we assume p27 to regulate gene transcription and thereby cause tumorigenesis when it is absent.

To address this issue, we performed genome-wide chromatin immunoprecipitation followed by sequencing (ChIP-Seq) with rat and human adrenomedullary cells to identify the sequences bound by p27-containing complexes and indirectly the TFs binding to p27. Therefore, we wanted to confirm the binding of p27 to adrenomedullary cells by investigating the presence of p27 in different cellular fractions. Once the binding was confirmed, we performed ChIP-Seq with adrenomedullary tissues from WT rats (with basal p27 levels) or adrenomedullary tissues of humans. DNA sequences bound by p27-contaning protein complexes were immunoprecipitated from rat and human tissue extracts using an anti-p27 antibody coupled with magnetic beads. Quantitative next generation sequencing (NGS) determined then the DNA sites bound by the p27-containing complexes, which indicated novel putative p27 interaction partners. Candidate TFs that bind to the enriched DNA sequences were tested for their direct interaction with p27 in adrenomedullary cells and cell lines using immunoprecipitation (IP). The interaction was validated by proximity ligation assay (PLA), which allows a high specific and sensitive detection and localization of protein-protein interactions.

The potential binding of p27 to promoter sequences in neuroendocrine cells and the associated regulation of gene transcription was then confirmed by the identification of transcriptional p27 target genes, comparing transcriptome analysis of adrenomedullary tissues from WT and MENX rats in correlation with the p27 ChIP-Seq data. The p27-dependent regulation of the expression of selected target genes was verified by modulating p27 levels in adrenal cell lines and tissues. To clarify a tissue-specific role of p27 as transcriptional regulator, p27 target genes were validated by their expression in endocrine tissues compared with nonendocrine tissues.

This newly discovered function of p27 as an indirect transcriptional repressor, if confirmed in other cell types than MEFs, may give insight into the mechanisms associated with the frequently observed p27 down-regulation in human cancers. Specifically, if p27 behaves as a transcriptional regulator also in neuroendocrine cells, we might be able to better understand why defects in p27 function mainly lead to tumors derived from these cells.

2 MATERIAL AND METHODS

2.1 Material

2.1.1 Instruments

Adhesive seal applicator	3M Deutschland, Neuss (Germany)
Centrifuge Biofuge fresco	Heraeus Instruments, Osterode (Germany)
Rotor: 75003328 1.5/2 ml	Thermo Fisher Scientific, Waltham (MA, USA)
Centrifuge Biofuge pico	Heraeus Instruments, Osterode (Germany)
Rotor: 75003328 1.5/2 ml	Thermo Fisher Scientific, Waltham (MA, USA)
Centrifuge Eppendorf 5415D	Eppendorf, Hamburg (Germany)
Rotor: F45-24-11 1.5 ml	Eppendorf, Hamburg (Germany)
Centrifuge Fisherbrand Mini	Fisher Scientific, Schwerte (Germany)
Rotors 0.2 ml, 1.5 ml	Fisher Scientific, Schwerte (Germany)
Centrifuge Rotanta 460R	Andreas Hettich, Tuttlingen (Germany)
Rotor: 5624 15 ml, 50 ml	Andreas Hettich, Tuttlingen (Germany)
Centrifuge Rotina 420R	Andreas Hettich, Tuttlingen (Germany)
Rotor: 4790 1.5 ml	Andreas Hettich, Tuttlingen (Germany)
Centrifuge Variofuge 3.0R	Heraeus Sepatech, Osterode (Germany)
Rotor: #8074, inserts #8078 15 ml, 50 ml	Heraeus Sepatech, Osterode (Germany)
Counting chamber Improved Double Neubauer Ruling	Brand, Wertheim (Germany)
Dispenser Multipette® plus	Eppendorf, Hamburg (Germany)
Electrophoresis Cell GT MINI-SUB®	Bio-Rad Lab., Munich (Germany)
Electrophoresis Mini-Cell XCell *SureLock*™ Novex	Invitrogen, Darmstadt (Germany)
Electrophoresis Transfer Cell Mini Trans-Blot®	Bio-Rad Lab., Munich (Germany)
Freezer -20°C Liebherr Comfort	Liebherr, Biberach an der Riss (Germany)
Freezer -80 °C HFC86-360	Heraeus Instruments, Osterode (Germany)
Freezing container NALGENE™ Cryo 1°C	Thermo Fisher Scientific, Roskilde (Denmark)
Fridge +4°C Liebherr Premium	Liebherr, Biberach an der Riss (Germany)
Gas burner Fuego SCS basic	WLD-TEC, Göttingen (Germany)
Gel documentation system	Vilber Lourmat, Eberhardzell (Germany)
Heating block Thermomixer® comfort 1.5 ml	Eppendorf, Hamburg (Germany)

Heating block Thermomixer® compact 1.5 ml	Eppendorf, Hamburg (Germany)
Heating block ThermoStat plus 1.5 ml	Eppendorf, Hamburg (Germany)
Hood Uniflow UVUB 1800	UniEquip, Planegg (Germany)
Ice machine	Ziegra, Isernhagen (Germany)
Incubator shaker Model G25	New Brunswick Sci., Edison (NJ, USA)
Incubator innova CO-170	New Brunswick Sci., Edison (NJ, USA)
Infinite M200 plate reader	Tecan, Crailsheim (Germany)
Magnetic stir bars, various sizes	NeoLab, Heidelberg (Germany)
Magnetic stirrer MR2000	Heidolph Instr., Schwabach (Germany)
Maxwell® 16	Promega, Mannheim (Germany)
Microplate Reader Model 680	Bio-Rad Lab., Munich (Germany)
Microplate Reader Varioskan™ LUX	Thermo Fisher Scientific, Langenselbold (Germany)
Microscope Axiovert 135	Carl Zeiss, Jena (Germany)
Microscope BX 43	Olympus, Hamburg (Germany)
Microscope CLSM FluoView FV1200	Olympus, Hamburg (Germany)
Microscope EVOS xl	Thermo Fisher Scientific, Langenselbold (Germany)
Microwave Privileg 1034HGD	Otto, Hamburg (Germany)
Microwave Whirlpool ProMicro 825	Bauknecht Hausg., Stuttgart (Germany)
MilliQ water purification system	Sigma-Aldrich, Steinheim (Germany)
Multichannel pipette Finnpipette® 50-300 µl	Thermo Fisher Scientific, Langenselbold (Germany)
NanoDrop™ 2000 Spectrophotometer	Thermo Fisher Scientific, Langenselbold (Germany)
4D-Nucleofector™ System (Core and X unit)	Lonza, Basel (Switzerland)
PCR cycler GeneAmp® PCR system 9700	Applied Biosystems, Darmstadt (Germany)
PCR cycler Real-Time 7300	Applied Biosystems, Darmstadt (Germany)
PCR cycler SensoQuest labcycler	SensoQuest, Göttingen (Germany)
PCR cycler TPersonal Thermocycler	Biometra, Göttingen (Germany)
pH meter inoLab® Level 1	WTW, Weilheim (Germany)
Pipette Discovery 100-1000 µl	Abimed, Langenfeld (Germany)
Pipette Discovery 20-200 µl	Abimed, Langenfeld (Germany)
Pipette Discovery 10-100 µl	Abimed, Langenfeld (Germany)
Pipette Discovery 2-20 µl	Abimed, Langenfeld (Germany)
Pipette Discovery 0.5-10 µl	Abimed, Langenfeld (Germany)
Pipette P1000	Gilson, Limburg-Offheim (Germany)

Pipette P200	Gilson, Limburg-Offheim (Germany)
Pipette P100	Gilson, Limburg-Offheim (Germany)
Pipette P20	Gilson, Limburg-Offheim (Germany)
Pipette P10	Gilson, Limburg-Offheim (Germany)
Pipettor accu-jet®	Brand, Wertheim (Germany)
Pipettor PIPETBOY acu	Integra Biosciences, Fernwald (Germany)
Pipettor pipetus®-akku	Hirschmann Laborg., Eberstadt (Germany)
Power supply Model 200/2.0	Bio-Rad Lab., Munich (Germany)
Power supply PowerPac 300	Bio-Rad Lab., Munich (Germany)
Pressure cooking pot Tender Cooker	Nordic Ware, Frankfurt (Germany)
Reaction tube rotator L29	A. Hartenstein, Würzburg (Germany)
Rocking table shaker UNITWIST-RT	Kister Biotech, Steinfurt (Germany)
Scales Sartorius basic	Sartorius, Göttingen (Germany)
Scales Sartorius universal	Sartorius, Göttingen (Germany)
Scanner 3000 7G with autoloader	Affymetrix, Ceveland (OH, USA)
Spectrophotometer NanoDrop® ND-1000	Thermo Fisher Scientific, Langenselbold (Germany)
Test-Tube-Rotator L29	A. Hartenstein, Würzburg (Germany)
Tweezers No.5	A.Dumont&Fils, Montignez (Switzerland)
Universal Oven UM 300	Memmert, Schwabach (Germany)
Vacuum Concentrator plus	Eppendorf, Hamburg (Germany)
Vortexer Reax top	Heidolph Instr., Schwabach (Germany)
Vortexer Vortex-Genie 2	Scientific Industries, Bohemia (NY, USA)
Water bath shaker #1083	G. f. Labortechnik, Burgwedel (Germany)
Water bath shaker SW21	Julabo Labortechnik, Seelbach (Germany)
X-ray cassette	Carl Roth, Karlsruhe (Germany)

2.1.2 Consumable Materials

Blotting paper grade 3m/N 65 g/m^2	Munktell & Filtrak, Bärenstein (Germany)
Cell Counting Slides for Luna	Biozym Sci. Hessisch Oldendorf (Germany)
Cell Culture Inserts for 24-well plates. 8.0 µm pores, Transparent PET Membrane. BD BioCoat™	BD Biosciences, Heidelberg (Germany)
Cell strainer Falcon 70 µm, nylon	BD Biosciences, Heidelberg (Germany)
Combitips® for Multipette® 12.5 ml	Eppendorf, Hamburg (Germany)
Cover slips 12 mm round	Carl Roth, Karlsruhe (Germany)

Cryogenic vials sterile 2 ml freestanding Falcon®	BD Biosciences, Heidelberg (Germany)
Cuvettes PLASTIBRAND® 1.5 ml semi-micro	Brand, Wertheim (Germany)
Gel cassettes 1.5 mm	Life Technologies, Carlsbad (Germany)
Glass slides SuperFrost® 76 x 26 mm	Carl Roth, Karlsruhe (Germany)
Membrane for Western Amersham™ Hybond™-ECL	GE Healthcare, Munich (Germany)
Microplates, TC 96 well, clear bottomed, white walled	Lonza, Basel (Switzerland)
Needles Sterican® Ø 0.60 x 60 mm 23G x 2 $^{3}/_{8}$”	B. Braun, Melsungen (Germany)
Needles Sterican® Ø 0.80 x 50 mm 21G x 2”	B. Braun, Melsungen (Germany)
Parafilm®	Carl Roth, Karlsruhe (Germany)
PCR plate (0.2 ml) Thermo-Fast® 96-well, non-skirted	Abgene/Thermo Scientific, Rockford (IL, USA)
PCR tube strips 0.2 ml	Eppendorf, Hamburg (Germany)
Petri dishes 100 x 15 56.7 cm^2 Nunclon™ Δ	Nunc, Roskilde (Denmark)
Petri dishes glass bottom poly-D-lysine coated no. 1.5	MatTek, Ashland (MA, USA)
pH indicator strips	Merck, Darmstadt (Germany)
Photographic film Amersham Hyperfilm™ ECL	GE Healthcare, Munich (Germany)
Pipettes, Pasteur glass 3.2 ml	Carl Roth, Karlsruhe (Germany)
Pipettes, serological CELLSTAR® 5 ml	Greiner BioOne, Frickenhausen (Germany)
Pipettes, serological CELLSTAR® 10 ml	Greiner BioOne, Frickenhausen (Germany)
Pipettes, serological CELLSTAR® 25 ml	Greiner BioOne, Frickenhausen (Germany)
Pipette tips Graduated Filter Tips TipOne® 0.1-10 µl	Starlab, Ahrensburg (Germany)
Pipette tips Graduated Filter Tips TipOne® 1-20 µl	Starlab, Ahrensburg (Germany)
Pipette tips Graduated Filter Tips TipOne® 1-100 µl	Starlab, Ahrensburg (Germany)
Pipette tips Graduated Filter Tips TipOne® 1-200 µl	Starlab, Ahrensburg (Germany)
Pipette tips Graduated Filter Tips TipOne® 101-1000 µl	Starlab, Ahrensburg (Germany)
Reaction tubes 1.5 ml	Eppendorf, Hamburg (Germany)
Reaction tubes 2 ml	Eppendorf, Hamburg (Germany)
Reaction tubes Falcon™ Blue Max 15 ml	BD Biosciences, Heidelberg (Germany)
Reaction tubes Falcon™ Blue Max 50 ml	BD Biosciences, Heidelberg (Germany)
Reaction tubes, RNase-free 1.5 ml	Zymo Research, Freiburg (Germany)
Scalpel, sterile, disposable	Aesculap, Tuttlingen (Germany)
Syringe Omnifix®, single-use 50 ml (60 ml)	Henke-Sass-Wolf, Tuttlingen (Germany)
Syringe-driven Filter Unit Millex® 0,22µm	Merck, Darmstadt (Germany)
Tissue culture flasks 25 cm^2, filter cap Nunclon™ Δ	Nunc, Roskilde (Denmark)
Tissue culture flasks 75 cm^2, filter cap	Greiner BioOne, Frickenhausen (Germany)
Tissue culture plates 6 well Nunclon™ Δ	Nunc, Roskilde (Denmark)

Tissue culture plates 24 well MULTIWELL™ flat	BD Biosciences, Heidelberg (Germany)
Tissue culture plates 48 well MULTIWELL™ flat	BD Biosciences, Heidelberg (Germany)
Tissue Grinder	Thermo Fisher Scientific, Langenselbold (Germany)
Tubes, plastic 5 ml 75x12 mm	Sarstedt, Nuembrecht (Germany)
Whatman® Gel Blot Paper GB003	Sigma-Aldrich, Steinheim (Germany)

2.1.3 Chemicals

β-mercaptoethanol >99%	Sigma-Aldrich, Steinheim (Germany)
Agarose LE for gel electrophoresis	Biozym, Hessisch Oldendorf (Germany)
Ampicillin sodium salt	Sigma-Aldrich, Steinheim (Germany)
Ampuwa® water	Fresenius KABI, Bad Homburg (Germany)
Ammonium Persulfate (APS) >98%	Sigma-Aldrich, Steinheim (Germany)
Antibody Diluent	Dako/Agilent, Santa Clara (CA, USA)
Bis-acrylamide ProtoGel® 30 % (w/v)	National diagnostics, Nottingham (UK)
Blotting-Grade Blocker	Bio-Rad Lab., Munich (Germany)
Bovine Serum Albumin (BSA) >98%	Sigma-Aldrich, Steinheim (Germany)
Butane Campingaz® CV360	CampingGaz, Hungen-Inheiden (Germany)
Chemiluminescent substrate SuperSignal® West Femto	Thermo Scientific, Darmstadt (Germany)
Chemiluminescent substrate SuperSignal® West Pico	Thermo Scientific, Darmstadt (Germany)
Chloroform, min. 99 % p.a.	Merck, Darmstadt (Germany)
Citrate buffer 10x	DCS, Hamburg (Germany)
Collagen A 0,1 % in HCl, Typ I, 1 mg/ml	Biochrom, Berlin (Germany)
Cresol red	AppliChem, Darmstadt (Germany)
DCS LabLine Antibody Diluent	DCS, Hamburg (Germany)
DMEM + GlutaMAX™, 4.5 g/l D_glucose, pyruvate	Fisher Scientific, Schwerte (Germany)
DMEM/F-12 (1:1) (1x) + L-Glutamine + 15mM HEPES	Fisher Scientific, Schwerte (Germany)
DMSO	Sigma-Aldrich, Steinheim (Germany)
dNTP Mix 10 mM each	Fermentas, St. Leon-Rot (Germany)
DTT 0.1 M	Fisher Scientific, Schwerte (Germany)
EDTA >99% p.a.	Carl Roth, Darmstadt (Germany)
Eosin Y alcoholic solution	Bio-Optica, Milano (Italy)
Ethanol, ASC, ISO	Merck, Darmstadt (Germany)
Ethidium bromide	Sigma-Aldrich, Steinheim (Germany)
Fetal bovine serum (FBS)	Fisher Scientific, Schwerte (Germany)

First strand buffer 5x	Fisher Scientific, Schwerte (Germany)
Formaldehyde 35 wt. % in H_2O	Sigma-Aldrich, Steinheim (Germany)
Fungizone™	Fisher Scientific, Schwerte (Germany)
Gel loading dye, blue 6x	New England Biolabs, Frankfurt (Germany)
Glyerol >99%	Sigma-Aldrich, Steinheim (Germany)
Goat Serum	PAA, Pasching (Germany)
HBSS 1x without $CaCl_2$/$MgCl_2$	Fisher Scientific, Schwerte (Germany)
HCl 5 M	NeoLab, Heidelberg (Germany)
Hematoxylin (Carazzi´s)	Bio-Optica, Milano (Italy)
Hoechst 33258 bisBenzimide	Sigma-Aldrich, Steinheim (Germany)
Horse Serum	Gibco, Darmstadt (Germany)
Hydrochloric acid 1M	Sigma-Aldrich, Steinheim (Germany)
Hydrogen Peroxide 30%	Merck, Darmstadt (Germany)
Isopropanol, ACS, ISO	Merck, Darmstadt (Germany)
Laemmli sample buffer 1x	Bio-Rad Lab., Munich (Germany)
LB broth base	Fisher Scientific, Schwerte (Germany)
Methanol, ACS, ISO	Merck, Darmstadt (Germany)
Mounting medium VECTASHIELD®	BIOZOL Diagnostica, Eching (Germany)
Thiazolyl Blue Tetrazolium Bromide (MTT)	Sigma-Aldrich, Steinheim (Germany)
NP-40 Tergitol®	Sigma-Aldrich, Steinheim (Germany)
Opti-MEM® Reduced Serum Medium	Fisher Scientific, Schwerte (Germany)
Paraformaldehyde	Merck, Darmstadt (Germany)
PBS powder pH 7.4	Sigma-Aldrich, Steinheim (Germany)
Penicillin-Streptomycin, liquid	Fisher Scientific, Schwerte (Germany)
Phenol Red	Sigma-Aldrich, Steinheim (Germany)
Photographic developer G153 A and B	Agfa Healthcare, Mortsel (Belgium)
Photographic fixer G354	Agfa Healthcare, Mortsel (Belgium)
PIPES >99%	Sigma-Aldrich, Steinheim (Germany)
Ponceau S practical grade	Sigma-Aldrich, Steinheim (Germany)
Protease inhibitor cocktail tablets complete mini	Roche Diagnostics, Mannheim (Germany)
Qubit® ds DNA HS Assay Kit	Life Technologies, Carlsbad (Germany)
Red blood cell Lysing Buffer	Sigma-Aldrich, Steinheim (Germany)
RIPA Buffer	Sigma-Aldrich, Steinheim (Germany)
RNaseZAP®	Sigma-Aldrich, Steinheim (Germany)
Roti®-Stock 10x TBS	Carl Roth, Karlsruhe (Germany)
RPMI 1640 + GlutaMAX™	Gibco, Darmstadt (Germany)

SDS 10 % (w/v) solution	Bio-Rad Lab., Munich (Germany)
SDS-PAGE running buffer Rotiphorese®, 10x	Carl Roth, Karlsruhe (Germany)
Sodium Azide >99%	Sigma-Aldrich, Steinheim (Germany)
Sodium chloride >99,5%	Merck, Darmstadt (Germany)
Sodium deoxycholate >97%	Sigma-Aldrich, Steinheim (Germany)
Sodium hydroxide tablets >99%	Merck, Darmstadt (Germany)
Stripping buffer for Western Blot Restore™ PLUS	Fisher Scientific, Schwerte (Germany)
TaqMan® universal PCR master mix 2x	PE Applied Biosys, Weiterstadt (Germany)
TBE Tris/Boric Acid/EDTA, 10x	Bio-Rad Lab., Munich (Germany)
TBS-T, 10x	Carl Roth, Karlsruhe (Germany)
TEMED 99%	Amresco, Solon (OH, USA)
Toluidine blue O (C.I. 52040) Certistain®	Merck, Darmstadt (Germany)
Transfection Reagent Lipofectamin™ 2000	Invitrogen, Darmstadt (Germany)
Triton X-100, >10% in H_2O	Sigma-Aldrich, Steinheim (Germany)
Trizma® base	Sigma-Aldrich, Steinheim (Germany)
TRIzol® reagent	Fisher Scientific, Schwerte (Germany)
Trypan blue solution 0.4 %	Sigma-Aldrich, Steinheim (Germany)
Trypsin, 0.05 % with EDTA	Fisher Scientific, Schwerte (Germany)
Tween 20	Carl Roth, Karlsruhe (Germany)
Citrate buffer, pH6, 10x	Sigma-Aldrich, Steinheim (Germany)
Xylol >99%	Merck, Darmstadt (Germany)

2.1.4 Buffers and Solutions

If not stated otherwise, all listed solutions were prepared in MilliQ-H_2O.

Agarose gel 1 % (w/v) agarose in 1x TBE boil until dissolved, cool to approximately 60 °C add 0.005 % (v/v) ethidium bromide	Lysis Buffer 1 (for ChIP) 50 mM Hepes-KOH (pH 7.5) 140 mM NaCl 1 mM EDTA 10 % Glycerol 0.5 % NP-40 0.25 % Triton X-100 1/10 Protease Inhibitor
Buffer N (for Cell Fractioning) 15 mM Tris-HCl (pH 7.5) 60 mM KCl 15 mM NaCl 5 mM $MgCl_2$ 1 mM $CaCl_2$ 1 mM DTT 2 mM Sodiumvanadat 250 mM Sucrose 1 mM PMSF	Lysis Buffer 2 (for ChIP) 10 mM Tris-HCl (pH 8.0) 200 mM NaCl 1 mM EDTA 0.5 mM EGTA 1/10 Protease Inhibitor
Elution Buffer (for ChIP) 50 mM Tris-HCl (pH 8.0) 10 mM EDTA 1 % SDS	Lysis Buffer 3 (for ChIP) 10 mM Tris-HCl (pH 8.0) 100 mM NaCl 1 mM EDTA 0.5 mM EGTA 0.1 % Sodium-Deoxycholat 0.5 % N-Lauroylsarcosine
Formaldehyde Solution (for ChIP) 50 mM Hepes-KOH 100 mM NaCl 1 mM EDTA 0.5 mM EGTA 11 % Formaldehyde	Lysis Buffer (for Cell Fractioning) 10 mM Pipes (pH 6.5) 10 mM EDTA 1 mM PMSF 1/10 Protease Inhibitor
IP Buffer 0.5 mM EDTA 1 % Triton X-100 1/7 Proteinase Inhibitor 1/10 Protease Inhibitor in PBS	Paraformaldehyde (2 %, pH 7.4) 2 % (w/v) paraformaldehyde in PBS 15 µl phenol red add 10 M NaOH until dissolved (colour change from pink to colourless) adjust pH to 7.4 with HCl

PCR master mix 6 % (w/v) sucrose 200 µM dATP 200 µM dCTP 200 µM dTTP 200 µM dGTP 10 % (v/v) 10x buffer (Biotherm, no $MgCl_2$) 3 % (v/v) $MgCl_2$ 40 ng/ml Cresol red	Separating gel (12 %) for SDS-PAGE (10 ml) 4 ml 30 % (w/v) acrylamide/bis 3.35 ml H_2O bidest. 2.5 ml 1.5 M Tris (pH 8.8) 100 µl 10% (w/v) SDS 50 µl 10 % (w/v) APS 5 µl TEMED
Ponceau dye 0.1 % (w/v) Ponceau S 5 % (v/v) acetic acid	Stacking gel (4 %) for SDS-PAGE (5ml) 670 µl 30 % (w/v) acrylamide/bis 3 ml H_2O bidest. 1.26 ml 0.5 M Tris (pH 6.8) 50 µl 10% (w/v) SDS 25 µl 10 % (w/v) APS 5 µl TEMED
RIPA buffer (for protein extraction) 50 mM Trizma® base 150 mM NaCl 0.1 % (w/v) SDS 0.5 % (w/v) sodium deoxycholate 1 % (w/v) NP-40 adjust to pH 8.0	TBS-T 10x (pH 7.6) 0.2 M Trizma® base 1.5 M NaCl 1 % (v/v) Tween 20 for 1x, dilute 1:10 in H_2O bidest
RIPA buffer (washing buffer for ChIP) 50 mM Hepes-KOH (pH 7.5) 500 mM LiCl 1 mM EDTA 0.7 % Sodium-Deoxycholat 1 % NP-40	TE buffer (for ChIP) 10 mM Tris-HCl (pH 8.0) 1 mM EDTA 50 mM NaCl

2.1.5 Commercially available Kits

BCA Protein Assay Pierce®	#23225; Fisher Scientific, Schwerte (Germany)
Duolink® In Situ Detection Reagents Red	#DUO92008; Sigma-Aldrich, Steinheim (Germany)
Cell Proliferation Reagent WST-1	#05015944001; Roche Diagnostics, Mannheim (Germany)
HistoMark Biotin Streptavidin-HRP	#5520-0023; SeraCare, Wedel (Germany)
Mycoplasma detection Kit	#PK-CA20-700-20; PromoKine, (Germany)
Maxwell® 16 simply RNA Tissue Kit	#AS1280; Promega, Mannheim (Germany)
Maxwell® 16 LEV Blood DNA Kit	#AS1290; Promega, Mannheim (Germany)

Peroxidase Substrate Kit DAB	#SK-4100; Vector Laboratories, Burlingame (CA, USA)
Protein A/G PLUS-agarose beads	#sc-2003; Santa Cruz Biotechnology, Heidelberg (Germany)
QIAprep® Spin Miniprep Kit	#27106; Qiagen, Hilde (Germany)
Qubit® ds DNA HS Assay Kit	#Q32851; Life Technologies, Carlsbad (Germany)
SF Cell Line 4D-Nucleofector™ X Kit	#V4XC-1024; Lonza, Basel (Switzerland)

2.1.6 Standards

Quick-Load® 100 bp DNA ladder	New England Biolabs, Frankfurt (Germany)
PageRuler™ prestained protein ladder	Fermentas, St. Leon-Rot (Germany)

2.1.7 Primers

For reverse transcription, random primers purchased from Promega were used. The primers for qPCR were ordered as pre-designed for the gene of interest from Thermo Fisher Scientific (Table 2). The Rotor Gene Q system quantifies PCR reaction products by calculating the cycle threshold (Ct) value for each sample during each replication cycle. By linear regression analysis, the relative amount of mRNA in each sample was calculated. Finally, values were normalized against a house keeping gene control (rat samples: *B2m*, human samples: *TBP*).

Table 2: TaqMan assays used for qPCR with the Rotor Gene Q system. [Rn: *Rattus norvegicus*, Hs: *Homo sapiens*]

Gene Symbol	Assays ID	Context Sequence
Apoc4	Rn01476208_m1	CCTGGCCTGCTTTGTAGCATCCATG
APOC4	Hs00957901_g1	GCCCGAGCACCTTCCGGGGCTTATG
B2m	Rn00560865_m1	GCTTGCCATTCAGAAAACTCCCCAA
Cdkn1b	Rn00582195_m1	CGTAAACAGCTCCGAATTAAGAATA
CDKN1B	Hs00153277_m1	AACCGACGATTCTTCTACTCAAAAC
Gata2	Rn00583735_m1	GCTCAGAAGGCCGGGAGTGTGTCAA
GATA2	Hs00231119_m1	GTTCCTGTTCAGAAGGCCGGGAGTG
Runx1	Rn01645281_m1	GAGCGGCAGAGGCAAGAGCTTCACT
RUNX1	Hs01021971_m1	CAGAGTCAGATGCAGGATACAAGGC
TBP	H00427620_m1	GCAGCTGCAAAATATTGTATCCACA

Tcf4	Rn00670364_g1	ACATTCACTCATGGTCGGGGCCCAC
TCF4	Hs00162613_m1	TTCATGCAAGATGGCCATCACAGCA
Zfp423	Rn00585834_m1	CCAGTGCCCCGGAAGAAGACGTACC
ZNF423	Hs00323880_m1	CAGACCGAGCTGCAGAACCACACGA
Zfp563	Rn01772782_m1	GTCTAGGAGAAGTCTGAGAAGTGGA
ZNF423	Hs00708147_s1	GAACAGAATACTGAAGATCAGTACA

2.1.8 siRNA

ON TARGETplus Non-targeting siRNA #1
#D-001810-01-05; GE Healthcare Dharmacon, Munich (Germany)

ON TARGETplus Rat *Gata2* (25159) siRNA - SMARTpool
#L-088673-02; GE Healthcare Dharmacon, Munich (Germany)

si*Cdkn1b* (rat)
siRNA made by order from siTOOLs Biotech GmbH; Planegg/Martinsried (Germany)

si*Runx1* (rat)
siRNA made by order from siTOOLs Biotech GmbH; Planegg/Martinsried (Germany)

2.1.9 Enzymes

Collagenase type II	Biochrome, Berlin (Germany)
Reverse transcriptase SuperScript® II	Life Technologies, Carlsbad (Germany)
Taq® DNA polymerase	Fermentas, St. Leon-Rot (Germany)

2.1.10 Antibodies

Primary antibodies for Western blotting

All primary western blotting antibodies shown in Table 3 were used in appropriate dilution with 3 % (w/v) BSA plus 0.1 % sodium azide. Antibodies were stored in dilution at 4 °C and could be re-used.

Table 3: Primary antibodies used for western blotting.

Antibody	Company	ID	Host	Dilution	band size
anti-β-actin (polyclonal)	OriGene Technologies Rockvill (MD, USA)	TA890010	rabbit	1:1000	~42 kDa

anti-E2F4 (polyclonal)	Santa Cruz Biotechnology, Heidelberg (Germany)	sc-866	rabbit	1:200	~44 kDa
anti-GATA2 (monoclonal)	Abcam, Cambridge (UK)	ab109241	rabbit	1:1000	~51 kDa
anti-p130 (polyclonal)	Santa Cruz Biotechnology, Heidelberg (Germany)	sc-317	rabbit	1:200	~130 kDa
anti-p27 (N-20) (polyclonal)	Santa Cruz Biotechnology, Heidelberg (Germany)	sc-527	rabbit	1:500	~27 kDa
anti-Runx1 (polyclonal)	Proteintech, Manchester (UK)	19555-1-AP	rabbit	1:1000	~49 kDa
anti-Znf423 (polyclonal)	Merck, Darmstadt (Germany)	ABN410	rabbit	1:2000	~145 kDa

Secondary antibodies for Western blotting

HRP-linked secondary antibodies (diluted in 5 % (w/v) skimmed milk in TBS-T) are displayed in Table 4. They were freshly prepared for each usage.

Table 4: HRP-linked secondary antibodies used for western blotting.

Antibody	Company	ID	Host	Dilution
anti-rabbit IgG	GE Healthcare, Little Chalfont (UK)	NA934-1ML	donkey	1:2000

Antibodies for Immunhistochemistry (IHC) on formalin-fixed paraffin embedded (FFPE) tissue sections

All antibodies were diluted in DCS antibody dilution buffer (DCS Innovative Diagnostik Systeme, Hamburg (Germany)) as indicated in Table 5.

Table 5: Primary antibody used for IHC on FFPE tissue sections.

Antibody	Company	ID	Host	Dilutions
anti-p27^{Kip1} (monoclonal)	BD Biosciences, Bedford (MA, USA)	610242	mouse	1:400

The secondary antibody for IHC was anti-mouse IgG antibody (#710039) produced in goat based on the Histomark Biotin Streptavidin HRP-system (Kirkegaard & Perry Laboratories; MA, USA). The antibody was prepared for ready-to-use applications by the company.

Antibodies for Immunofluorescence (IF) on FFPE tissue sections or on cells

The shown antibodies for IF (Table 6) were diluted in ready-to-use antibody diluent from Dako/Agilent.

Table 6: Primary antibodies for IF on FFPE tissue sections.

Antibody	Company	ID	Host	Dilutions
anti-GATA2 (monoclonal)	Abcam, Cambridge (UK)	ab109241	rabbit	1:500
anti-p27^{Kip1} (monoclonal)	BD Biosciences, Bedford (MA, USA)	610242	mouse	1:500
anti-RUNX1 (polyclonal)	Abcam, Cambridge (UK)	ab35962	rabbit	1:1000
anti-Znf423 (polyclonal)	Merck, Darmstadt (Germany)	ABN410	rabbit	1:500

Secondary antibodies were used from Cell Signaling Technology (MA, USA). With respect to the host species of the primary antibody, secondary antibodies tagged with either Alexa fluor 555 (#4413 or #4409) or Alexa fluor FITC (#4412 or #4408) were choosen.

Antibodies for Immunoprecipitation (IP)

For IP experiments, 10 µg of each primary antibody shown in Table 7 were used.

Table 7: Antibodies used for IP experiments.

Antibody	Company	ID	Host
anti-GATA2 (monoclonal)	Abcam, Cambridge (UK)	ab109241	rabbit
anti-p27^{Kip1} (monoclonal)	BD Biosciences, Bedford (MA, USA)	610242	mouse
anti-p27 (C-19) (polyclonal)	Santa Cruz Biotechnology, Heidelberg (Germany)	sc-528	rabbit

anti-p27 (N-20) (polyclonal)	Santa Cruz Biotechnology, Heidelberg (Germany)	sc-527	rabbit
anti-p27 (F-8) (monoclonal)	Santa Cruz Biotechnology, Heidelberg (Germany)	sc-1641	mouse
anti-RUNX1 (polyclonal)	Abcam, Cambridge (UK)	ab35962	rabbit
Znf423 (polyclonal)	Merck, Darmstadt (Germany)	ABN410	rabbit
anti-mouse IgG	Invitrogen, Grand Island (NY, USA)	10400C	mouse

Antibodies for chromatin immunoprecipitation (ChIP)

Antibodies for ChIP experiments in cells and adrenomedullary tissues were utilized with 10 µg (Table 8).

Table 8: Antibodies used for ChIP experiments.

Antibody	Company	ID	Host
anti-p27^{Kip1} (monoclonal)	BD Biosciences, Bedford (MA, USA)	610242	mouse
anti-mouse IgG	Invitrogen, Grand Island (NY, USA)	10400C	mouse

Antibodies for proximity ligation assay (PLA)

To analyse protein-protein interactions, we performed PLA experiments and used following antibodies (Table 9) for that experiments.

Table 9: Antibodies used for PLA.

Antibody	Company	ID	Host
anti-GATA2 (monoclonal)	Abcam, Cambridge (UK)	ab109241	rabbit
anti-p27^{Kip1} (monoclonal)	BD Biosciences, Bedford (MA, USA)	610242	mouse
anti-RUNX1 (polyclonal)	Abcam, Cambridge (UK)	ab35962	rabbit

2.1.11 Bacteria strains and cultured cell lines

One Shot® TOP10 *E. coli* competent cells	Invitrogen, Grand Island (NY, USA)
primary mouse embryonic fibroblasts (MEFs)	mouse embryos established in our laboratory
primary rat embryonic fibroblasts (REFs)	rat embryos established in our laboratory
HEK293T cells	CRL-11268™ courtesy of Dr Natasa Anastasov (ISB, HMGU, Munich, Germany)
PC12	CRL-1721™ purchased from LGC Standards
MPC 4/30 PRR	courtesy of Dr Karel Pacak (National Institutes of Health, Bethesda, MD, USA)
MTT	courtesy of Dr Graeme Eisenhofer (Departments of Clinical Chemistry and Laboratory Medicine, University of Dresden, Germany)
HeLa	courtesy of Dr Sonia Paixao (MPI for Neurobiology, Munich, Germany)
MCF7	courtesy of Dr Natasa Anastasov (ISB, HMGU, Munich, Germany)

2.1.12 Human Adrenal Tissues

The human adrenal and PCC samples used for ChIP-Seq and further gene expression studies were kindly provided by the Imperial College Healthcare Tissue Bank in the Hammersmith Hospital London. The Tissue Bank application number is R13041 confirmed in July 2012.

2.1.13 Animals

The phenotype and genotype of MENX rats have previously been described (Molatore and Pellegata, 2010). MENX rats were group housed under controlled conditions (temperature 23 °C, 12-h/12-h light/dark cycle). The rats had access to standard rodent chow (Altromin Spezialfutter GmbH) and water *ad libitum*. All experiments and procedures were approved by local authorities (TVA-Az.: 55.2-1-54-2532-225-2013) and complied with German animal protection law.

2.1.14 Desinfections

Antifect® FD10	Schülke & Mayr, Norderstedt (Germany)

Pursept®-A Classic Fresh	Merz, Frankfurt a.M. (Germany)
Ethanol 70 % (v/v) in water for bacteriology	
Ethanol 80 % (v/v) in water for cell culture	

2.1.15 Software

Rotor-Gene Q 2.3.1.49	Qiagen, Hilde (Germany)
AimImageBrowser	Carl Zeiss, Jena (Germany)
AxioVision 4.6	Carl Zeiss, Jena (Germany)
Integrative Genome Viewer (igv)	https://www.broadinstitute.org/igv/home (Robinson *et al*., 2011)
LabSens	Olympus Soft Imaging Solutions, Münster (Germany)
MEME-Suite (MEME-ChIP, FIMO, CentriMo)	http://meme.nbcr.net/meme/ (Bailey *et al*., 2009)
SkanIt™ Software for Microplate Reader	Thermo Fisher Scientific, Waltham (MA, USA)
MatInspector	Genomatix GmbH, Munich (Germany)
MS Office 2010	Microsoft, Unterschleißheim (Germany)

2.2 Methods

2.2.1 Molecular biology methods

DNA and RNA isolation

The extraction of RNA or DNA of cells or tissues was performed by the Maxwell® 16 device (Promega GmbH). Cell pellets or homogenized tissue samples were treated with Homogenization Solution and Lysis Buffer (components of the Maxwell® 16 simply RNA Tissue Kit and the Maxwell® 16 Cell DNA Purification Kit) following the manual instructions. The lysed cells or tissues were given to a Maxwell® 16 LEV Cartridge, part of the Promega Purification Kits. The remaining purification process was fulfilled by the Maxwell® extractor automatically. The generated extracts were diluted in 40-60 µl of nuclease-free water. The DNA and RNA content of the samples were measured at a wavelength of 260 nm by the NanoDrop™ 2000 Spectrophotometer. To assess the purity of DNA or RNA the ratio of absorbance at 260 nm and 280 nm were measured.

Accepted ratios for pure DNA and RNA are approximately 1.8/2.0. If the ratios are lower contaminations with proteins, phenol or other absorbers around 280 nm might exist.

Agarose gel electrophoresis

For analysing PCR products, 1 µl of PCR sample was mixed with 5 µl of 6x loading dye and loaded onto a 1 % agarose gel containing 0.005 % ethidium bromide. Samples were separated in 1x TBE buffer alongside a DNA standard (1 kb ladder) at 100 V. Ethidium bromide incorporation visualizes the DNA bands under UV light.

Quantitative real time PCR (qRT-PCR)

Reverse transcription was performed to generate cDNA from RNA templates for further PCR-based analysis of RNA extracts. 0.1-1 µg of total RNA was incubated for 10 min at RT with 1 µg of random primers in 11 µl of reaction volume. Afterwards, components listed in Table 10 were added per reaction batch and incubated for 1 h at 42 °C. The reaction was stopped by a heating step at 95 °C for 5 min. The generated cDNA was stored at -20 °C until further use.

Table 10: Reverse transcription PCR components.

Reagents	**Volume**
5x first strand buffer	4 µl
DTT (0.1 M)	2 µl
dNTP Mix (10 mM each)	1 µl
RNaseOUT	1 µl
SuperScript™ II reverse transcriptase	1 µl

For gene expression studies at mRNA levels, specific genes were amplified by TaqMan™ PCR (Thermo Scientific™). 1 µl of gene expression assays from Thermo Scientific™ (Table 2) was mixed with 10 µl of a 2x TaqMan™ master mix and 5 µl of Ampuwa. The mixture was given into 0.1 ml tubes (appropriate for the Rotor-Gene Q 72-well rotor) and 4 µl of Ampuwa-diluted reverse transcription product was added. All samples were pipetted in duplicates. In parallel, a negative control samples was loaded where 4 µl Ampuwa was added to 16 µl master mix instead of reverse transcript product. Next to the genes of interest, species-dependent endogenous controls were loaded for normalization of cDNA input: *B2m* for rat

and mouse samples (encoding β_2 microglobulin) and TBP for human samples (encoding TATA-binding protein). The Rotor-Gene Q system was run for 40 cycles (steps 3 to 4) with a program shown in Table 11.

Table 11: Rotor-Gene Q qPCR set-up.

Step	Temperature [°C]	Time
1	50	2 min
2	95	10 min
3	94	15 sec
4	60	1 min
5	4	Pause

2.2.2 Cloning - transformation and plasmid isolation

For bacterial transformation, a vial of One Shot® TOP 10 chemically competent *E. coli* were thawed on ice and mixed gently with 1 µg of plasmid DNA. After a 30 min incubation on ice heat shock of bacteria was performed for 30 sec at 42 °C. Following a few minutes cooling down on ice, the bacteria recovered in 1 ml pre-warmed LB medium for 1 h at 37 °C and 300 rpm in a shaking incubator. 100 µl of bacteria solution were given on agar plates containing the appropriate selection antibiotic (100 µg/ml Ampicillin, 50 µg/ml Kanamycin). Bacterial colony growing occurred overnight at 37 °C, so that clones could be picked and inoculated in 4-20 ml of LB medium the next day. After overnight incubation at 37 °C, 10 ml of the bacterial culture were used for plasmid isolation by the QIAprep Spin Miniprep Kit from Qiagen™ following the manual instructions. Glycerol stocks were generated from every plasmid containing bacteria solution for long-term storage.

2.2.3 Cell culture methods

Passage of adherent cell lines

All cells were incubated at 37 °C in an atmosphere of 5 % CO_2 handled under sterile conditions (sterile hood with controlled airflow). Media and trypsin were pre-warmed to 37 °C before use. In order to avoid complete confluence of cells following cell death, the density of cells was reduced by enlarging the size of cell culture flasks or by reducing the cell number before complete confluence was reached. For this purpose, cells were washed with

PBS to remove calcium and trypsin inhibitors from the serum-containing medium and treated with 0.05 % trypsin/EDTA for approximately 5 min at 37 °C to break cell-cell and cell-matrix contacts. The enzymatic effect of trypsin was inhibited by adding serum-containing medium (v/v) to the cells. Cells were split in a ratio between 1:3 and 1:10 every two to four days depending on cell type and their growth kinetics. As to forestall changes in phenotype and functional differentiation, cells were passaged for a limited number of times (35 passages at most) to avoid differential changes in phenotype and function. Media conditions for all used cell lines or primary cells are displayed in Table 12.

Table 12: Composition of used cell culture media. Origin of cell lines see 2.1.11 [HS: horse serum; FBS: fetal bovine serum; P/S: Penicillin/Streptomycin (each 5 000 u/ml); A/A: Antibiotic/Antimycotic solution (10 000 u/ml penicillin, 10 mg streptomycin, 25 µg amphotericin B)]

Cell line / primary cell type	commercial medium	additional ingrediens
HEK293T	DMEM	10 % FBS 1 % P/S
Hela	DMEM	10 % FBS 1 % P/S
MCF7	DMEM	10 % FBS 1 % P/S
MPC	RPMI	10 % HS 5 % FBS 1 % P/S
MTT	RPMI	10 % HS 5 % FBS 1 % P/S
PC12	DMEM/F12	15 % HS 2,5 % FBS 1 % P/S
primary adrenomedullary cells	RPMI	10 % FBS 1 % A/A

Cryoconservating and thawing cells

For cryoconservation cells with low passage numbers were expanded in a 25 cm^2 flasks to approximately 80 % confluence (within two to three passages after thawing a cell line). Cells were detached by trypsin treatment and pelleted by centrifugation (1000 x g and RT for 5 min). Cells were resuspended in 2 ml serum-containing medium plus 10 % (v/v) DMSO. The cell suspension was given into two cryogenic vials (1 ml/vial), which were transferred to a freezing container filled with isopropanol placed at -80 °C overnight. The circumfluent

isopropanol layer ensured a continuous temperature reduction of 1 °C/min. Afterwards, the frozen cells were placed in liquid nitrogen (-196 °C) for long time storage.

For thawing, vials of cryoconserved cells were taken from the liquid nitrogen tank and rapidly thawed in a 37 °C water bath for one to two minutes and quickly transferred to 10 ml pre-warmed cell-specific serum-containing medium. Rapid dilution of the freezing medium is essential due to the cytotoxicity of the cryoprotectant DMSO at RT. To finally get rid of the DMSO, cells were centrifuged at 1000 x g at RT for 5 min, resuspended in fresh serum-containing cell medium and transferred to 25 cm^2 tissue culture flasks.

Mycoplasma test

While fungal or other bacterial infections are usually easily detectable and destructible by antimycotics and antibiotics, mycoplasma contaminations often elude detection. Therefore, every new cell line was routinely tested for contamination by the mycoplasma test kit from PromoKine. 1 ml cell culture supernatant was centrifuged at 250 x g for 5 min at RT to pellet cellular debris. The supernatant was transferred into a fresh sterile tube and centrifuged a second time at 20 000 x g for 10 min at RT to sediment mycoplasma. The pellet was resuspended in 50 µl of buffer solution. 5 µl of suspension was heated to 95 °C for 3 min and mixed with 35 µl of H_2O and 10 µl reaction mix for PCR amplification. The tubes were placed in a PCR thermal cycler and the program set to conditions shown in Table 13; steps 2-4 were repeated for 35 cycles. Afterwards the sample was analyzed by agarose gel electrophoresis. Only mycoplasma free cells were used for experimental set-ups.

Table 13: Mycoplasma PCR set-up.

Step	Temperature [°C]	Time
1	94	30 sec
2	94	30 sec
3	60	120 sec
4	72	60 sec
5	94	30 sec
6	60	120 sec
7	72	5 min

Automated cell counting

10 µl of cell suspension were mixed 1:1 with trypan blue to selectively color and distinguish dead cells. 10 µl were given into a LUNA™ disposable slide and counted by the LUNA™ Automated cell counter (algorithm gives cell number per 1 ml). Within a cell concentration range of 5 x 10^4 to 1 x 10^7 cells/ml and cell diameter of 3-60 µm, LUNA™ software accurately distinguishes between live and dead cells and disregards debris.

Transient transfection

Nucleofection of cells was performed by electroporation performed with the Amaxa 4D-Nucleofector. Cells were resuspended with the desired cell number of 2×10^6 cells per reaction in solution and supplement mixtures according to the manufacturing instructions. Additionally, 1 nM siRNA (from siTOOLs Biotech) or 1 µg plasmid DNA were mixed with cell suspension and transferred into a nucleofection cuvette provided by the company. Nucleofection was conducted with the X-unit of the Amaxa Nucleofector device and electroporation was processed with optimized pulses (Table 14) in order to maximize transfection efficiency without significantly altering viability of the cells. Cells were resuspended in 400 µl of 37 °C pre-warmed cell culturing medium and plated into tissue culture dishes.

Table 14: Optimized buffer and pulse conditions for cell lines and adrenomedullary primary cells used for transfection via the Amaxa Nucleofector device from Lonza.

Cell line / primary cell type	Buffer	Supplement	Pulse
PC12	Solution SF	1	EI-100
primary adrenomedullary cells	Buffer P3	3	DS-150

Primary cell culture of adrenomedullary cells

After dissection of the rat, the adrenal medullas were separated from the cortex with a forceps. The tissue was transferred into a 60 mm Petri dish containing 5 ml HBSS with 1 % antibiotic/antimycotic solution for washing. Afterwards the tissue was injected with sterile type 2 collagenase and was chopped with razor blade into pieces smaller than 0.5 mm. These pieces were transferred into a 15 ml conical tube and filled up with 8 ml type 2 collagenase. The tissue suspension was incubated in a 37 °C water bath for 45 min. Every

15 min, the suspension was mixed by briefly pipetting to ensure proper digestion of connective tissues. To inactivate the collagenase activity, 1 ml of FBS and 10 ml of serum-containing medium were added. The cell suspension was passed through a 70 µm cell strainer and centrifuged at 1 000 x g for 5 min. The supernatant was discarded and the cell pellet was resuspended in 300 µl red blood cell lyses buffer, incubated at RT for 3 min and centrifuged again (same condition as before). Finally, the cells were resuspended in 1 ml serum-containing medium and counted automatically by the LUNA™ cell counter.

2.2.4 Biochemistry methods

Protein extraction

Frozen cell pellets were thawed on ice and resuspended in 50-80 µl of RIPA buffer with protease inhibitor (cOmplete™ Protease inhibitor cocktail). Tissues were minced by a tissue grinder and resuspended in 100 µl of RIPA buffer with protease inhibitor. After 20 min incubation on ice, the cell lysates were spun down at 13 000 g at 4 °C for 10 min to remove cell debris. The protein extracts were stored at -20 °C.

Protein quantification

The content of extracted proteins was measured using the Pierce™ bicinchoninic acid (BCA) Protein Assay Kit. A standard curve was created based on appropriated, different concentrated BSA solutions *ad* 50 µl volume. In parallel, 1 µl of protein sample was mixed with 49 µl of Ampuwa. 500 µl BCA solution (1:50 mixture of Pierce™ Protein Assay Reagent A and Reagent B) was added to protein samples and BSA samples, respectively. After 20 min of incubation at 60 °C, the OD was measured by a Spectrophotometer at 560 nm. The amount of protein in the given sample was estimated by comparing the value for OD_{560} to the standard curve.

SDS-PAGE

Regarding their electrophoretic mobility proteins were separated by discontinuous sodium dodecyl sulphate polyacrylamide gel electrophoresis (SDS-PAGE). Protein extracts (35 µg to 50 µg) and 2x/4x Laemmli buffer plus 5 % (v/v) β-mercaptoethanol were mixed 1:1 and denatured at 95 °C for 5 min. Proteins were electrophoretically separated in 1x SDS running buffer on discontinuous polyacrylamide gels (4 % stacking gel and 12 % separating gel) at

90 V until the samples have passed the stacking gel. Afterwards the voltage was increased to 130 V. A pre-stained protein ladder was run alongside the samples in each gel to allow the identification of the protein of interest based on its molecular weight.

Western blot transfer

To detect specific proteins of cell or tissue samples they have to be made accessible for suitable antibodies. Therefore proteins were blotted by a wet blot system (Bio-Rad Laboratories) from the SDS gel onto a thin nitrocellulose membrane with non-specific protein-binding properties. The SDS gel was placed onto the nitrocellulose membrane bilaterally embedded in two sponges and four sheets of whatman filter paper. The blotting chamber was completely filled with 1x transfer buffer and plugged in a power supply to generate a constant electric field of either 50 V for overnight transfer or 100 V for 2 h transfer at 4 °C. To determine the quality of the transfer and the separating pattern of the proteins the membrane was reversibly stained with Ponceau S solution for several minutes at RT. The staining solution was removed by washing the membrane three times for 5 min in TBS-T washing buffer.

Protein detection

Proteins transferred to a nitrocellulose membrane can be detected by specific antibodies. To prevent non-specific antibody-binding, the membrane was blocked with 5 % (w/v) skimmed milk for 1 h at RT under gentle agitation. The blocking reagent was removed from the membrane by three 5 min washes in TBS-T. The specific primary antibody was diluted in a 3 % BSA solution and added to the membrane for either overnight (at 4 °C) or 1 h (at RT) incubation. Unbound primary antibody was removed washing the membrane three times for 5 min with TBS-T. Subsequently, a species-specific horseradish peroxidase-coupled secondary antibody was diluted in 5 % (w/v) skimmed milk and added to the membrane for 1 h at RT. Following three more washes with TBS-T, a chemiluminescent agent (Super Signal West Pico Chemiluminescent Substrate) was mixed 1:1 and was given on the membrane for 5 min at RT in the dark. The membrane was exposed on a sheet of photo film afterwards. For re-probing western blot membranes with a different primary antibody the membrane was treated with Restore™ Fluorescent Western Blot Stripping Buffer for 15 min at RT. The stripping buffer was removed and the membrane was rinsed with water following three

washes for 5 min each at RT in TBS-T. With the incubation of the membrane in skimmed milk the detection process described above was started all over.

Immunoprecipitation (IP)

Frozen cell pellets (at least 4 x 10^6 cells) were thawed on ice and resuspended in 300 µl of IP buffer with protease inhibitor (cOmplete™ Protease inhibitor cocktail). After 30 min on ice, the cell lysates were spun down at 13 000 g and 4 °C for 10 min to remove cell debris and IP lysates were stored at -20 °C until further use.

For IP, 500 µg of IP protein lysate were mixed with 10 µg of specific primary antibody (*ad* 500 µl IP buffer). After 60 min shaking incubation at 4 °C, 40 µl of protein A/G agarose beads were added and incubated further overnight at 4 °C. Then the beads were washed five times with IP buffer (spin 1 min, 1 000 rpm, 4 °C). Afterwards, 30 µl of 4x Laemmli buffer were added to the beads. To elute the IP product from the beads and denature proteins, the mixture was incubated at 95 °C for 5 min. The IP was checked by western blotting.

WST-1 proliferation assay

PC12 cells were seeded with a number of 10 x 10^4 cells per well into a 96-well-plate. 24 h post-transfection 10 µl/well of the ready-to-use WST-1 reagent from Roche Diagnostics were added to the cells. The stable tetrazolium salt WST-1 is cleaved to a soluble formazan by a complex cellular mechanism that occurs primarily at the cell surface. This bioreduction is largely dependent on the glycolytic production of NAD(P)H in viable cells. Therefore, the amount of formed formazan dye directly correlates to the number of metabolically active cells. The OD was measured by a Spectrophotometer at 450 nm.

2.2.5 Immunhistological stainings

Preparation of tissues

Tissues were fixed in 4 % buffered formalin of at least one day and paraffin-embedded afterwards. Two to 4 µm sections were cut and stained with haematoxylin and eosin (H&E) for histopathological examination or used for immunohistochemical or immunofluorescence stainings.

Preparation of cells

Cells were fixed in 4 % PFA, immobilized in a plasma-thrombin-solution and paraffin-embedded afterwards. Two to 4 µm sections were cut and stained with haematoxylin and eosin (H&E) for histopathological examination or used for immunohistochemical or immunofluorescence stainings.

Haematoxylin and eosin (H&E) staining

Tissue sections were stained by immersing the tissue slides into haematoxylin for 4 min. Excess haematoxylin was removed by washing the slides in running water for 5 min. The staining of the nuclei should fade from violet to blue. The tissue slides were counterstained using eosin for 20 sec and subsequently washed with running water for additional 5 min. Finally, the stained tissue slides were dehydrated using an ascending alcohol series (50 %, 70 %, 96 % and 100 %) and treated with xylol. The slides were sealed with cover slips.

Immunohistochemistry (IHC)

IHC makes it possible to visualize the distribution and localization of specific cellular components within cells and in the proper tissue context. By IHC, discrete tissue components can be identified because of the interaction of target antigens with specific primary antibodies and enzyme-conjugated secondary antibodies. In the presence of substrate and chromogen, the enzyme forms a colored deposit at the sites of antibody-antigen-binding. The visible protein-specific staining can be analyzed microscopically.

First, paraffin sections were deparaffinized (two washes in xylol for 10 min) and hydratized in 100 % ethanol (2 times, 5 min), 90 % ethanol (5 min) and 70 % ethanol (5 min). Afterwards the slides were washed in distilled water and Tris-buffered saline plus 0.05 % Tween 20 (TBS-T, pH 7.0) for 5 min each. To block endogenous peroxidase activity and minimized non-specific background staining, the samples were incubated in hydrogen peroxide (H_2O_2) solution (0,3 % H_2O_2 in methanol) for 5 min. After washing twice for 5 min in TBS-T the antigen retrieval was performed to enable antibody-binding and improve staining intensity. Therefore, the sections were microwaved for 30 min at 1 000 W in citrate acid monohydrate buffer (pH 6,0). Afterwards, the slides were washed in TBS-T for 5 min to cool them down. To avoid unspecific antibody-binding, the slides were blocked with normal goat serum for 30 min at RT and washed once with TBS-T. Following, the slides were incubated with a

primary antibody against the specific protein of interest overnight at 4 °C in a wet chamber. The next day, the samples were washed 3 times in TBS-T for 5 min and incubated with biotinylated secondary antibodies for 45 min. The secondary antibody is conjugated to biotin beads, which can bind to the avidin-enzyme complex. After the incubation time, the slides were washed 3 times for 5 min in TBS-T to remove the antibody and incubated in streptavidin-horseradish peroxidase for 30 min at RT. The slides were washed 3 times for 5 min in TBS-T and treated with DAB staining solution to enable visualization. The slides were counterstained with haematoxylin for 10 sec and washed under running water for 4 min. The slides were dehydrated in increasing concentrations of ethanol (70 %, 96 % and 100 %) with 2 min incubation at each concentration. Subsequently, the sections were incubated in xylol twice for 10 min and mounted with cover slips. Images were recorded using an Olympus BX43 microscope.

Immunofluorescence (IF)

For the IF staining we used sections originated from paraffin embedded tissue samples. Before the staining was proceeded, the sections had to be deparaffinized, rehydrated and cooked as described for IHC. After boiling, the slides were transferred rapidly into TBS-T for 5 min and the primary antibody, diluted in Dako REAL™ solution, was added on the tissue sections. In case of co-immunofluorescent stainings, a mixture of 2 primary antibodies was applied. After the pre-treatment, the slides were incubated with the first antibody dilutions in humid surroundings at 4 °C overnight. The next day, the samples were washed 3 times in TBS-T for 5 min. The secondary antibody was diluted in Dako REAL™ solution and incubated for 60 min, followed by 3 washing steps in TBS-T for 5 min each. For co-staining, a mixture of both secondary antibodies was used - each antibody conjugated to a different fluorophore (FITC or Alexa555). The cell nuclei were stained with DAPI in the dark for 3 min followed by 1 min washing in distilled water. Finally, the slides were covered with vectashield® mounting medium and cover slips. The IF staining was imaged with a confocal fluorescence microscope. The tissue slides were long-term stored at -20 °C in the dark.

Proximity Ligation Assay (PLA)

The proximity ligation assay was performed by using the Duolink® In Situ-Fluorescence Kit and Duolink® Detection Reagents Red from Sigma. Cells were prepared as described above and FFPE sections were used for PLA performed following the manufacturer´s protocol. The

signal detection produced by protein interaction partners was done by the use of a confocal fluorescence microscope from Olympus.

2.2.6 Cell fractioning

Cell nuclei preparation

To verify the binding properties of specific proteins, cells from adrenomedullary WT tissues and cell lines were separated due to their cell compartments. The cell nuclei were isolated by homogenizing tissue and resuspending cell pellets of cell lines in 300 µl of Buffer N. Immediately the same volume of Buffer N plus 0,6 % NP-40 detergent was added. After a 5 min incubation on ice the homogenate was centrifuged at 2 000 g for 5 min at 4 °C. The supernatant containing the cytoplasmic fraction of cells were transferred into a fresh tube, whereas the cell pellet containing the cell nuclei was washed 2 times with Buffer N to get rid of the detergent. The cell nuclei were resuspended in 300 µl Buffer N and 10 µl of that solution was spun down again and resuspended in 10 µl of 2 M NaCl for spectrophotometric measurement by the NanoDrop^{TM} 2000 Spectrophotometer. Microscopically intact preparation of clean nuclei had an A260/A280 ratio of 1.6-1.7 and an A230/A260 ratio of 0.9-1.0 (Bellard *et al.*, 1989). For overnight storage, the cell nuclei were given into a suspension of Buffer N with 70 % glycerol and stored at -80 °C.

Micrococcal nuclease digestion of cell nuclei

To clarify whether a protein of interest binds to the active or inactive portion of the chromatin the cell nuclei were digested by micrococcal nucleases (MNases). At first, the cell nuclei were washed 3 times with Buffer N to remove the glycerol from overnight storage. The cell nuclei pellet is resuspended with 300 µl pre-warmed Buffer N and incubated at 37 °C for 10 min. The cell nuclei were pelleted (5 000 rpm, 5 min) and digested by 0.8 u and 3.2 u of MNase per 10^7 nuclei at 37 °C for 10 min. Afterwards the samples were given on ice for 15 min and centrifuged for 10 min at 12 800 g and 4 °C. The supernatant contained the euchromatin and was given into a fresh tube. The pellet was resuspended in 300 µl ice-cold EDTA (2 mM, pH 8.0) and incubated on ice for 10 min. A centrifugation step (12 800 g, 10 min, 4 °C) separated the nuclear matrix (pellet) and the heterochromatin in the supernatant. The pellet was resuspended in 300 µl ice-cold EDTA (2 mM, pH 8.0) and stored at -20 °C, same with the euchromatin and heterochromatin fraction. During each fractioning

step, a small aliqout of the sample was taken for further western blot analysis to detect the proteins of interest bound to the different cell fractions. To depict the successful digest by MNases, the DNA of the chromatin fractions was isolated by the Maxwell® 16 device (Maxwell® 16 Cell DNA Purification Kit) and 15 µl out of a 50 µl DNA lysate were loaded onto a 1.5 % agarose gel. Ethidium bromide staining showed the classical nucleosomal ladder due to increasing concentrations of MNase.

2.2.7 ChIP-Seq

Chromatin immunoprecipitation (ChIP) comprises a multistep protocol that enables detection of protein-DNA interactions to investigate the potential of proteins to regulate gene transcription. In brief, cells or tissues are fixed with formaldehyde to crosslink the protein-DNA complexes of the chromatin. The nuclear chromatin is then purified and fractioned by sonication. The sonicated chromatin is subjected to immunoprecipitation with an antibody against p27. Subsequently, the co-precipitated DNA was analyzed by quantitative next generation sequencing (NGS). The method was performed according to a protocol from Nature Protocols published in 2006 (Lee *et al*., 2006). The protocol was originally generated for the ChIP-chip approach. Nevertheless, we followed the protocol until the extraction of the immunoprecipitated DNA. Since our aim was the identification of p27 interacting proteins in adrenomedullary tissues to investigate a predicted role of p27 as transcriptional co-regulator, we chose this protocol because it was well-described and because the recommended buffers and incubation steps could be used not only for cells (*e.g.* cell lines or primary cell cultures), but also for tissue samples.

Cell fixation and crosslinking

The tissue was taken directly after rat sectioning and was minced finely in 100 µl of PBS on ice. The minced tissue was transferred into a fresh tube where 2 vol of PBS were added. For crosslinking of proteins to the chromatin, 11 % of fresh formaldehyde solution was added for a 15 min fixation of the tissue at RT on a rotating device. 1/10 vol of 1.25 M glycine was added and incubated for 5 min at RT under rotation to quench the formaldehyde reaction. The tissue suspension was centrifuged (1 100 g, 4 °C, 5 min) and the pellet was washed twice with PBS and was used for ChIP immediately or stored at -80 °C until use.

To harvest cell cultures (1 x 10^8 cells) for ChIP the medium was aspirated and the cells were washed once with PBS. 10 ml of PBS was given onto the cell culture flask and 1/10 vol (1 ml) 11 % formaldehyde was added and incubated for 10 min at RT. 1/10 vol of 1.25 M glycine was added for 2 min. Afterwards, the fixed cells were washed two times with PBS and harvested by a silicon scraper. The cells were pelleted (700 g, 5 min) and washed once with PBS before they were snap frozen in liquid nitrogen. The cells were used for ChIP immediately or stored at -80 °C until use.

Nuclear extraction

The tissue or cell pellet was resuspended in 1 ml Lysis Buffer 1 and incubated for 10 min at 4 °C under rotation. The cells were pelleted (1 350 g, 5 min, 4 °C) and resuspended in 1 ml Lysis Buffer 2. Again, 10 min incubation and centrifugation followed as previously described. The cell pellet was mixed with 1 ml Lysis Buffer 3 for sonication.

Sonication

50 µl of the nuclear extract were taken as pre-sonication control. The chromatin lysate resuspended in Lysis Buffer 3 was shared by sonication with an amplitude of 20 % for 30 sec per cycle. During sonication, the tubes were hold on ice. After every second sonication cycle, 10 µl of the lysate were loaded onto an agarose gel and checked for their fragment sizes. When the DNA was shared in 500 to 1 000 bd fragments, 1/10 vol 10 % Triton X-100 was added and the cell debris was pelleted (20 000 g, 10 min, 4 °C). 50 µl of the solution was mixed with 150 µl elution buffer and incubated overnight at 65 °C for reversal crosslinking. The fragmented DNA was transferred into cryovials for snap freezing in liquid nitrogen and storage at -80 °C.

Quality control of sonicated chromatin

The overnight incubated sonication product (50 µl) was mixed with 200 µl TE Buffer and 0.2 mg/ml of RNase A. The RNase A reaction was performed within 2 h at 37 °C. In addition, 0.2 µg/ml Proteinase K was given to degrade proteins in 2 h at 55 °C. After RNA and protein degradation, 400 µl phenol:chroroform:isoamyl alcohol was added, the solution was vortexed, incubated on ice for 1 min and centrifuged fullspeed for 15 min at 4 °C. The aqueous layer was transferred into a fresh tube containing 32 µl 2.5 M NaCl and 2 µl of 20 µg/ml glycogen. 800 µl ethanol was added and the precipitation reaction was performed

overnight at -20 °C or at least 2 h at -80 °C. The DNA precipitate was pelleted for 30 min at fullspeed and 4 °C and washed twice with 80 % ethanol (ice-cold). The ethanol was removed carefully and the pellet was air-dried for 20 min. The DNA was resolved in 50 µl Tris-HCl (10 mM, pH 8.8) and 5 µl were loaded onto a 1 % agarose gel to check the fragment size. In case of successful fragmentation, the majority of the DNA was expected to be shared to fragments of 200 to 500 bp length.

IP

For the chromatin IP, magnetic Dynabeads™ coupled with protein G were used to precipitate specific protein-DNA-complexes. Prior to the IP, the beads were prepared one day in advance. 50 µl of them were washed three times in 0.5 % BSA in PBS (blocking solution). The beads were incubated shaking overnight at 4 °C in 250 µl blocking solution plus 10 µg of a specific primary antibody. The next day, the beads were washed three times in blocking solution to get rid of the antibody. The beads were solved in 100 µl of blocking solution and 300 µl of sonication product, which was thawed slowly on ice and incubated overnight at 4 °C on a rotator to perform the IP reaction. The next day, the IP lysate was washed five times with RIPA washing buffer. The beads with the bound protein-DNA-complexes were resolved in 1x TE buffer plus 50 mM NaCl. The beads were pelleted (1 000 g, 3 min, 4 °C) and the TE was removed. The beads were vortexed in 235 µl elution buffer and incubated 30 min at 65 °C. Afterwards, the beads were centrifuged for 2 min at fullspeed and 200 µl were taken for reversal crosslinking at 65 °C overnight (the residual 20 µl were used for western blotting). Afterwards, the DNA was isolated as described in the QC part above. The DNA concentration was measured by a Qubit® 2.0 fluorometer.

Sequencing

The precipitated p27 ChIP samples were sequenced commercially by quantitative next generation sequencing (NGS) done by IMGM Laboratories GmbH (Martinsried, Germany).

3 RESULTS

3.1 p27 ChIP-Seq

High levels of the p27 protein are mostly found in the nucleus of quiescent cells (Shirane *et al*., 1999). This feature applies to rat and human adrenomedullary tissues as well (Figure 10). The well characterized role of p27 in the cell nuclei is its function as cyclin-cdk inhibitor. However, beside that classical role in cell cycle regulation, p27 was recently reported to regulate gene transcription in MEF cells (Pippa *et al*., 2012). Whether p27 can act as transcriptional regulator in other cells or tissue types is still unclear. To address this scientific question, we investigated the potential ability of p27 to bind to the chromatin in adrenomedullary cells. We selected chromatin immunoprecipitation followed by quantitative next generation sequencing (ChIP-Seq) as method of choice to verify an association between p27 and specific DNA sequences of target gene promoters. Given that p27 does not possess a DNA-binding domain, its role as transcriptional regulator needs to be mediated by the interaction with TFs. This approach allows the identification of DNA sequences that are pulled-down by an anti-p27 antibody, which should indicate a function of p27 as gene transcription regulator. No data of p27 ChIP-Seq experiments on adrenal cells have been reported so far.

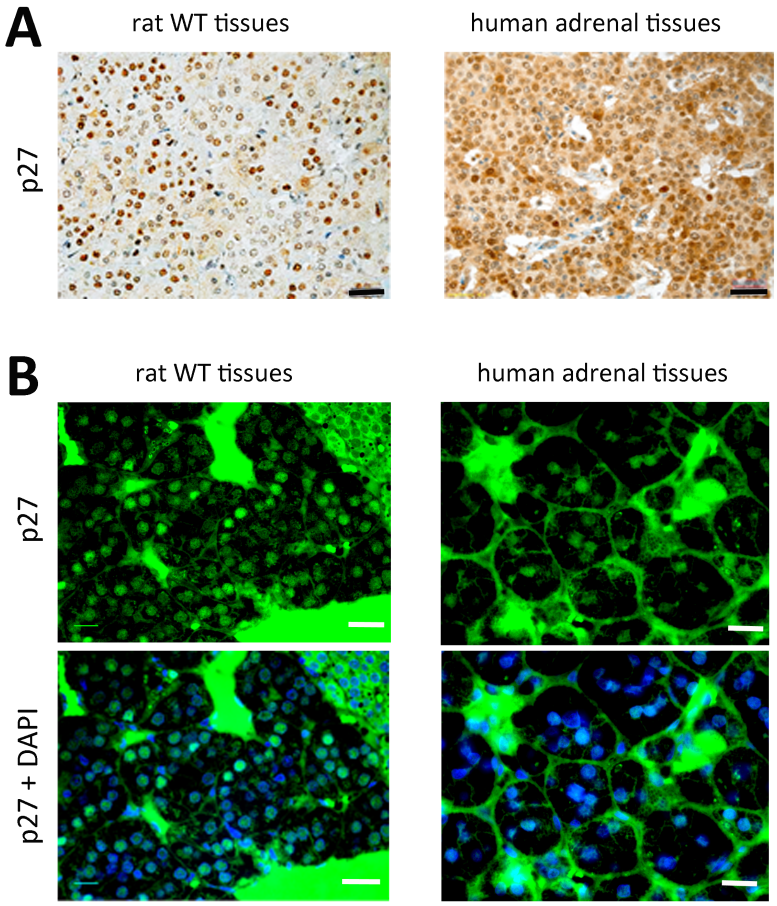

Figure 10: Expression of p27 in rat and human adrenomedullary tissues. (A) IHC of the medulla of adrenal glands of one WT rat tissue sample and one human adrenomedullary tissue sample. The staining of p27 could be observed in the majority of the cell nuclei [scale bars: 20µm; p27: 1:400]. **(B)** IF of p27 in rat WT and human tissues of the adrenal medulla. The upper pictures show p27 (green), whereas the lower row represents the merged channels for p27 (green) and DAPI (blue), which counterstained the cell nuclei. [scale bars: 10µm; p27: 1:400] [Representative data from rat (n=6) and human (n=4) samples.]

3.1.1 Optimization of the p27-IP in adrenal cell lines and tissues for further ChIP-Seq experiments

A prerequisite for a successful IP is to have a highly specific primary antibody. Indeed, the primary antibody specificity plays a crucial role for efficient and reliable ChIP experiments (Orlando *et al.*, 1997). Therefore, we tested several anti-p27 antibodies for their suitability for IP experiments. We tested four different anti-p27 antibodies: (1) monoclonal α-mouse $p27^{Kip1}$ from BD Transduction Laboratories™ (Immunogen: mouse aa 1-197 [full-length p27]), (2) polyclonal α-rabbit p27-N20 from Santa Cruz Biotechnology (Immunogen: human p27 N-terminus), (3) polyclonal α-rabbit p27-C19 from Santa Cruz Biotechnology (Immunogen: human p27 C-terminus) and (4) monoclonal α-mouse p27-F8 from Santa Cruz

Biotechnology (Immunogen: mouse aa 1-197 [full-length p27]). For IP experiments, 10 µg of antibody were utilized to immunoprecipitate p27 in different cell lines: PC12 (rat PCC cell line), REF (rat embryonic fibroblasts), MCF7 (human breast cancer cell line), HeLa (human cervix epithelial cells) and MEF (rat embryonic fibroblasts). The IP reaction was carried out using cell lysates mixed with each one of the mentioned anti-p27 antibodies and incubated overnight at 4°C. Afterwards, the immunoprecipitated p27 was detected by western blotting. IP samples were loaded onto a SDS-PAGE, transferred to a nitrocellulose membrane and probed with an anti-p27 antibody (Figure 11). The antibody used for western blotting was made in a different species compared to the antibody used for IP experiments to avoid unspecific detection of the light chain of the IP-antibody at 25 kDa, which would interfere with the detection of p27 having a molecular weight of 27 kDa.

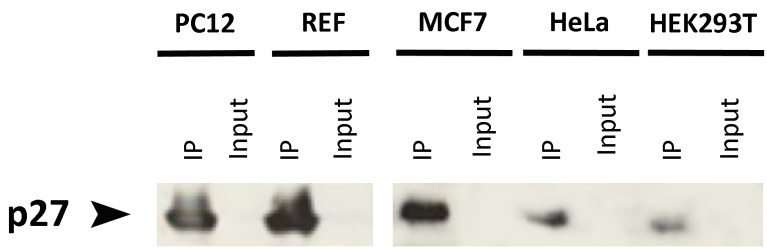

Figure 11: p27-IP experiments with cell lysates of different cell lines. In PC12, REF, MCF7, HeLa and HEK293T cells p27 could be immunoprecipitated successfully by the use of the monoclonal α-mouse anti-p27 antibody from BD Transduction Laboratories™. [p27: 1:500, 27 kDa]

In order to test whether increased p27 protein levels would give more effective results in p27-IP experiments, we treated PC12 cells with proteasome inhibitors to stabilize p27. MG132 is a membrane-permeable proteasome inhibitor, that blocks the cleavage of poly(A) polymerase and apoptosis in PC12 cells, but also temporarily increases the p27 protein level (Giasson *et al*., 1999; Lee *et al*., 2005; Molatore *et al*., 2010; Saito *et al*., 1992). Bortezomib is an anti-cancer drug and the first therapeutic proteasome inhibitor for treating relapsed multiple myeloma and mantle cell lymphoma. In our lab, Bortezomib was found to stabilize p27 in neuroendocrine tumor cells (Lee *et al*., 2011; Molatore *et al*., 2010). The conditions to treat PC12 cells with MG132 and Bortezomib had already been optimized. Following these treatments, we observed a 3-fold (MG132) and 3.1-fold (Bortezomib) increase in p27 levels in PC12 whole cell lysates (input) (Figure 12). Bortezomib- and MG132-treated PC12 cells were then lysed for p27-IP experiments, to check whether the increased levels of the protein

have a positive impact on the p27-IP efficiency. Despite the increased p27 levels, no higher amount of the protein was immunoprecipitated (Figure 12). Hence, we did not further pursue the use of proteasome inhibitors and we performed all subsequent p27-IPs in PC12 cells without pre-treating them with MG132 and Bortezomib. For p27-IP experiments with PC12 cells, we standardized the pre-incubation of the cells in starvation medium without serum. This led to an increase in p27 levels, since cells that undergo quiescence due to lack of nutrients in the medium elevate the expression of p27.

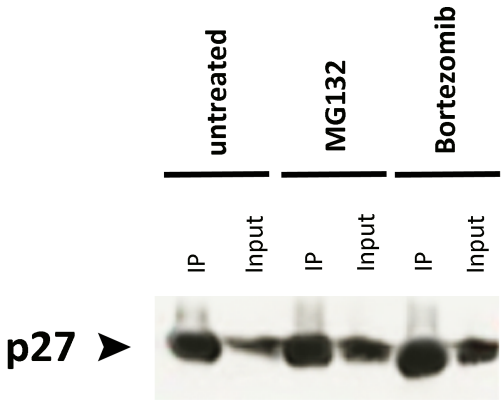

Figure 12: p27-IP experiments with PC12 cells treated with proteasome inhibitors MG132 and Bortezomib in comparison with untreated PC12 cells. Although the endogenous p27 level increased due to the proteasome inhibitor treatments (see inputs), no enhanced IP-efficiency could be detected in these cells (see IP). For p27-IP the monoclonal α-mouse anti-p27 antibody was used. [p27: 1:500, 27 kDa]

The monoclonal anti-p27 antibody from BD Transduction Laboratories™ could be identified as the most specific and efficient in IP experiments, since there was only one specific protein band with a size of 27 kDa detectable by western blotting (Figure 13). As control, a normal mouse anti-IgG antibody (Mouse IgG Isotype Control, Invitrogen™) was used, which is comparable to the IgG family of the specific anti-p27 antibody (isotype stated by the company: mouse IgG1). By western blotting, the BD antibody showed no bands in the IgG control sample. The other three anti-p27 antibodies showed more than one specific band or a considerably fainter p27 band by western blot analyses, indicating less specific or less efficient antibody-binding abilities for p27, respectively, in the different cell lines (data not shown).

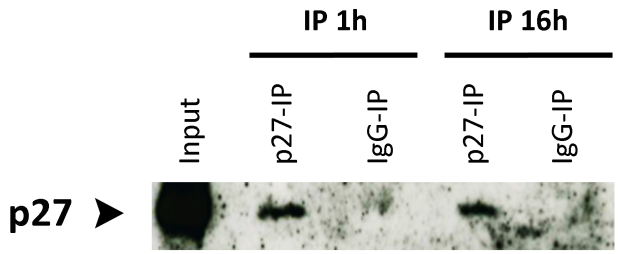

Figure 13: p27-IP in PC12 cells starting from 500 µg of protein and performed with the optimized anti-p27 antibody. The p27-IPs were performed either 1 hour (1h) at 4 °C or overnight (16h) at 4 °C. The duration of the incubation time had no effect on the efficiency of the p27-IP, since the detected signal is similar with both conditions. The negative control (IgG-IP) did not pull-down p27, which indicates a high specificity of the anti-p27 antibody. [p27: 1:500, 27 kDa]

Pippa *et al*. (2012) demonstrated for the first time the ability of p27 to bind to the chromatin in MEF cells by using ChIP on chip experiments. The TFs p130 and E2F4 were identified as interaction partners of p27, which are necessary for its indirect chromatin-binding and transcriptional regulatory function (Pippa *et al*., 2012). To investigate, whether these two TFs are interaction partners of p27 also in adrenomedullary cells - our cell type of interest - we performed co-IP experiments. For that, the p27-IP was performed on PC12 cells and adrenomedullary cell lysates of WT rats, and p130 and E2F4 were detected by western blotting with specific antibodies. As positive control, cell lysates of MEF cells were run in parallel for p27-IP and for western blotting. As shown in Figure 14, the interaction between p130 or E2F4 and p27 could not be confirmed in adrenomedullary cells (PC12 cell line and WT rat adrenomedullary tissue). Only in MEF cells the pull-down of p130 or E2F4 together with p27 could be shown, as expected based on the study of Pippa *et al*. (2012) (Figure 14).

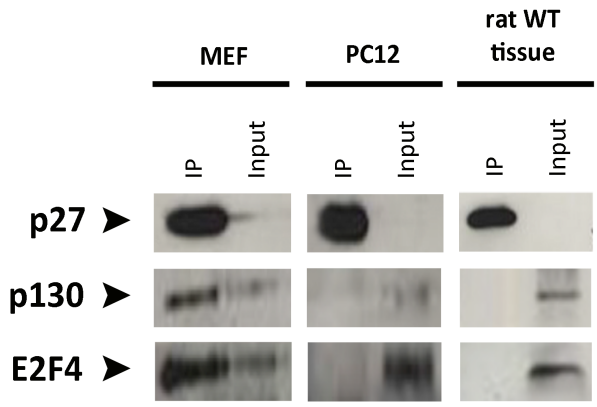

Figure 14: Co-IP experiments of adrenal cells and MEF cells for the validation of p27 to pull-down p130 and E2F4. In PC12 cells as well as in adrenomedullary tissues from a WT rat, neither p130 nor E2F4 could be detected by p27 co-IP. MEF cells were used as control cells, since an interaction of p27

with p130 and E2F4 was reported by Pippa *et al*. (2012). [p27: 1:500, 27 kDa; p130: 1:200, 130 kDa; E2F4: 1:200, 44 kDa]

These findings suggest that if p27 regulates transcription in adrenomedullary cells then it does so through the interaction with TFs other than p130 and E2F4. These TFs permit the association of p27 to the chromatin. Based on this hypothesis, we decided to perform ChIP-Seq experiments with adrenomedullary tissues from WT rats expressing endogenous full-length p27 to verify whether p27 binds to the DNA in these cells, and to identify novel interaction partners of p27 mediating this function. With regard to the tested anti-p27 antibodies for IP experiments, we proceeded further ChIP-Seq experiments with the α-mouse monoclonal anti-p27 antibody from BD Transduction Laboratories™, which recognizes the full-length p27.

3.1.2 p27 binds to the chromatin of WT rat adrenomedullary tissues

To investigate the ability of p27 to bind to chromatin in adrenal cells, we used PC12 and MPC cells, as well as adrenomedullary tissues of WT rats and isolated the cell nuclei by using 5 mM $MgCl_2$. Following the protocol of Remboutsika *et al*. (1999), the chromatin was isolated from the cell nuclei by hypotonic lysis in the presence of 10 mM EDTA (Sealy *et al*., 1989) and separated by micrococcal endonuclease digestion and further EDTA treatments into three different fractions: euchromatin, heterochromatin and the nuclear matrix/insoluble portion of the chromatin (Figure 15 A). In the PC12 and MPC cell lines, the binding of p27 to euchromatin and the nuclear matrix could be detected (Figure 15 B), whereas the rat adrenomedullary tissue (the tissue of interest used for further ChIP-Seq studies) showed an exclusive association of p27 to the nuclear matrix (Figure 15 B). For p27, a signal was not detectable in the cell nuclei fraction of these cells. It could be shown only in the concentrated and purified nuclear matrix fraction. The euchromatin and the nuclear matrix fraction are characterized as transcriptionally active DNA (Ludérus *et al*., 1992; Singer and Green, 1997). Thus, these experiments support the ability of p27 to bind to transcriptionally active chromatin, thereby potentially regulating gene transcription. This finding is an essential basic requirement to proceed with ChIP-Seq experiments.

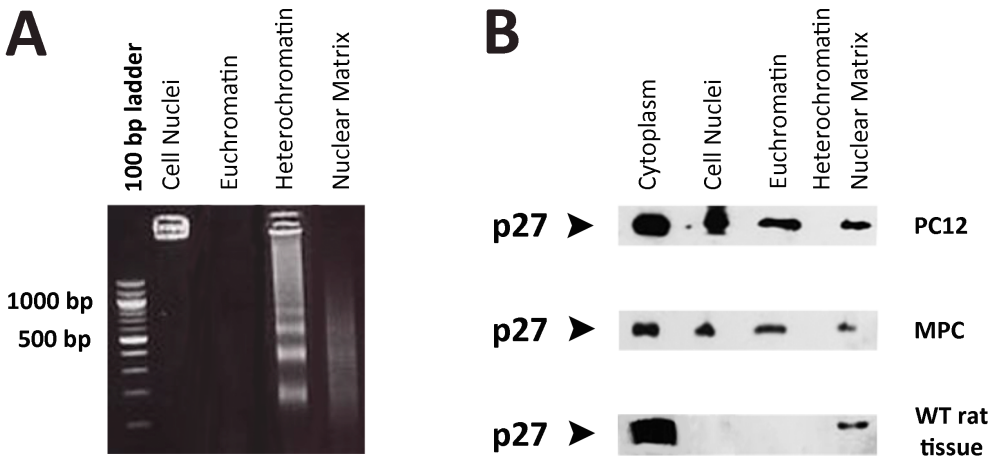

Figure 15: p27 associates to the chromatin in adrenal cells. (A) Agarose (1 %) gel electrophoresis showed the different nuclear fractions of rat WT adrenomedullary tissues (n=3; each sample was a pool of 3 adrenal medullas from 3 different rats). **(B)** In PC12 cells, MPC cells and rat adrenomedullary tissues, p27 could be detected in the euchromatin and in the nuclear matrix by western blotting. In addition, p27 could be observed to bind to euchromatin in PC12 and MPC cells. Representative data for PC12 and MPC cells from three technical replicates. [p27: 1:500, 27 kDa]

3.1.3 Establishment of the p27 ChIP-Seq method

ChIP-Seq experiments are genome-wide location analyses that combine chromatin immunoprecipitation with a highly specific antibody for the protein of interest and NGS to identify protein-DNA interactions that occur in living cells. Protein-DNA interactions are captured *in vivo* by chemical crosslinking to ensure a representative status of protein-DNA interactions dependent on the current living state of a cell population, or of differentiated cells in tissue samples. Cell lysis, DNA fragmentation and immunoaffinity purification of the desired protein are the most essential steps enabling a successful ChIP-Seq in the chosen cells or tissues. These steps will co-purify DNA fragments that are associated with the protein of interest; finally they will be sequenced. Various computational and bioinformatics approaches are then applied to identify and normalize the enriched pulled-down sequences containing the binding site of certain TFs. The general workflow of the whole p27 ChIP-Seq procedure is shown in Figure 16.

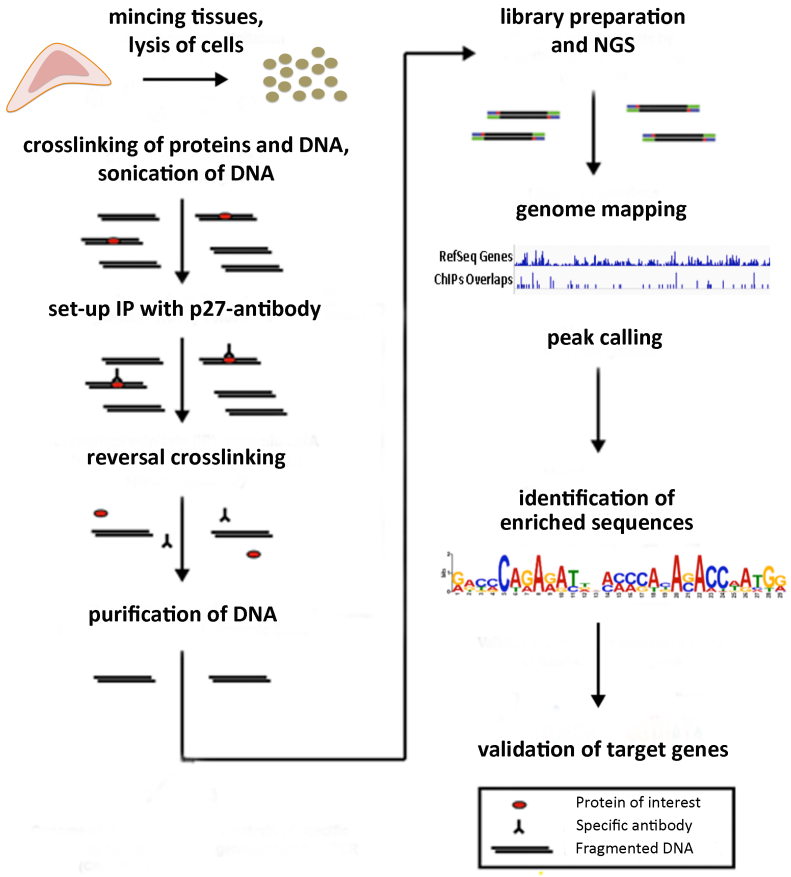

Figure 16: ChIP-Seq workflow with an anti-p27 antibody. Adrenomedullary tissues from WT rats and human individuals needed to be minced in single cells for lysis and crosslink proteins with DNA. Afterwards, the anti-p27 antibody pulled-down p27-bound DNA fragments by IP. The DNA was purified and sequenced. Sequencing generated several million short reads, which were mapped to the reference human or rat genome by short reads alignment programs (Langmead *et al*., 2009). Identification of ChIP enriched regions was accomplished by peak calling algorithms (Chen and Zhang, 2010; Wilbanks and Facciotti, 2010). Identified ChIP enriched regions were subsequently validated.

As mentioned in the protocol of Lee *et al*. (2006), the ChIP-Seq method contains critical steps such as the amount of input material, protein-DNA crosslinking, DNA fragmentation, and specific IP. Each of these steps needs to be optimized for every individual cell line or tissue type. Since the amount of ChIP-input material was predicted to be high, in order to spare precious animal tissue samples, we first performed preliminary ChIP experiments using PC12 and MEF cell lines. MEFs were an interesting model because p27 is able to interact with TFs and regulate gene transcription in these cells as mentioned in 1.4 (Pippa *et al*., 2012). The PC12 cells were used as an adrenal cell line model to verify whether p27 may be a transcriptional regulator also in these cells. Noteworthy, both cell lines were found to harbor an intact WT *Cdkn1b* gene by sequencing.

To perform the p27 ChIP protocol optimization with the indicated cell lines, MEF and PC12 cells were expanded to reach a total cell number of 5×10^7 to 1×10^8 cells for a proper amount of input material. The ChIP protocol started with the fixation of cells and the simultaneous crosslinking of endogenous associated DNA and proteins. The cells were fixed using a 11 % formaldehyde solution for ten minutes initially followed by gentle collection using a cell scraper. They were then snap frozen in liquid nitrogen and stored at -80 °C until further use. Since the concentration of formaldehyde solution or the duration of the incubation time can be adjusted to avoid over- or under-crosslinking, this is indicated as the first critical step in the ChIP protocol. Following the protocol´s instructions, cells were lysed by several incubation steps in three different lysis buffers. Afterwards, the DNA was fragmented into sequences of 500 to 1 000 bp in size; this represents the second critical step of the chosen method. The fragmentation of the DNA into the mentioned fragment sizes is necessary for a successful IP and needs to be performed accurately. Following the protocol´s recommendations, the fragmentation was done mechanically by sonication, where the number and duration of sonication cycles and the used amplitude was crucial for an ideal fragmentation result. These parameters depend on the sonication device used for these experiments. To ensure that the fragmentation was stopped at the most suitable time point, agarose gel electrophoresis was done during the several sonication cycles to check for DNA fragmentation. The fragmentation control by gel electrophoresis was conducted after every other sonication cycle of 30 seconds with an amplitude of 80 %. Sonication is critical since the right sonication tip needs to be used according to the reaction volume and the chosen amplitude to prevent foaming and enable the required circulation of the sample. In our experiment, the cells or tissues were sonicated into 1 ml of lysis buffer with a sonication tip indicated as suitable for reaction volumes of 1 ml, and an amplitude of 80 %. Furthermore, the sonication was performed with samples held continuously on ice; this prevents heat build-up and degradation of proteins and DNA. After these tests, the best working sonication condition for both MEF and PC12 cell lines were 4 cycles for 30 seconds at 80 % amplitude (Figure 17).

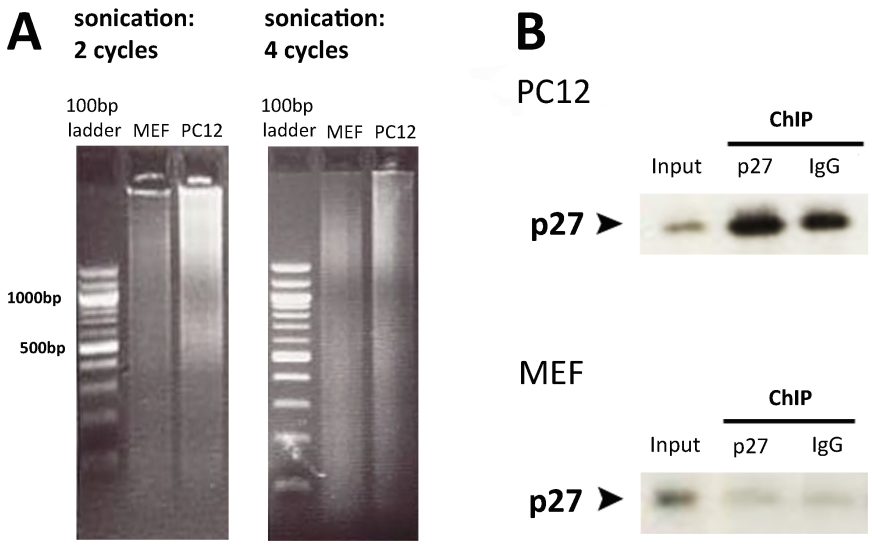

Figure 17: p27-ChIP experiments with PC12 and MEF cells. (A) The size of DNA sequences obtained by sonication was checked by agarose (1 %) gel electrophoresis. The left lane shows the MEF cell fragments and the right lane shows the PC12 cell fragments after two and four cycles of sonication. For MEF and PC12 cells, the suitable fragmentation (around 500 bp) was reached after four sonication cycles. **(B)** After p27 ChIP experiments, the p27 pull-down was checked by western blotting using an anti-p27 antibody. The success of the p27 ChIP was confirmed in PC12 and MEF cells. [p27: 1:500, 27 kDa]

For the ChIP, special resins are necessary to pull-down antibody-coupled protein-DNA fragments. We used magnetic beads coupled with protein G since they are highly recommended for antibodies having an IgG1 backbone, such as the anti-p27 antibody from BD Transduction Laboratories™. As negative control for the input, the same amount of cell lysate was incubated in parallel without the primary antibody. This should indicate the specificity of the anti-p27 antibody for ChIP experiments in MEF and PC12 cells. The most important step of the ChIP method is the IP. The anti-p27 antibody was already tested for its ability to pull-down the p27 protein in these cells (Figure 11). The protocol recommends the usage of 10 µg of the anti-p27 antibody. This amount was evaluated in extracts of PC12 and MEF cells and found to be suitable for ChIP procedures as it was able to pull-down p27 (Figure 17). For western blotting, we used an anti-p27 antibody derived from a species (rabbit) different from the species where the IP antibody (mouse) was produced. Thus, in order to avoid unspecific detection of the light chain of the IP-antibody, which has a size very similar to that of p27.

The final steps of the ChIP are: 1) reversal crosslinking of immunoprecipitated protein-DNA fragments; 2) protein degradation by proteinase K treatment; 3) extraction of the

immunoprecipitated DNA. Reversal crosslinking and protein degradation was performed as recommended by incubating the samples at 65 °C for six hours to overnight. Then, samples were treated with proteinase K (0.2 g/ml) for two hours at 55 °C. The DNA extraction was performed using phenol:chloroform:isoamyl alcohol. DNA concentration was measured by NanoDrop™ and Qubit® Fluorimeter to confirm the success of the ChIP procedure with regard to DNA amount and purity. Contaminations could be detected by calculating the 230/260 and 280/260 ratios that the NanoDrop™ technology assesses automatically. The DNA measurement using the Qubit® fluorimeter is highly sensitive and accurate since the specific Qubit® ds DNA HS assay contains advanced dyes that only fluoresce when bound to double-stranded DNA and no other contaminants (*e.g.* RNA or proteins). Therefore, this method enables the measurement of very small amounts of DNA: ranging from 0.2 ng to 100 ng.

The ability to immunoprecipitate DNA with the anti-p27 antibody in PC12 cells, demonstrated that p27 binds to the chromatin in these cells, which could show indication of a potential regulation of gene transcription. These results suggest that PC12 cells are a promising model to further validate the results of p27 ChIP experiments performed with adrenomedullary tissues. In general, the successful p27 ChIP of MEF cells and PC12 cells following the protocol from Lee *et al*. (2006) encouraged us to go on with the optimization of the method for adrenomedullary tissues.

3.1.4 p27 ChIP-Seq experiments revealed p27 to associate with specific TFs in adrenomedullary tissues

p27 ChIP-Seq experiments were performed using adrenomedullary tissues from WT rats and humans, which express endogenous p27. The optimal amount of input material was determined by conducting five independent p27 ChIP runs with a different number of adrenal medullas of WT rats as input material. Due to the necessity to start from a high amount of tissue input material, only two replicates of the rat tissues and one human sample could be generated. The rat samples consisted of two pooled samples each containing three or four adrenal medullas from different WT rats (age- and gender-matched) (Figure 18 A). Since the adrenal glands are one of the first organs to undergo necrosis after death, the availability of human tissue material for research is rare. Tissue pieces from three individuals were pooled to get the sample that we used in the p27 ChIP experiment (Figure

18 A). At the end, using at least three rat adrenal medullas as input was sufficient to get a suitable amount of immunoprecipitated DNA for NGS (Figure 18 A). Initially, the adrenal glands were taken right after the rats were sacrificed and before any tissue degradation could start. Since only the medulla of rat adrenal glands was needed for p27 ChIP experiments, we separated the medulla from the cortex by performing an incision through the capsule and cortex and we then squeezed out the medulla by slight pressure. Concerning the human samples, we cut frozen adrenal medullary tissues into small pieces (Figure 18 A).

In contrast to the ChIP in cell lines (described above in paragraph 3.1.3), how successful the ChIP on tissues will be, depends on an initial step: the mechanically mincing of tissues by a tissue grinder. Therefore, the rat and human adrenomedullary tissues were homogenized thoroughly to generate a cell suspension. Afterwards, the DNA of the tissue samples was shared by sonication and checked for fragmentation by agarose gel electrophoresis (Figure 18 B). The number of sonication cycles depended on the original size of the minced tissue pieces and, especially for the human samples, on their consistency and nature. For the optimized number of adrenal medullas from rats (three to four adrenal medullas), six sonication cycles á 30 seconds with an amplitude of 77 % were necessary. Samples were always kept on ice. For the amount of human material (one piece - each 3 mm^2 in diameter - of 3 different human adrenal samples) seven cycles à 30 seconds were performed with an amplitude of 81 %; always performed on ice. The IP with the optimized anti-p27 antibody was performed overnight using magnetic beads coupled with protein G. Finally, the success of the p27 ChIP was verified by western blotting using an anti-p27 antibody generated in a different species than the anti-p27 antibody used for ChIP experiments. In parallel to the p27 ChIP, the whole procedure was performed using a control anti-mouse IgG-antibody using the same rat and human input material and the same conditions to prove the specificity of the anti-p27 antibody. As expected, a signal for p27 could be detected by western blotting exclusively in the lane where the rat and human p27 ChIP was loaded, whereas no unspecific signal was observed in the lane where the IgG-control was loaded (Figure 18 C). In contrast to the protocol for ChIP in the cell lines, the DNA was extracted for the ChIP samples using the Maxwell® device from Promega GmbH and not by phenol:chloroform:isoamyl alcohol procedure. In general, quality and amount of DNA improved by using the automated DNA extraction method with the Maxwell® device. For each p27 ChIP sample, a matching input DNA control sample was prepared by following the same protocol with the exception that

the DNA fragments were purified without p27-IP. These input samples were also sequenced in parallel to the p27-specific ChIP samples for further normalization and statistical validation.

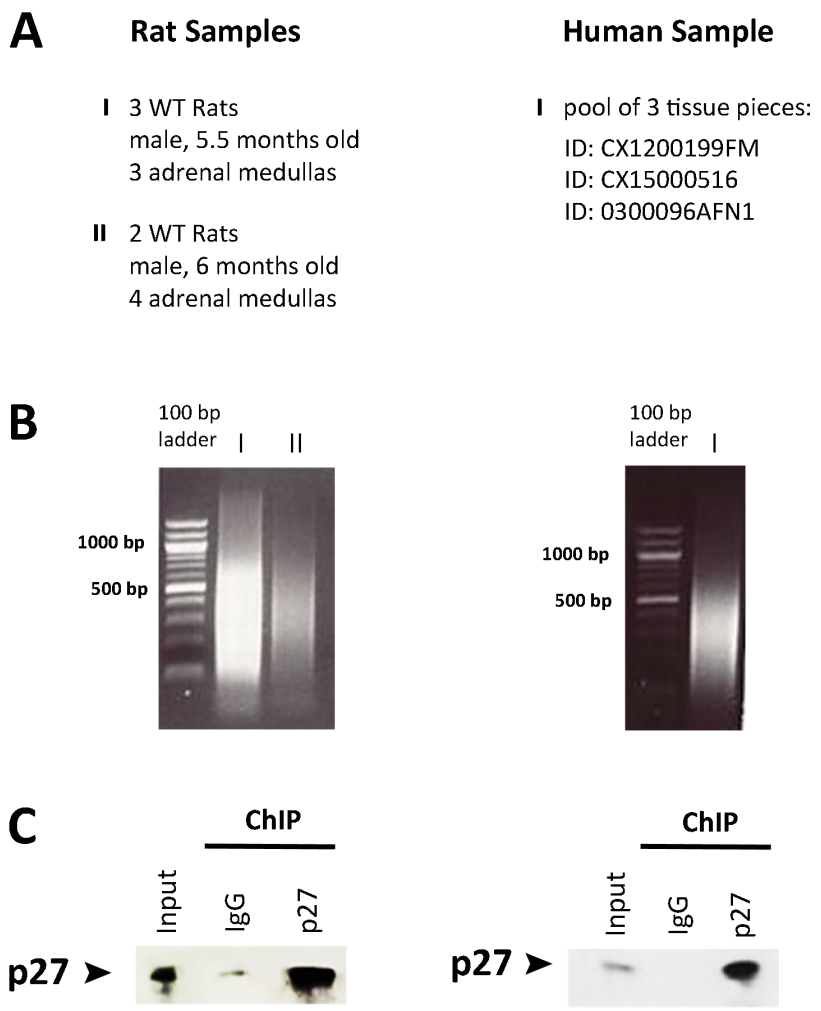

Figure 18: p27 ChIP-Seq experiments of rat and human adrenomedullary tissues. (A) Two rat samples were prepared for p27 ChIP-Seq as replicates. Both samples were generated as pool of at least three adrenal medullas from at least two different rats. One human sample was generated as pool of three tissue pieces from three different human individuals. **(B)** After sonication and p27 ChIP, the size of DNA fragments was checked by gel electrophoresis to verify whether they were suitable for NGS. Both rat and human samples showed a suitable fragment size distribution of 100-500 bp. **(C)** To check the success of p27 ChIPs, western blotting was performed with an anti-p27 antibody from a species different than that of the p27 ChIP-antibody. As control, the same input material was used for ChIP with an unspecific anti-IgG antibody run in parallel to the p27 ChIP. The DNA extracted from the encircled rat and human input and p27 ChIP samples were sent for quantitative NGS to the company IMGM Laboratories. [p27: 1:500, 27 kDa]

The DNA obtained from the encircled samples shown in Figure 18 C was sent to IMGM Laboratories (Martinsried, Germany) for NGS. Our DNA samples were sent at a final

concentration of around 15 ng/µl in 15 µl of reaction volume (>200 ng in total). All following sequencing steps were done by IMGM. By the Illumina TruSeq® ChIP Sample Preparation Kit, from p27 ChIP samples a sequencing library was prepared. The samples were purified, size-selected by agarose gel electrophoresis and adapter-ligated fragments were amplified. Then, quality control of all samples was done by the Bioanalyzer 2100 (Agilent Technologies). Finally, sequencing was performed by Illumina NextSeq500®. All p27-ChIP sequencing samples showed an average fragment length of 275 - 300 bp and a concentration of around 500 nM. The NextSeq500® sequencing runs were performed by the company and .fastq-files were generated as sequencing raw data. The quality control values for the sequencing samples were: cluster density (around 95 k/mm^2), >Q30 bases (92 %), sequencing yield (28 mio reads) and PF reads (27 mio reads). The sequencing raw data generated by the IMGM facility were forwarded to us to conduct further bioinformatics/statistical analyses and validation.

ChIP-Seq experiments revealed that p27 binds to chromatin of rat and human adrenomedullary tissues and significantly associates with a number of TF binding sites and probable gene promoters (Table 15, Figure 20). The pooled human sample analyzed by p27 ChIP-Seq showed a lower significance for specific peaks after genome mapping compared to the rat data (Figure 19). Based on this finding and on the fact that only one pooled human sample was used for p27 ChIP-Seq, we decided to focus on the rat data for further statistical analysis.

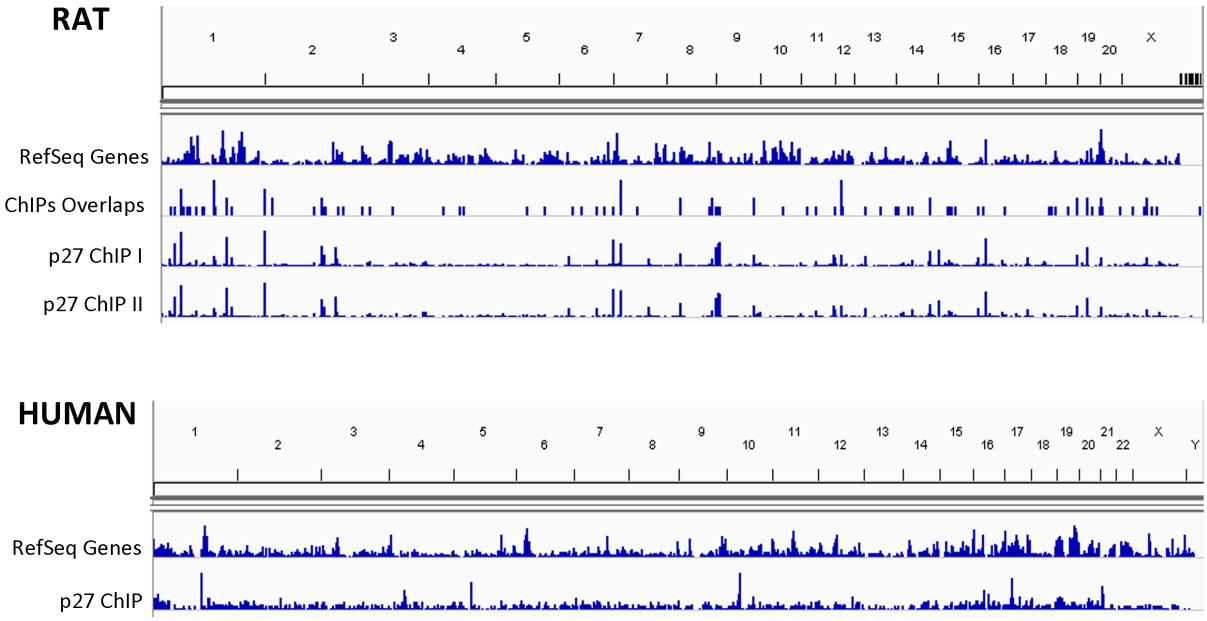

Figure 19: Rat and human p27 ChIP-Seq data displayed with the integrative genome viewer (igv browser). After genome mapping and peak calling, p27 ChIP-Seq peaks were visualized on a rat/human reference genome (chromosomes are displayed). Both rat p27 ChIP samples (ChIP I and ChIP II) were calculated as overlap and were normalized against the input control. The upper line of the rat samples shows the reference rat genome (Rn4). The human sample was normalized to the input control as well and displayed in comparison with the human reference genome (Hg18) shown in the upper line.

To validate the specificity of the identified binding sites, *de novo* motif analysis - using the sequences from the 1 000 most significant peaks - was performed with two different motif analysis tools: MEME-ChIP and Genomatix. MEME discovers novel, ungapped motifs in a series of DNA, such as those generated by ChIP-Seq. A motif is defined as a sequence pattern that occurs repeatedly in a group of related sequences. As indicated in Figure 20, the output of MEME represents motifs as position-dependent letter-probability matrices that represent the four nucleotides. The size of the letters indicates the probability to be located at each position in the pattern: the bigger the letter, the higher the probability. To analyze and annotate the data generated by ChIP-Seq, MEME uses statistical modeling techniques to automatically choose the best width, number of occurrences, and description for each motif. The second sequence analysis tool, the Genomatix Suit, is able to perform several tasks, *e.g.* scientific analysis and visualization of genomic data, generation of networks and pathways or literature searches. Furthermore, the Genomatix tool 'Overrepresented transcription factor binding sites or modules' searches enriched TF binding sites within a set of input

sequences and generates statistics on single TF binding sites and TF binding site pairs (described as modules, which consist of two TF binding sites at a distance of 10 to 50 bp) including overrepresentation values and Z-scores (Table 16). The TF binding site descriptions used for the analysis are from the Genomatix tool 'MatBase' or can be user-defined matrices created with 'MatDefine'. All occurrences of matches are calculated by 'MatInspector'. The overrepresentation values are based on the background of occurrences of the TF binding sites within the whole genomic sequences of the selected species, within all promoters of the selected species and within a user-defined background.

The analysis of the p27 ChIP-Seq data by MEME was done by our collaboration partner Enzo Lalli (University of Nice). Through massively parallel sequencing millions of short sequences are generated, called reads. These sequencing reads were mapped to the rat genome (version Rn4) or human genome (version Hg18) using Bowtie2 with default settings (Langmead *et al*., 2009). Enriched p27-binding sites were identified for its location in the genome by the use of the CisGenome v2 SeqPeak algorithm. Hence, duplicates of p27 ChIP samples and one input control sample were analyzed with algorithm standard parameters: read extension length: 150, local rate window: 10 kb, local rate cut-off 1^{e-005} (Ji *et al*., 2008). Afterwards, Enzo Lalli imported the sequences to the MEME suite for further annotation and motif analysis (Bailey *et al*., 2009). The MEME Suite is a motif-based sequence analysis tool, which is freely available online: www.meme-suite.org/tools/meme-chip (Bailey and Elkan, 1994). The MEME tool takes 150 bp sequences surrounding the summits of the 1000 most significant peaks, which were sorted by their p-values. Based on that, the most enriched sequences for TF biding sites were analyzed and displayed as motif sequence pattern. For further motif distribution analyses, the MEME suite offers algorithms, such as FIMO and CENTRIMO, to show the single occurrences of motifs or the local distribution of a motif (Bailey *et al*., 2009).

Based on the analysis of the rat p27 ChIP-Seq data set with the MEME-ChIP Suite, the most significantly enriched sequence was the binding site of the Zinc finger protein 423 (ZNF423), and the second most enriched sequence was the binding site of the runt-related transcription factor 1 (RUNX1) (Figure 20). Both ZNF423 and RUNX1 are TFs implicated in cancer, where they can repress or activate tumorigenesis (Blyth *et al*., 2005; Huang *et al*., 2009b). The *de novo* motif analyses for the rat p27 ChIP-Seq peaks found an enrichment for

ZNF423 and RUNX1 recognition sites, which suggested that p27 might directly or indirectly interact with these TFs. The peaks containing the binding sites of ZNF423 and RUNX1 were identified using the motif scanning tool 'FIMO' (Grant *et al*., 2011), an analyzing tool part of the MEME-ChIP software. FIMO (Find Individual Motif Occurrences) scans a sequence database to search for the presence of known independent motifs in the sequences obtained from the ChIP-Seq data. The FIMO analysis revealed that 11.3 % (146) of the rat p27 ChIP-Seq peaks (1294 motif counts in total) harbored a ZNF423 binding site, while 20.6 % (266) contained a RUNX1 binding site. Furthermore, 'CentriMo' analysis (Bailey and Machanick, 2012) was used to profile the distribution of ZNF423 sites and RUNX1 sites in ZNF423/RUNX1-containing peaks. CentriMo (Central Motif Enrichment Analysis), another tool in the MEME suite, takes a set of TFBS matrixes/motifs and a set of equal-length sequences from the p27 ChIP-Seq data and plots the position of the best match of each motif on the sequences. Thereby, the 'local enrichment' of each motif is computed by counting the number of times its best match occurs in each sequence and by applying a statistical test to see if the local enrichment is significantly different in comparison with a control set of sequences from the database (by Fisher's exact test). The peaks for ZNF423 and RUNX1 in our p27 ChIP-Seq data revealed no central enrichment as calculated by CentriMo (Figure 20).

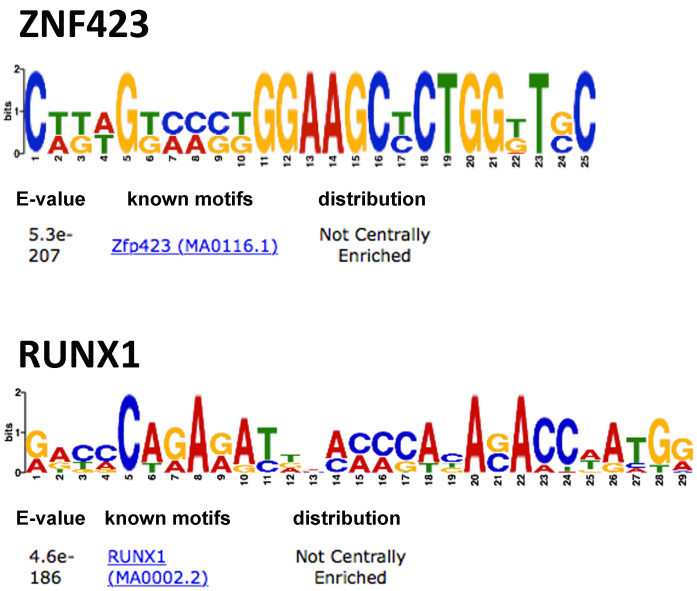

Figure 20: Most significantly enriched motifs of rat p27 ChIP-Seq experiments obtained by using the MEME-ChIP Suite. Consensus binding motifs for ZNF423 and RUNX1 could be identified as most significantly enriched sequences in rat p27 ChIP-Seq samples normalized against binding motifs for the input sample.

Among ZNF423 and RUNX1, all significantly enriched motifs analyzed by the MEME Suite are displayed in Table 15. Significantly enriched genes are *Zfp423, RUNX1, HNF4A/Rxra/Esrrb, Spdef, Bhlhb2, Tcfe2a/Znf238, NFATC2/NFATC1, TBX15/TBX1/TBX5, Nkx1, TFCP2, Sox8, Myc/MAX, Ascl2/Tcf3/Tcf12, Runx3/Runx2, Foxl1, TBX21, SPDEF, MEF2B/MEF2D/MEF2C, MLXIPL/MLX/SREBF2* and *MZF1/Crx*. Some sequences are closely related to the binding site of differente TFs and shown together for the same motif.

Table 15: Significantly enriched TF binding sites in p27 ChIP-Seq adrenomedullary rat samples analyzed by the MEME Suite. For some enriched sequences (motifs) more than one gene could be identified as related to the identified motifs.

Gene Symbol	E-value	Gene Symbol	E-value
Zfp423	5.3 e-207	Sox8	7.6 e-7
RUNX1	4.6 e-186	Myc/MAX	1.2 e-6
HNF4A/Rxra/Esrrb	6.5 e-169	Ascl2/Tcf3/Tcf12	1.4 e-5
Spdef	1.4 -146	Runx3/Runx2	1.4 e-5
Bhlhb2	2.7 e-18	Foxl1	3.2 e-5
Tcfe2a/Znf238	1.8 e-16	TBX21	8 e-5
NFATC2/NFATC1	9.2 e-12	SPDEF	6.4 e-4
TBX15/TBX1/TBX5	2 e-11	MEF2B/MEF2D/MEF2C	2 e-3
Nkx1	1.7 e-7	MLXIPL/MLX/SREBF2	4.3 e-3
TFCP2	3.2 e-7	MZF1/Crx	2.5 e-2

When analysis of the data using the MEME Suite was done, we identified the overrepresented TF binding sites in the rat data set after normalization of the two p27 ChIP-Seq replicates against the input sequences. The TF binding site overrepresentation analysis uses pre-defined binding site matrices from the MatBase/MatInspector library provided by the Genomatix Genome Analyzer. The list we obtained comprised the TF families that were significantly over-represented/enriched in the rat p27 ChIP-Seq data set, and were sorted by their Z-scores for overrepresentation over the genome. In total, 66 binding site families could be found as overrepresented in the p27 ChIP-Seq data set of rat adrenomedullary tissues (Table 16). The overrepresentation of V$HAML, the binding site family for RUNX1, is 1.07 fold over the genomic background and 1.15 fold over the promoter background compared to the database for *Rattus norvegicus* provided by Genomatix. V$HAML is on

position 38 out of 66 regarding its significant promoter overrepresentation. The overrepresentation for V$OAZF, the binding site family for ZNF423, is 1.61 fold over the genomic background and 0.96 fold over the promoter background. It is shown, that V$OAZF is on position 51 out of 66 regarding its significant promoter overrepresentation. Although the binding sites for ZNF423 and RUNX1 were not identified as the most overrepresented by the Genomatix tool, they were listed as significantly overrepresented. The results of the analysis of the ChIP-Seq data set done with both MEME Suite and Genomatix Suite confirmed that using this approach on adrenomedullary tissues allows the reproducible detection of specific TF binding sites, suggesting that p27-containing complexes bind DNA at defined sequences, reflecting the p27 DNA-binding specificity.

Table 16: List of overrepresented TF binding sites identified based on the analysis of rat p27 ChIP-Seq data by Genomatix. The TF families for Znf423 (V$OAZF) and Runx1 (V$HAML) were highlighted in grey. Both TF families are overrepresented in the rat p27 ChIP samples when compared with the genome background. The MatInspector matrices use different prefixes to differ between seven groups (V$, I$, P$, F$, N$, B$ and O$). The prefix V$ stands for vertebrates, whereas the prefix O$ is a synonym for general core promoter elements.

TF Families	Overrep. genome	Z-score genome	Overrep. promoter	Z-score promoter
O$TF3C	7.79	5.91	6.56	5.26
V$GCF2	26.8	41.69	5.65	16.35
V$CHOP	2.25	1.73	3.3	2.73
V$NDPK	6.85	19.22	3.22	10.62
V$BEDF	8.75	22.52	2.79	9.19
V$MAZF	6.02	17.93	2.68	8.97
V$AARF	1.75	0.97	2.42	1.69
V$CSEN	2.75	3.73	2.35	3.09
V$PLAG	3.94	13.55	2.16	7.23
V$PROX	2.02	2.49	2.03	2.51
V$CTCF	5.93	17.04	2.03	6.05
V$THAP	1.64	1.07	1.78	1.29
V$TAIP	1.75	2.38	1.76	2.43
V$EREF	1.95	2.73	1.62	1.92
V$ZF03	1.24	0.77	1.6	1.88
V$SP1F	3.91	13.56	1.58	4.21
V$BZIP	1.16	0.42	1.57	1.54
V$RU49	1.56	1.51	1.56	1.5
V$MEF3	1.59	2.06	1.53	1.89
V$RUSH	1.03	0.15	1.52	2.79
V$HMTB	1.06	0.12	1.5	1.58
V$CAAT	1.29	1.66	1.5	2.73
V$HICF	1.61	1.71	1.49	1.4
V$MYT1	1.11	0.76	1.44	2.79
V$PBXC	1.29	1.41	1.43	2.02
V$AP1F	1.18	0.86	1.38	1.77
V$TEAF	1.16	0.47	1.35	1.1
V$HEAT	1.11	0.79	1.3	2.12
V$PAX1	1.41	0.39	1.29	0.23
V$ZF02	2.6	9	1.29	2.28
V$EGRF	3.01	10.66	1.29	2.28
V$BTBF	1.17	0.16	1.26	0.33
V$SNAI	1.71	0.93	1.24	0.23
V$AP4R	1.82	1.91	1.24	0.58
V$ZF06	1.44	0.65	1.22	0.27
V$DICE	1.34	0.81	1.2	0.43
V$YBXF	1.37	0.76	1.16	0.27
V$HAML	1.07	0.22	1.15	0.53
V$KLFS	1.82	6.51	1.14	1.41
V$FXRE	1.23	0.34	1.13	0.12
V$PTF1	1.22	0.37	1.13	0.17
V$PEG3	1.31	0.56	1.13	0.16
V$NFKB	1.4	1.62	1.13	0.5
V$NF1F	1.17	0.59	1.09	0.26
V$RORA	1.02	0.03	1.07	0.28
V$ETSF	1.15	1.34	1.05	0.43
V$RXRF	1.09	0.76	1.03	0.23
V$ZFHX	1.07	0.19	1.01	-0.07
V$DMTF	1.56	1.29	1.01	-0.1
V$XBBF	1.07	0.48	0.98	-0.19
V$OAZF	1.61	1.13	0.96	-0.3
V$GCMF	1.11	0.48	0.93	-0.49
V$ZBED	1.37	0.61	0.88	-0.51
V$ZF11	1.34	0.62	0.88	-0.53
V$STAF	1.28	0.9	0.88	-0.65
V$MYOD	1.04	0.16	0.83	-1.19
V$ZF01	1.14	0.11	0.81	-0.7
V$ZICF	1.42	0.92	0.76	-1.01
V$HESF	1.16	0.56	0.72	-1.56
V$EBOX	1.06	0.18	0.7	-1.88
V$ZF57	1.59	0.77	0.68	-1.06
V$NOLF	1.05	0.01	0.66	-1.55
V$NRSF	1.07	0.11	0.61	-1.93
V$AP2F	1.33	1.08	0.61	-2.24
O$MTEN	1.17	0.05	0.27	-2.98

Figure 20 shows the TFBS for ZNF423 (E value: 5.3 e-207) and RUNX1 (E-value: 4.6 e-186), which could be identified by MEME as most enriched in p27 ChIP-Seq samples performed in rat adrenomedullary cells. Furthermore, the motifs could be observed as exclusively for *Znf423* and *Runx1*. Additionally, by Genomatix, both ZNF423 and RUNX1 could be identified as overrepresented in the p27 ChIP-Seq dataset (Table 16). Therefore, we decided to focus further studies on these two candidates.

3.2 Expression and interaction studies of p27 with Runx1 and Znf423 in adrenal cells

We checked different human and rat tissues for their *Runx1* and *Znf423* mRNA expression levels. When WT rat adrenal tissue samples were compared with adrenal tissues from homozygous p27-Mut MENX rats (with PCC) by qRT-PCR, *Runx1* (3.4 fold) and *Znf423* (11 fold) expression levels were increased in the mutant animals (Figure 21 A). Western blotting analyses showed that Znf423 and Runx1 were equally expressed in WT and mutant animals (Figure 21 B). In case of human PCC samples, it has been reported that p27 levels are reduced in 50.6 % of cases (Pellegata *et al*., 2007). The *RUNX1* mRNA levels were -50 % reduced in tumors as well. In contrast, *ZNF423* expression levels were increased 1.6 fold in tumor samples compared with human adrenal tissue samples (Figure 21 C). Furthermore, all available adrenal PCC cell lines (PC12, MPC, MTT) showed a relatively high level of Znf423 and Runx1 proteins (Figure 21 D).

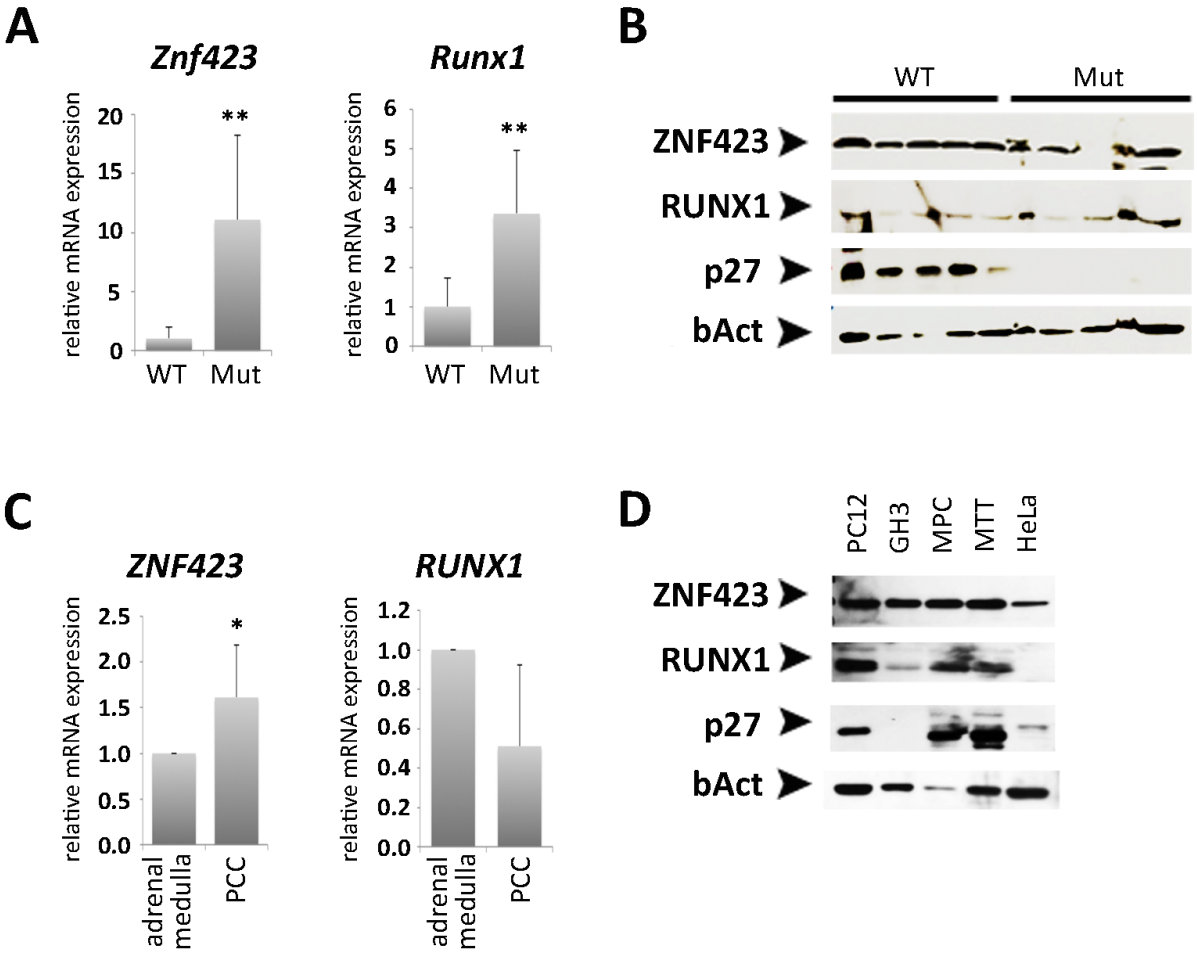

Figure 21: Expression studies of *Znf423/ZNF423* and *Runx1/RUNX1* in rat and human tissue samples and different cell lines. (A) In rat adrenomedullary tissues - WT vs. p27 mutants (Mut) - *Znf423* and *Runx1* showed a significantly increased mRNA expression level in p27 mutated tissues. [WT: n=6, Mut: n=10; **: p<0.01 by Fisher´s exact test] **(B)** WT and p27 mutant rat adrenomedullary tissues were loaded onto a western blot gel and analyzed for the expression levels of ZNF423, RUNX1 and p27. No changes in the expression levels of ZNF423 and RUNX1 were detected in p27-mutated rats (Mut) in comparison with WT rat tissues (WT). In contrast, p27 levels could be shown to be reduced in mutant rats due to the causative p27 mutation. β-Actin (bAct) was used as loading control. **(C)** At mRNA level, *ZNF423* and *RUNX1* were analyzed for their expression in healthy and tumorous adrenal tissues of human individuals. *ZNF423* showed an overexpression level in human tumor tissues, whereas *RUNX1* showed a not significantly reduced expression level in tumors. [adrenal medulla: n=2, PCC: n=8; *: p<0.05 by Fisher´s exact test] **(D)** ZNF423, RUNX1 and p27 were detected in different cell lines by western blotting. All PCC cell lines PC12, MPC and MTT could be shown to express ZNF234 and RUNX1 at detectable level. As loading control the house keeping gene β-Actin (bAct) was used. [ZNF423: 1:2000, 100 kDa; RUNX1: 1:1000, 49 kDa; p27: 1:500, 27 kDa; bAct: 1:1000, 42 kDa]

Validating the interaction of p27 with the identified candidate TFs ZNF423 and RUNX1 is important to support the hypothesis that they form a complex with transcriptional regulatory ability. Thus, we first looked for a possible co-localization of p27 and the TFs ZNF423 and RUNX1 given that if they interact they have to co-localize in cells and tissues.

Therefore, co-IF was performed using an anti-p27 antibody together with an anti-Runx1 or anti-Znf423 antibody in rat and human adrenomedullary tissues. The two primary antibodies were chosen from different species to allow us to distinguish the signal of each protein thanks to specific fluorophore-labeled secondary antibodies. In formalin-fixed paraffin embedded (FFPE) PC12 cells and FFPE MPC cells, p27 and ZNF423 or RUNX1 could be observed as co-localized in the cell nuclei (Figure 22). For this study FFPE cells were used to facilitate the reproducibility of stainings since these cells could be considered as identical to each other regarding cell cycle and replication. Furthermore, the use of FFPE blocks is time-saving since the cells do not need to be expanded and fixed again before performing the stainings.

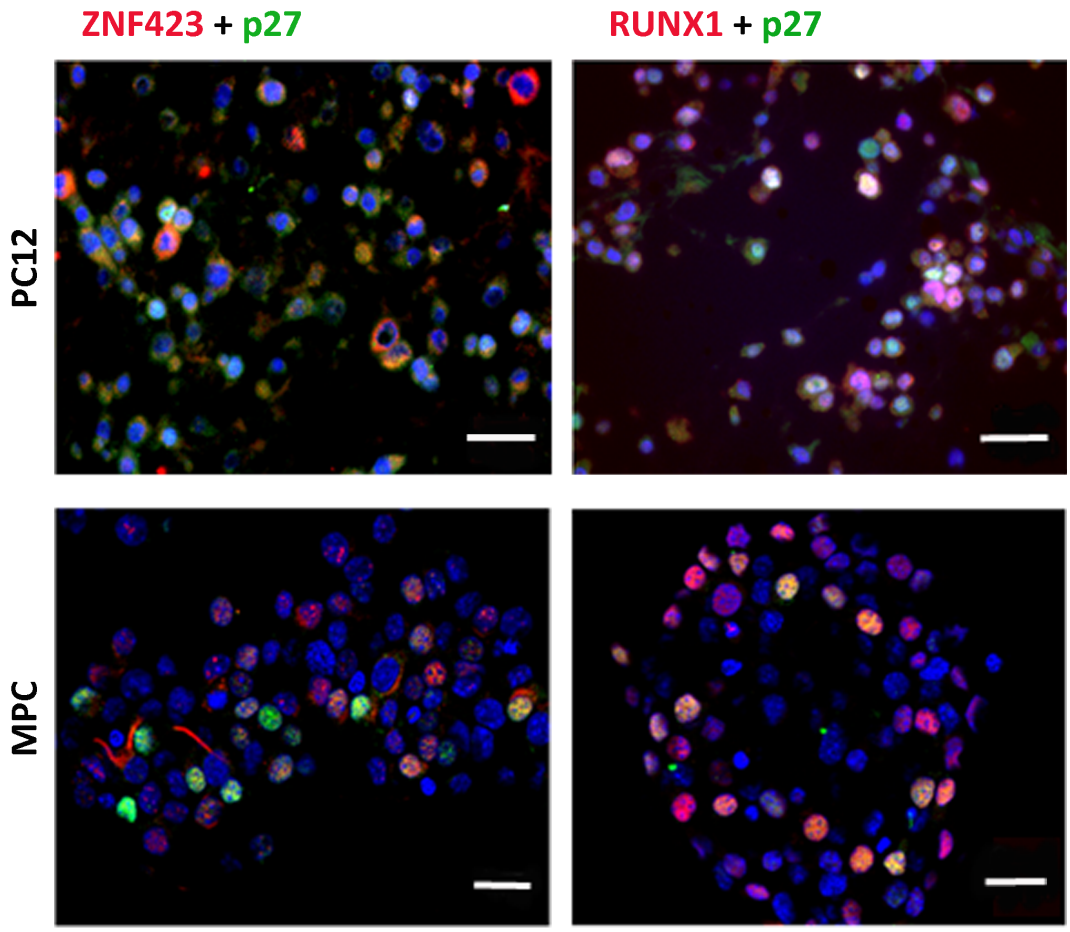

Figure 22: Co-IF experiments in PC12 and MPC cells. In PC12 and MPC cells, ZNF423 and RUNX1 (red) could be observed in cell nuclei of some cells together with p27 (green). This indicated a co-localization of ZNF423 and RUNX1 with p27 in these cells. Representative pictures of four technical replicates for each condition. [scale bar: 20 µm; ZNF423: 1:500; RUNX1: 1:1000; p27: 1:400]

FFPE tissues for rat and human adrenal medulla were also stained with the identical antibodies. Similar to the cell lines, human adrenomedullary cells showed a co-localization of p27 and ZNF423 or RUNX1, as well (Figure 23 A). In case of rat adrenal tissues, ZNF423 could be observed to be expressed in cell nuclei together with p27. In contrast, RUNX1 IF showed a strong unspecific cytoplasmic staining (Figure 23 B). Since RUNX1 is a TF, it is expected to be located in the cell nuclei. In other rat tissues (lung and colon), RUNX1 was localized in the cell nuclei as expected, which excluded a species dependent issue. Rather, this suggests that it is an adrenal-specific issue: for reasons we cannot explain the antibody gives unspecific signal only in this tissue.

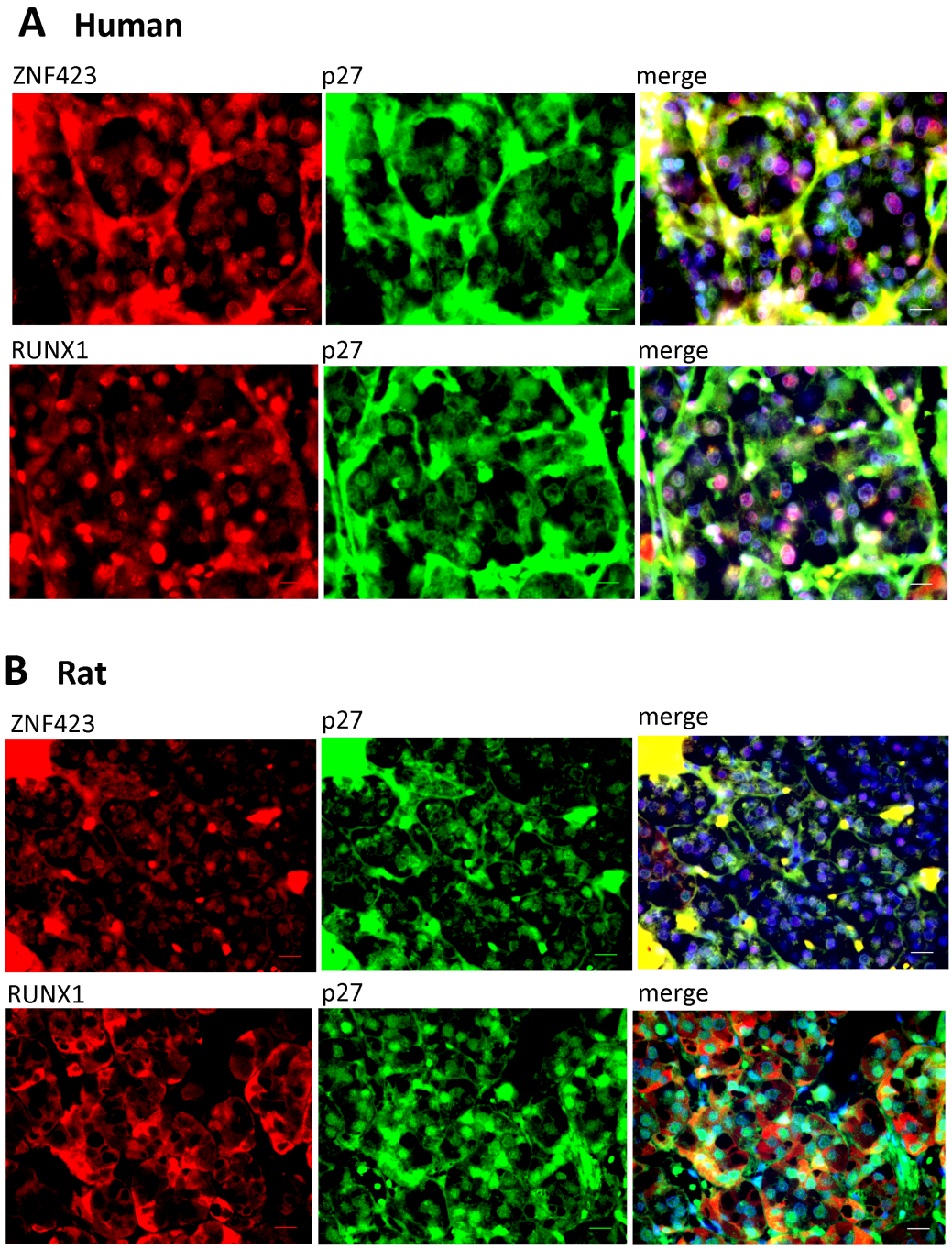

Figure 23: Co-IF of human and rat adrenomedullary tissues. (A) In human adrenomedullary tissues (n=4), ZNF423 and RUNX1 co-localized with p27 in cell nuclei. **(B)** In rat adrenomedullary tissues (n=6), the staining of ZNF423 could be observed in cell nuclei, although it was faint. In contrast, the available anti-Runx1 antibody showed an unspecific staining in the cytoplasm of adrenomedullary cells. Therefore, no conclusion could be made regarding co-localization of RUNX1 and p27 in the rat tissues. [scale bar: 10 µm; ZNF423: 1:500; RUNX1: 1:1000; p27: 1:400]

Moreover, cell fractionation of PC12 and MPC cells and adrenomedullary WT rat tissues showed that the three proteins (p27, ZNF423 and RUNX1) are present in the euchromatin and/or the nuclear matrix fraction (Figure 24). p27 could not be detected in the cell nuclei

fraction of WT rat tissues - probably because p27 is too diluted in comparison to the concentrated nuclear matrix fraction. This approach confirmed the nuclear localization of p27, ZNF423 and RUNX1, which was expected based on their cellular functions.

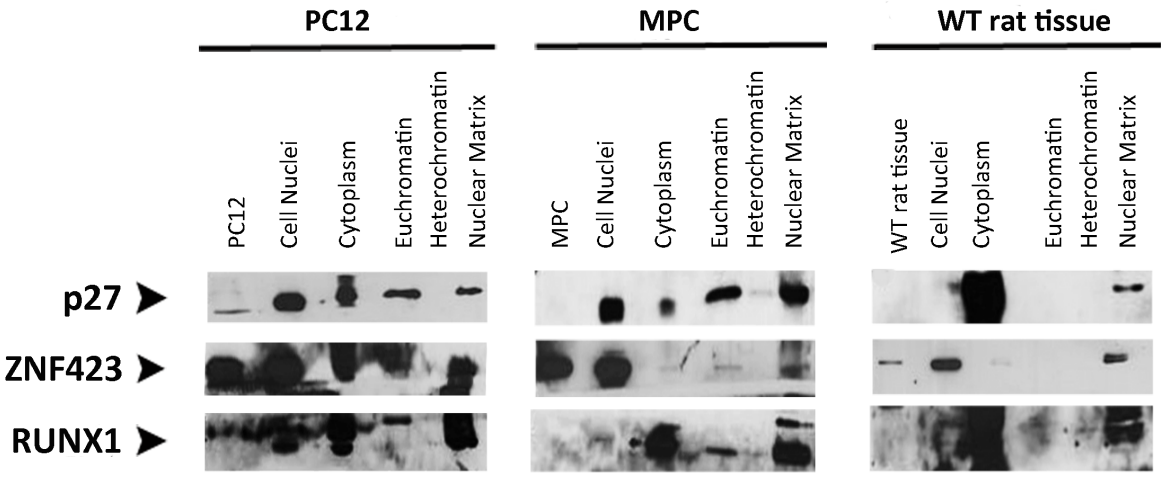

Figure 24: Fractionation of PC12 cells, MPC cells and WT rat adrenomedullary tissues to validate localization of p27, ZNF423 and RUNX1. p27 and ZNF423 could be observed as localized in the nuclear matrix and euchromatin of PC12 and MPC cells. RUNX1 could be detected in the nuclear matrix fraction of PC12 cells. In MPC cells, RUNX1 is expressed in the euchromatin fraction, as well. In WT rat adrenomedullary tissue (n=3), p27, ZNF423 and RUNX1 could be shown to be expressed in the nuclear matrix fraction. [p27: 1:500, 27 kDa; ZNF423: 1:2000, 100 kDa; RUNX1: 1:1000, 49 kDa]

In addition to the co-localization of p27 with ZNF423 and RUNX1, we performed co-IP experiments to verify the putative interaction of these proteins. IP was conducted with an anti-p27 antibody on lysates of PC12 cells and adrenomedullary tissues of WT rats. The western blotting membrane was probed with antibodies against ZNF423 and RUNX1. For ZNF423, no signal was detectable, which indicates no direct interaction of p27 with ZNF423 in these cells/tissues, whereas we could detect RUNX1. In PC12 cells RUNX1 was pulled-down together with endogenous p27 (cells were transfected with a GFP-containing plasmid as control) and also with exogenous overexpressed p27 (Figure 25). To overexpress p27, PC12 cells were transfected with a plasmid containing the human p27 coding sequence with a C-terminal HA-tag. To confirm these findings, reciprocal experiments were performed: IP was done using anti-Runx1 or anti-Znf423 antibodies and the pulled-down p27 was detected by western blotting. In Runx1-IP samples, a pull-down of p27 could be detected by western blotting (Figure 25), indicating a physiological interaction of p27 and RUNX1 in PC12 cells and adrenomedullary rat tissues. Unfortunately, ZNF423 by itself could not be detected by

western blotting after the ZNF423-IP in PC12 cells (data not shown). After performing additional test IPs, we concluded that the available anti-Znf423 antibodies (Znf423, Merck; OAZ (E-6), Santa Cruz Biotechnology) are probably not suitable for IP experiments in PC12 cells and adrenomedullary rat tissues.

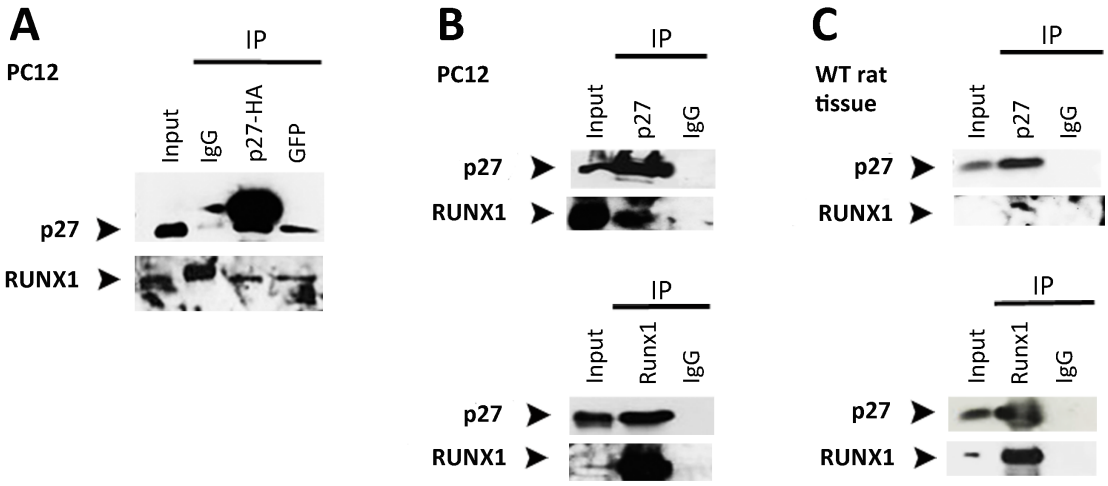

Figure 25: Co-IP experiments of p27 and RUNX1 in PC12 cells and WT rat adrenomedullary tissues. (A and B) In PC12 cells, RUNX1 could be observed to interact with endogenous p27 and with exogenously expressed p27 (cells were transfected with an overexpression plasmid containing p27 tagged with an HA-tag). **(C)** In adrenomedullary tissues of WT rats (n=3), RUNX1 could be shown to be pulled-down together with p27, and *vice versa*. [p27: 1:500, 27 kDa; RUNX1: 1:1000, 49 kDa]

Furthermore, the interaction of p27 and RUNX1 was confirmed by proximity ligation assay (PLA) in FFPE PC12 cells. This method detects protein-protein interactions *in situ* by using two antibodies, which recognize and bind to each of the two potentially interacting targets. These antibodies are conjugated to a matched pair of short single-stranded oligonucleotides. If the two respective targets interact, and hence remain in very close proximity, the oligonucleotide probes will hybridize and ligate with two additional oligos to form a continuous circular DNA structure. The DNA polymerase will amplify these circular molecules through simple, reliable rolling-circle amplification. The result is a highly amplified circular DNA molecule that can be detected by standard fluorescent methods, and that acts as a quantitative marker of interaction between the two proteins. The individual p27 and RUNX1 proteins are located in the nuclei of PC12 cells (Figure 22). Following PLA, a fluorescent signal was detected in the cell nuclei, thereby demonstrating that there is a close proximity between p27 and RUNX1 (Figure 26 A). As negative control, the PLA was performed with only one of the two antibodies (Figure 26 B) or in cells with siRNA-mediated knockdown of *Cdkn1b*

or *Runx1* (Figure 26 C). This approach indirectly proves the interaction of p27 and RUNX1 in PC12 cells. Since no signal was detected in the PLA samples when using an anti-p27 and an anti-Znf423 antibody (data not shown), we concluded that either the available anti-Znf423 antibodies did not work for PLA or that there is only a co-localization of p27 and Znf423 in PC12 cell nuclei (Figure 22), but no direct interaction, hence no close proximity, between these two proteins.

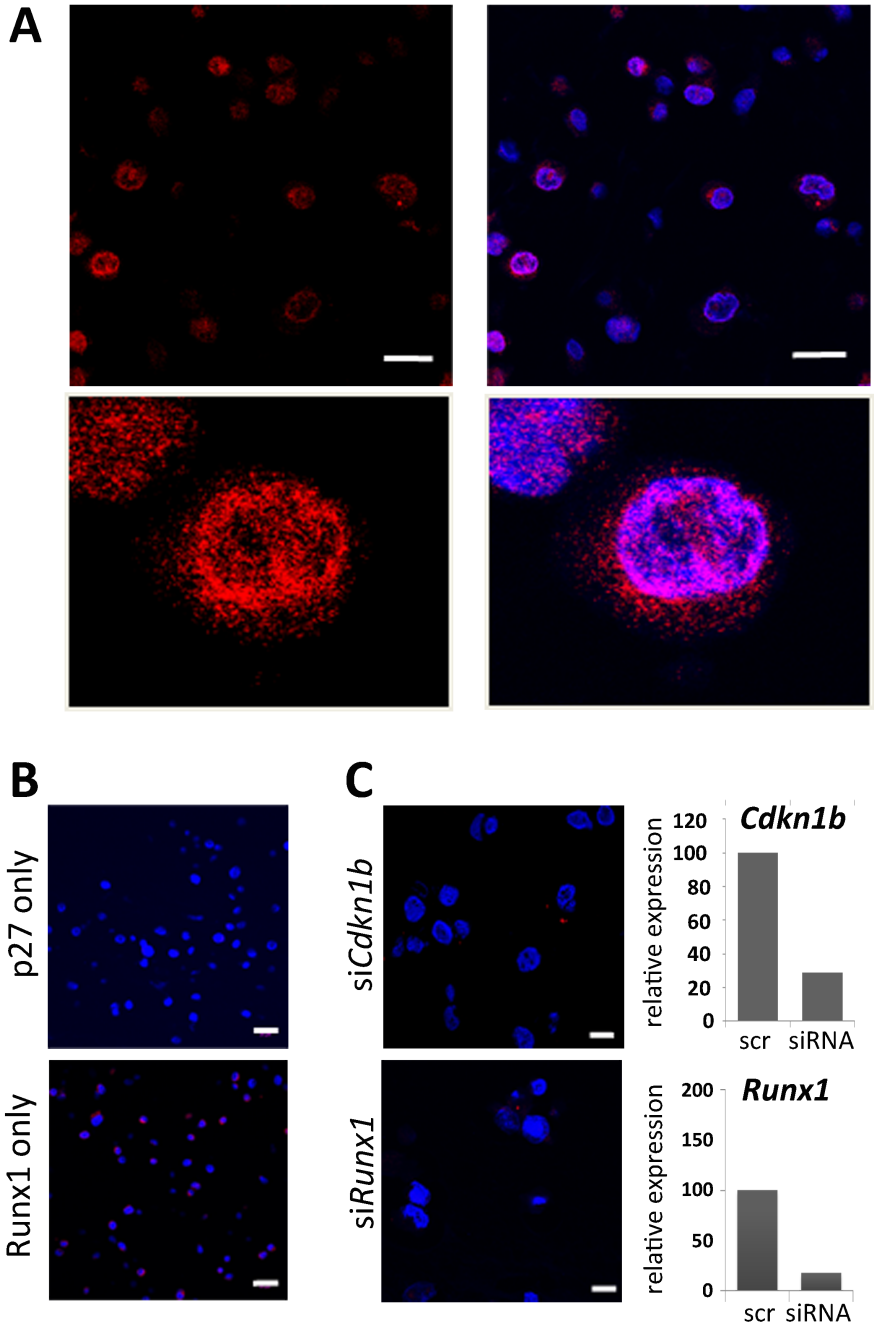

Figure 26: PLA of PC12 cells with anti-p27 and anti-Runx1 antibodies. (A) Anti-p27 [$p27^{Kip1}$ (BD Transduction Laboratories™) 1:400] and anti-Runx1 [Runx1 (Abcam) 1:1000] antibodies were used for PLA experiments in PC12 cells. A positive signal (red) could be detected due to the close proximity

of p27 and RUNX1 in PC12 cells. **(B)** As negative control, PLA was performed with only one primary antibody. Neither the anti-p27 alone (p27 only) nor the anti-Runx1 antibody alone (Runx1 only) gave a detectable signal indicating high specificity of the antibodies. **(C)** As further negative control, PC12 cells were transfected with siRNA against *Cdkn1b* (p27) and *Runx1* before performing PLA experiments. There was no signal observed in PC12 cells upon siRNA-mediated gene knock down. The right panels show the reduced mRNA level of *Cdkn1b* and *Runx1* due to siRNA treatment. [scale bars: 20 µm; scr: scrambled negative transfection control]

3.3 RUNX1 recruits p27 to specific target gene promoters

3.3.1 Identification of RUNX1 target genes by investigating the correlation of p27 ChIP-Seq data and rat adrenal tissue microarray data

Previous studies conducted in our lab included gene expression mRNA microarrays of adrenomedullary tissues from eight homozygous mutant MENX rats (with adrenal lesions), which were compared with pooled samples from the adrenal medulla of WT rats (Molatore *et al*., 2010). Further analyses of the p27 ChIP-Seq data in correlation with adrenal tissue microarray data were done in collaboration with Dr. Juan Higareda Almaraz from the Institute of Diabetes and Cancer (IDC, HMGU, Germany). More precisely, in the microarray data, we looked for the level of expression of the target genes of RUNX1 in tumor *versus* WT adrenal. Moreover, we checked the expression level of the candidate TFs that we obtained by ChIP-Seq as potential partners of p27. Then, gene expression data were correlated with ChIP-Seq results. Specifically, genes differentially expressed between tumor and WT adrenal were filtered based on their proximity to a p27 ChIP-Seq peak. These analyses result in the regulatory network generated by Juan Higareda Almaraz and illustrated in Figure 27.

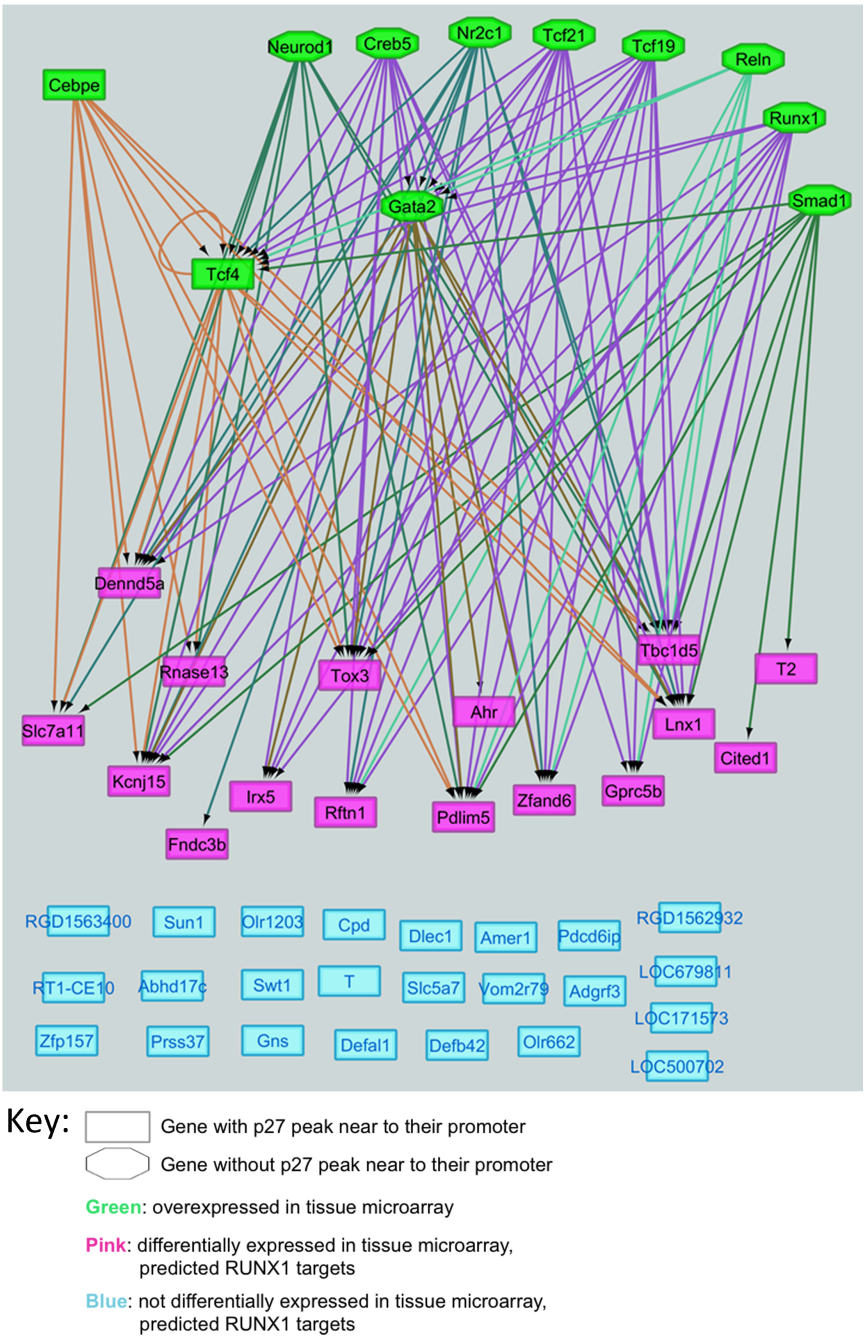

Figure 27: Regulatory network of the correlation study of rat p27 ChIP-Seq data with rat adrenal tissue microarray data. As indicated in the figure key, all genes in rectangles have p27 ChIP peaks near to their promoters and are differentially expressed in adrenomedullary tissue microarrays. Furthermore, the green (*Tcf4* and *Gata2*) and pink genes are predicted RUNX1 target genes and therefore chosen for further literature research and validation studies. [generated by Juan Higareda Almaraz (IDC, HMGU, Germany)]

Genes shown in rectangles are those with p27 ChIP-Seq peaks close to their promoters (1 kb up- or down-stream): *Cebpe, Tcf4, Dennd5a, Slc7a11, Rnas13, Kcnj15, Fdc3b, Irx5, Tox3, Rftn1, Ahr, Pdlim5, Zfand6, Gprc5b, Lnx1, Tbc1d5, T2* and *Cited1*; while those in octagons

showed no detectable peaks: *Neurod1, Creb5, Gata2, Nr2c1, Tcf21, Tcf19, Reln* and *Smad1*. The different colors are based on the differential expression status of the genes, based on the microarray data and on the transcriptional activity of these genes. Green genes (*Cebpe, Tcf4, Neurod1, Creb5, Gata2, Nr2c1, Tcf21, Tcf19, Reln* and *Smad1*) are TFs overexpressed in PCC tumors based on the tissue microarray data. Genes in pink (*Dennd5a, Slc7a11, Rnas13, Kcnj15, Fdc3b, Irx5, Tox3, Rftn1, Ahr, Pdlim5, Zfand6, Gprc5b, Lnx1, Tbc1d5, T2* and *Cited1*) are targets of the differentially expressed TFs, which are differentially expressed in the tissue microarray data, and have p27 peaks close to their promoters. The regulatory relationship between the genes is based on actual experimental evidence downloaded Juan Higareda Almaraz from the ENCODE project, Homer and TRANSFACT database. These analyses detected only eleven genes, which could be identified as differentially expressed in tumor tissues, as having p27 ChIP-Seq peaks near their promoters and as being regulated by RUNX1 (predicted RUNX1 targets): *Tcf4, Dennd5a, Kcnj15, Irx5, Tox3, Rtftn1, Pdlim5, Gprc5b, Lnx1* and *Tbc1d5*. It is important to mention, that there are three TFs that bind DNA at a consensus sequence/binding site similar to that of RUNX1 (namely CREB5, TCF21, TCF19). Based on the biological function of the eleven candidate genes and their putative link to RUNX1, we have chosen *Tcf4* as the most promising RUNX1 target gene for further validation in adrenomedullary cells. TCF4 was shown to be involved in AML and is known to act in a HDAC-dependent manner, like RUNX1 (Cheng *et al*., 2016; Zhang *et al*., 2008). *Gata2* was more highly expressed in the PCC *versus* WT medulla. Therefore, we decided to include this gene in further studies.

3.3.2 Identification of RUNX1/p27 target genes based on mRNA microarray data of PC12 cells with knockdown of *Runx1* or *Cdkn1b*

To determine the genes transcriptionally regulated depending on the presence of p27 or RUNX1, PC12 cells were transfected with siRNA against *Cdkn1b* or *Runx1* to reduce the expression of the proteins. The cells were transfected (electroporated) with 1 µg of siRNA using the Nucleofector™ from Lonza. The siRNAs were generated by siTOOLs Biotech based on the siPOOLs Technology, described as highly complex and defined pools of 30 individual siRNAs against the same gene. This approach dilutes the off-target effects of each siRNA molecule and increases on-target specificity. Furthermore, these siPOOLs should generate more robust and reliable knockdown results given that each gene is targeted by multiple

siRNAs. 24 h post-transfection, the cells were collected and RNA was extracted for further microarray-based transcriptome profiling. To verify the efficacy of gene silencing, the expression levels of *Cdkn1b* (reduction of -84 %) and *Runx1* (reduction of -81 %) were measured by qRT-PCR (Figure 28). GeneChip™ Rat Gene 1.0 ST arrays were used (Affymetrix, now part of Thermo Fisher Scientific). The Rat Gene 1.0 ST arrays are a combination of Affymetrix' Whole Transcript Assays and high-density arrays, which provide a more complete and more accurate picture of overall gene expression. The rat gene 1.0 ST arrays contain hundreds of thousands of probes designed to cover every exon of every transcript present on the array. The high transcript coverage (median 22 probes per gene) yields accurate detection for genome-wide expression changes (Okoniewski *et al*., 2007).

In collaboration with Dr. Martin Irmler from the Institute of Experimental Genetics (IEG, HMGU, Germany) the quality of the RNA samples was assessed, the arrays were run and statistical analyses were conducted. Two replicates per condition were prepared in our lab: PC12 cells transfected with si*Cdkn1b*, PC12 cells transfected with si*Runx1* and PC12 cells transfected with non-targeting scrambled siRNA (Figure 28). The quality of the RNA was determined by a 2100 Bioanalyzer Instrument (Agilent Genomics) by Martin Irmler. The Bioanalyzer software generates an electropherogram and gel-like image, which provides a better assessment of RNA quality by showing a detailed picture of the size distribution of RNA fragments. Additionally, the Bioanalyzer displays results, such as sample concentrations, the ribosomal ratios and the RNA integrity numbers (RIN values). The RIN software algorithm allows the classification of total eukaryotic RNA, based on a numbering system from 1 to 10, with 1 being the most degraded profile and 10 being the most intact profile; this software takes the entire electrophoretic trace into account. The RIN values for all prepared samples laid between 9.9 and 10, which indicated intact total RNA. In term of quality control, the cluster dendogram and PCA (principal component analysis) analysis showed good quality of samples and accordance between biological replicates (Figure 28).

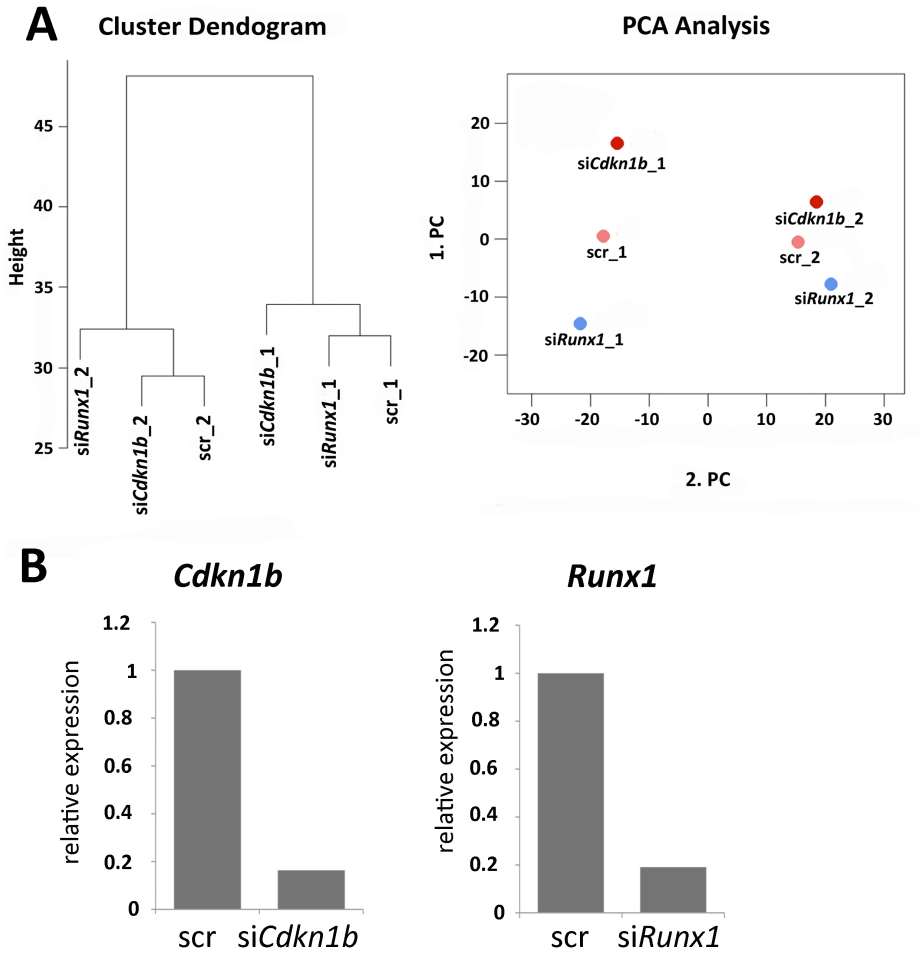

Figure 28: Quality control of microarray samples of PC12 cells treated with siRNA against *Cdkn1b* or *Runx1*. (A) The cluster dendogram displayed the samples according to replicates. The PCA analysis visualized the sample pattern of all conditions and replicates. **(B)** qRT-PCR analyses proved the knockdown of *Cdkn1b* (-84 %) and *Runx1* (-81 %) in PC12 samples. [scr: scrambled negative control; PCA: principal component analysis; PC: principal components]

After the microarrays were run, the siRNA samples were normalized to the scrambled control sample, and relative expression levels of all detected genes were obtained by Martin Irmler. This analysis disclosed several genes differentially expressed among samples. In Table 17, we compared both data sets (si*Cdkn1b* and si*Runx1*) and reported genes concordantly up- or down-regulated upon knockdown of *Cdkn1b* or *Runx1*. Based on the hypothesis that p27 is a transcriptional repressor, as it was demonstrated by Pippa *et al*. (2012) in MEF cells, we selected potential target genes that were more highly expressed when *Cdkn1b* or *Runx1* levels were reduced. Using a cut-off of 1.58 fold overexpression in the si*Runx1* data set, the genes *Zfp563, Apoc4, Ralgapa2, Maneal* and *Serpini1* were pointed out.

Table 17: PC12 mRNA microarray data after si*Cdkn1b* and si*Runx1* transfection. The displayed genes were selected for their differential expression level in PC12 cells after *Cdkn1b* and *Runx1* knockdown (in comparison with the scrambled negative control). Genes in blue are significantly overexpressed, whereas genes in red are down-regulated. General criteria for selecting genes were a fold change of more than 1.3 fold in comparison with the scrambled control in both directions. Based on these criteria, the data set of PC12 si*Runx1* cells contained 523 genes and the data set of PC12 si*Cdkn1b* contained 488 genes. [scr: scrambled negative control, FC: fold change, Av: average]

siRunx1	Symbol	FC>1.3x, p<0.05, Av>16 (523)		sip27	Symbol	FC>1.3x, p<0.05, Av>16 (488)
	Mir23b	2.08			Mir23b	1.61
	Zfp563	1.53			Zfp563	1.53
	Apoc4	1.70			Apoc4	1.32
	Ralgapa2	1.65			Ralgapa2	1.45
	Maneal	1.58			Maneal	1.44
	Serpini1	1.58			Serpini1	1.37
	Kng1	1.53			Kng1	1.36
	Osbpl6	1.48			Osbpl6	1.49
	Qpctl	1.39			Qpctl	1.48
	Clec2g	1.41			Clec2g	1.47
	Gbp5	1.48			Gbp5	1.44
	Rftn2	1.32			Rftn2	1.44
	Zfp626	1.38			Zfp626	1.43
	Olr1425	1.40			Olr1425	1.43
	U2surp	1.34			U2surp	1.40
	Atad2b	1.33			Atad2b	1.39
	Wdr13	1.40			Wdr13	1.38
	Gsc2	1.32			Gsc2	1.34
	Swt1	1.34			Swt1	1.34
	Lacc1	1.34			Lacc1	1.33
	Chic2	1.32			Chic2	1.32
	Fam214b	-1.38			Fam214b	-1.52
	Iba57	-1.31			Iba57	-1.51
	Lgals2	-2.10			Lgals7	-1.57
	Adrb3	-2.02			Adrb3	-1.33
	Fdxacb1	-1.58			Fdxacb1	-1.51
	Tifa	-1.57			Tifa	-1.32
	Slc6a6	-1.50			Slc6a4	-1.42
	Prrx2	-1.52			Prrx1	-1.41
	Hmbox1	-1.50			Hmbox1	-1.32
	Gpr183	-1.43			Gpr183	-1.48

These genes were then investigated for their biological function and for the commercial availability of molecular tools, such as antibodies, qRT-PCR assays or siRNAs, necessary to perform further studies. *Ralgapa2* was excluded from the selected candidates since its function is reported as tumor suppressor gene in hepatocellular and bladder cancer (Kodama *et al*., 2016; Saito *et al*., 2013). Based on the microarray data of PC12 cells treated with si*Cdkn1b*, the *Ralgapa2* gene is overexpressed when p27 levels are reduced. Since we

knew that a reduced p27 level leads to tumor formation in adrenomedullary cells, the detection of this gene as overexpressed under these conditions did not fit with its presumed function as a tumor suppressor. The same issue applies to *Serpini1*, which is reported to be a tumor suppressor in gastric cancer (Yamanaka *et al*., 2012). For *Maneal*, no rat TaqMan™ assays are available and no studies about *Maneal* in association with p27 or cancer are published. More promising genes were *Znf563* and *Apoc4,* the two most overexpressed genes, and *Kng1*. Although there are no publications on *Znf563*, it was selected since it was the most overexpressed gene in the si*Cdkn1b* data set (1.53 fold). Following *Runx1* knockdown, the overexpression level of *Znf563* in PC12 cells was also increased by 1.53 fold. *Apoc4* was the most up-regulated gene in the si*Runx1* data set (1.7 fold) and showed a 1.32 fold increase after *Cdkn1b* knockdown. In addition, it was already known to be involved in colorectal and breast cancer development (Kheirelseid *et al*., 2010; Philley *et al*., 2017).

Since GO term analyses display a functional profile of data sets to better understand underlying biological processes, we performed GO term enrichment analyses, which showed dysregulated genes belonging to certain GO groups ('diseases and disorders', 'molecular and cellular functions' and 'physiological system development and functions') (Figure 29). Common categories within these GO groups of si*Cdkn1b*-transfected or si*Runx1*-transfected *versus* scrambled siRNA-transfected control PC12 cells are 'cardiovascular disease' (group 'diseases and disorders'), 'cell-to-cell signaling', 'cell morphology' and 'cellular development' (group 'molecular and cellular functions'), and 'embryonic development' and 'organismal development' (group 'physiological system development and functions') (Figure 29). So, the knockdown of *Cdkn1b* or *Runx1* changes the expression of genes belonging to different functional categories. However, some degree of overlap was observed, supporting the findings that there are genes commonly regulated by the two proteins.

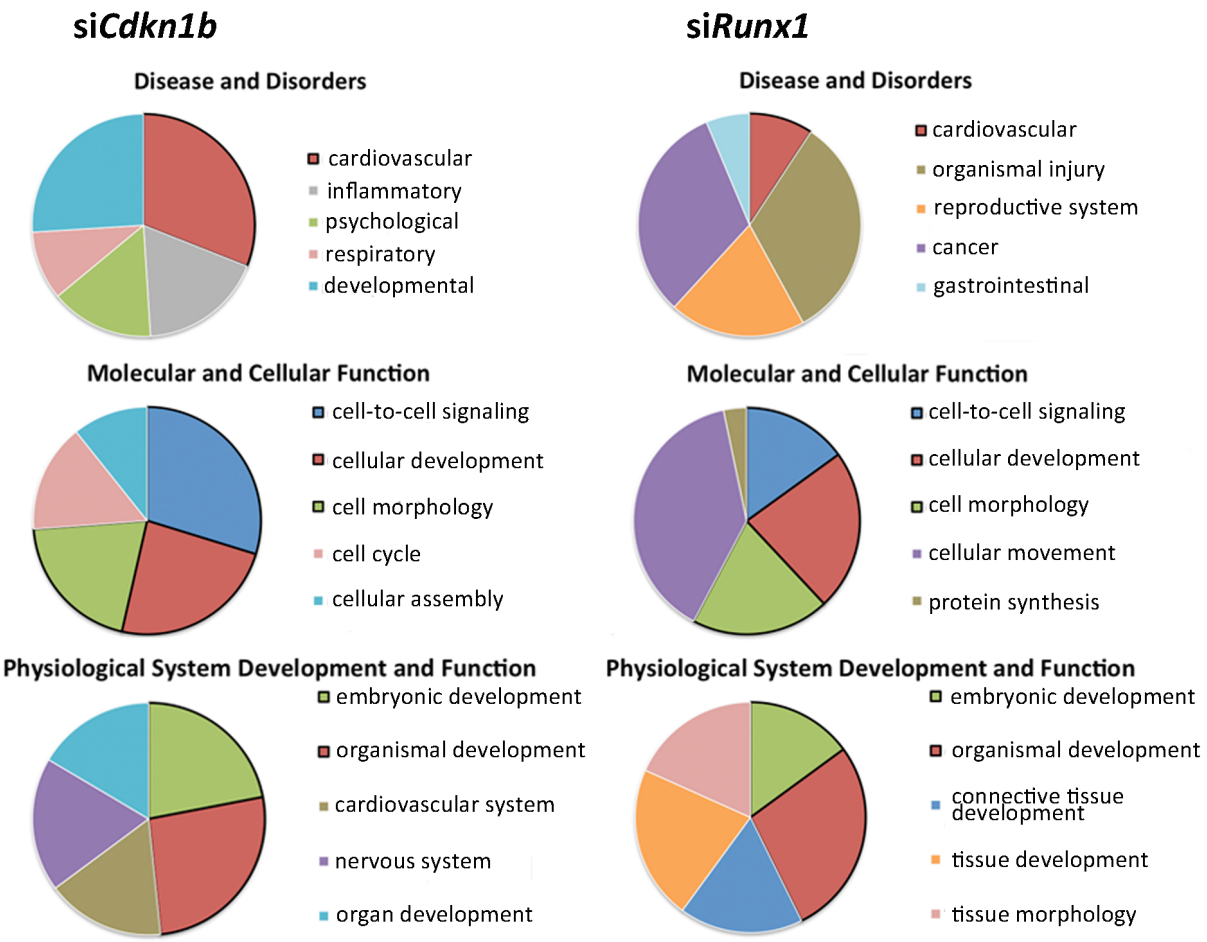

Figure 29: GO term analysis of microarray studies of PC12 cells with *Cdkn1b* or *Runx1* knockdown. Reduced expression levels of *Cdkn1b* (left) or *Runx1* (right) in PC12 cells led to commonly enriched GO categories: 'cardiovascular disease' (red in the upper diagrams), 'cell-to-cell signaling' (blue in the middle diagrams), 'cellular development' (red in the middle diagrams), 'cell morphology' (green in the middle diagrams), 'embryonic development' (green in the lower diagrams) and 'organismal development' (red in the lower diagrams).

To get an impression of the effect of RUNX1 on functional cellular processes in correlation with p27, we performed a proliferation assay in PC12 cells. These cells showed a two-fold increase in proliferation following *Runx1* knockdown (≈80 %); the same could be seen in these cells after *Cdkn1b* knockdown (≈80 %) (Figure 30).

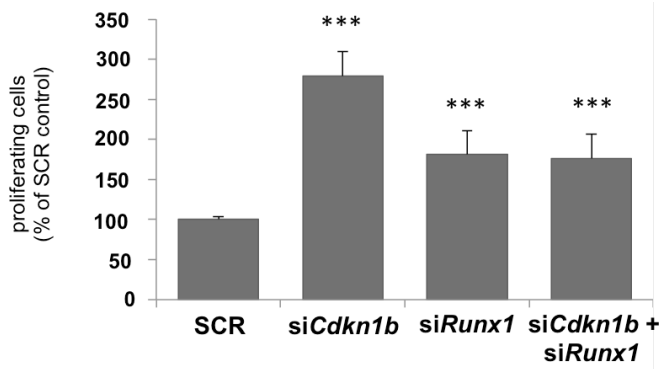

Figure 30: Proliferation (WST-1) assay of PC12 cells after *Cdkn1b* and *Runx1* knockdown. *Cdkn1b* (p27) and *Runx1* were down-regulated for around -80 % when compared with the scr control. This led to a 2.8 fold increase of PC12 cell proliferation following *Cdkn1b* knockdown and to an 2 fold increase after *Runx1* or *Cdkn1b*-*Runx1* double knockdown. [SCR: scrambled negative control; ***: p<0.001 by student´s t-test]

3.3.3 Validation of the putative p27/RUNX1 target genes *Znf563, Apoc4, Tcf4* and *Gata2*

By microarray analyses in PC12 cells following *Cdkn1b*- or *Runx1*-knockdown, *Znf563* and *Apoc4* were up-regulated (Table 17). The mRNA expression level of both genes was checked by qRT-PCR in human and rat adrenal tissues. Human PCC samples and unaffected adrenal tissue samples were compared and no change in expression of *ZNF563* was observed in tumor samples. In rats, the *Znf563* level is increased 1.9 fold in tumor *versus* WT tissues (Figure 31 A). *APOC4* mRNA expression showed an extremely reduced level (-95 %) in human PCC samples, whereas no changes in *Apoc4* levels could be observed in rat tumor samples (Figure 31 B). The expression of *Tcf4*/*TCF4* and *Gata2*/*GATA2* was also validated in human and rat samples. When human PCCs were compared to unaffected adrenal tissues, *GATA2* and *TCF4* showed significantly increased expression in tumor samples (*GATA2*: 17 fold and *TCF4*: 2.3 fold). Also in the rat tumor samples, *Tcf4* (3 fold) and *Gata2* (5.2 fold) expression was significantly increased *versus* WT adrenal (Figure 31 C and D).

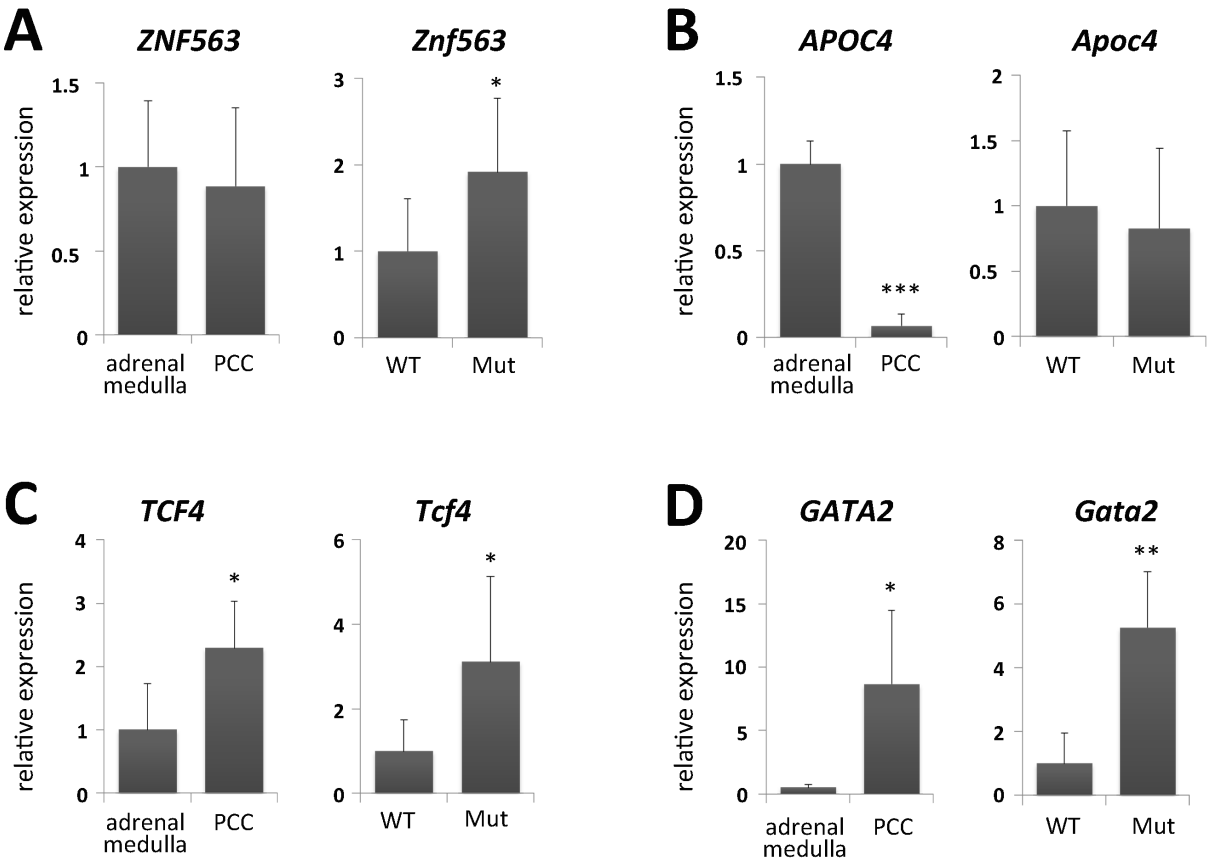

Figure 31: qRT-PCR analyses of putative p27/RUNX1 target genes in human and rat PCC tissues. (A) *Znf563* could be observed as overexpressed in rat tumor tissues (Mut), whereas *ZNF563* showed no changed expression level in human tumor tissues. **(B)** *APOC4* is dramatically reduced in human PCC tissues, but *Apoc4* is not differentially expressed in rat tissues. **(C and D)** *TCF4/Tcf4* and *GATA2/Gata2* could be shown as significantly overexpressed in human and rat tumor tissues. [Rat tissues: WT: n=6, Mut: n=10; Human tissues: adrenal medulla: n=2, PCC: n=8; *: p<0.05; **: p<0.01; ***: p<0.001 by student´s t-test]

Since *Znf563, Apoc4, Tcf4* and *Gata2* were identified as putative RUNX1 targets, we wanted to investigate the expression of these genes following siRNA-mediated knockdown of *Cdkn1b* and *Runx1* in both PC12 and WT rat adrenomedullary primary cells. Cells were transfected, collected 24 h later (optimized time point) and RNA was analyzed by qRT-PCR. Primary adrenomedullary cells from WT animals are difficult to cultivate, since they are highly sensitive, and are difficult to transfect, thereby leading to low transfection efficiency. Furthermore, the total number of isolated primary cells is low (around 1 million cells per animal, when both adrenal glands are pooled). Therefore, cells were treated with siRNA against *Cdkn1b* and/or *Runx1* to have enough cells for subsequent RNA extraction; the number of primary cells was not enough to collect them for protein extraction. In PC12 cells, the expression level of *Cdkn1b* and *Runx1* was reduced in average by around -80 % upon

transfection of the appropriate siRNAs (Figure 32 A). On average, around -50 % reduction of *Cdkn1b* expression and around -40 % reduction of *Runx1* level could be achieved in WT primary cells following siRNA transfection. When we performed *Cdkn1b*-*Runx1*-double knockdown in PC12 cells, the expression level of *Cdkn1b* was not further reduced, whereas the level of *Runx1* reached a -60 % reduction (Figure 32 B). *Znf563* expression was increased 1.75 fold upon *Cdkn1b* and *Runx1* double knockdown in PC12 cells, whereas the single knockdowns had no effect on *Znf563* levels. In contrast, in WT rat primary cells, *Znf563* is overexpressed (22-43 %) upon single and double knockdown of *Cdkn1b* and *Runx1* (Figure 32). In case of *Apoc4* expression, we observed no altered expression pattern in WT rat primary cells, but a 3.8 fold overexpression in PC12 cells when *Cdkn1b* or *Runx1* were knocked down and up to an 11 fold increased upon *Cdkn1b*-*Runx1*-double knockdown (Figure 32). These data confirm the microarray analyses. *Gata2* and *Tcf4* were identified as de-regulated in microarray analyses of adrenal tissues (see 3.3.1). Moreover, they were fished out as promising predicted RUNX1 targets by database analyses. Although better transfection efficiency for siRNAs was achieved in PC12 cells, the influence of the knockdown of *Cdkn1b* and *Runx1* expression levels of *Gata2* and *Tcf4* was lower in PC12 compared with primary cells (Figure 32). *Gata2* expression was reduced only -22.4 % after *Cdkn1b* knockdown in PC12 cells and no remarkably de-regulated *Gata2* expression was seen following *Runx1* knockdown (Figure 32 A). *Cdkn1b*-*Runx1*-double knockdown led to a slightly more reduced level of *Gata2* when compared with *Cdkn1b* single knockdown in both cell models. *Tcf4* expression was only suppressed by si*Cdkn1b* in PC12 cells (reduction of -10 %) (Figure 32 A). In WT primary adrenomedullary cells, *Gata2* was reduced to -50.9 % due to the silencing of *Cdkn1b* and -35.8 % due to that of *Runx1*. *Tcf4* showed a reduced expression level of only -22.1 % after si*Cdkn1b* transfection or -14.4 % after *Runx1* knockdown in primary cells (Figure 32 B).

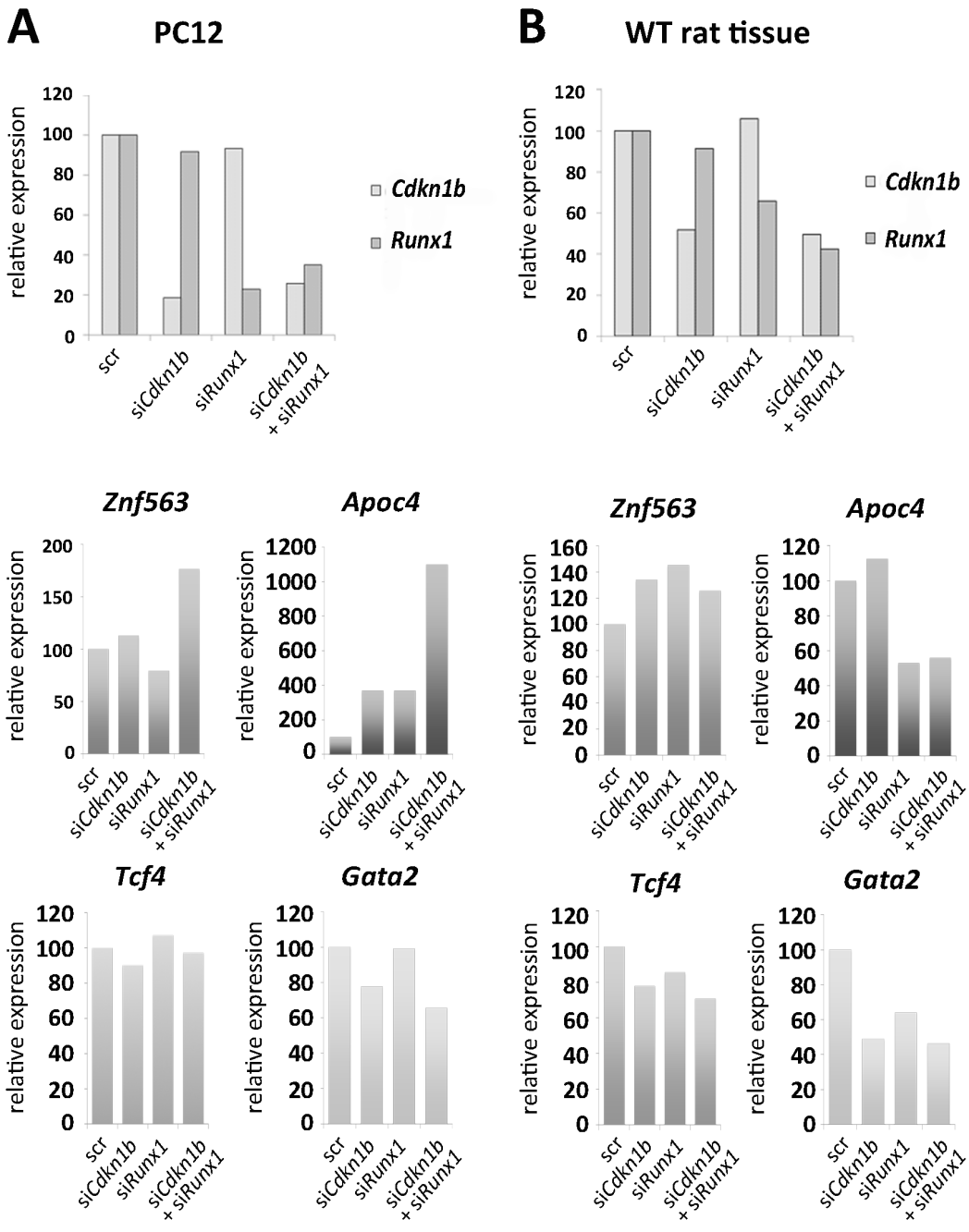

	PC12			WT rat tissue		
	si*Cdkn1b*	si*Runx1*	si*Cdkn1b* si*Runx1*	si*Cdkn1b*	si*Runx1*	si*Cdkn1b* si*Runx1*
Znf563	-	↘	↑	↑	↑	↑
Apoc4	↑	↑	↑	-	↓	↓
Tcf4	-	-	-	↘	↘	↘
Gata2	↘	-	↘	↓	↘	↓

Figure 32: Expression analysis of putative p27/RUNX1 targets in PC12 cells with down-regulated *Cdkn1b* or/and *Runx1*. (A) In PC12 cell experiments [n=2], *Znf563* and *Apoc4* showed an increased expression level after *Cdkn1b*-*Runx1*-double knockdown. Additionally, *Apoc4* was overexpressed

upon *Cdkn1b* and *Runx1* single knockdown, whereas *Tcf4* and *Gata2* showed no differential expression upon gene silencing. **(B)** In WT rat adrenomedullary tissues [n=2], *Apoc4* and *Gata2* were down-regulated following *Runx1* or *Cdkn1b*-*Runx1*-double knockdown. Silencing of *Cdkn1b* decreases *Gata2* levels. *Znf563* showed a slightly increase in expression when *Cdkn1b* and *Runx1* were down-regulated. In contrast, *Tcf4* could be observed as slightly down-regulated upon *Cdkn1b* and *Runx1* knockdown. [scr: scrambled transfection negative control]. As overview, the table below shows all four validated genes and their differential expression under certain conditions in adrenal cells/tissues. Blue arrows indicate an up-regulation (more than 50 %) of the displayed genes. Dark red arrows indicate a down-regulation (-50 % and more), whereas light red arrows describe a slight reduction of gene expression up to -50 %.

Since the p27 mutation in MENX rats leads exclusively to the development of neuroendocrine tumors, we checked the expression level of the putative p27/RUNX1 target genes in adrenal and non-endocrine tissues (liver and kidney) of WT rats compared with MENX rats. In addition, expression levels of these genes were checked on http://www.ncbi.nlm.nih.gov/, where RNA-Seq studies on different tissues are available (Figure 33). *Znf563* showed in consideration of all displayed tissues no different expression in endocrine *versus* non-endocrine tissues. Similarly, *Apoc4* is relatively equally expressed in all tested tissues without any significant difference between endocrine and non-endocrine tissues. *Tcf4* and *Gata2* are more expressed in adrenal tissues of rats in comparison with liver and kidney (Figure 33 A). In the overview including other validated organs, the expression profile in endocrine and non-endocrine tissues is similar. But in general, *Tcf4* and *Gata2* showed an overexpression when p27 is mutated like in tissues of MENX rats, what indicates a p27-dependent expression pattern.

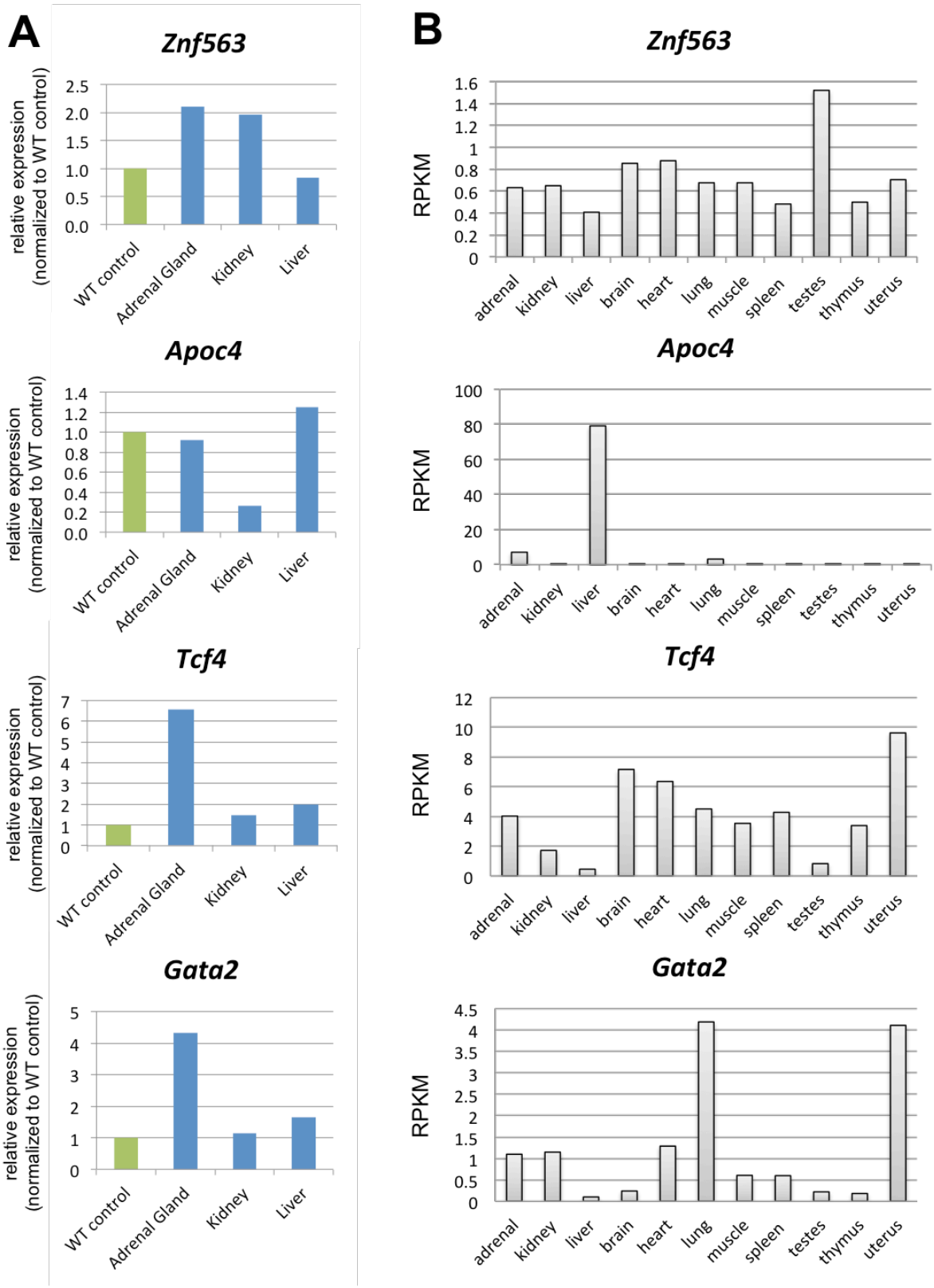

Figure 33: Expression profiles of RUNX1 target genes. (A) qRT-PCR results of *Znf563, Apoc4, Tcf4* and *Gata2* on rat tissue samples; in comparison of MENX rats with WT rats. [n=2] **(B)** RNA-Seq transcriptomic BodyMap from 21 weeks old Fischer 344 rats available on http://www.ncbi.nlm.nih.gov/. [RPKM: reads per kilobase per million mapped reads]

It has been reported that the TF GATA2 can regulate *Runx1* expression in some cells (Shi *et al*., 2014). Therefore, we decided to check whether this also occurs in our cell systems. PC12 cells were treated with siRNA against *Gata2* and expression levels of *Runx1* and *Cdkn1b* were investigated by qRT-PCR and western blotting. The silencing of *Gata2* had no effect on protein levels of p27 or RUNX1 (Figure 34). *Runx1* was not affected by the *Gata2-Cdkn1b*-double knockdown (Figure 34 A). Similarly: when both *Gata2* and *Runx1* were silenced, no changes in the levels of *Cdkn1b* could be detected by qRT-PCR (Figure 34 A) or of p27 by western blotting (Figure 34 B). Noteworthy, in the double knockdown experiments the degree of down-regulation of *Cdkn1b* (-54 %) and *Runx1* (-33.3 %) was significantly reduced compared to the single knockdown (Figure 34 A).

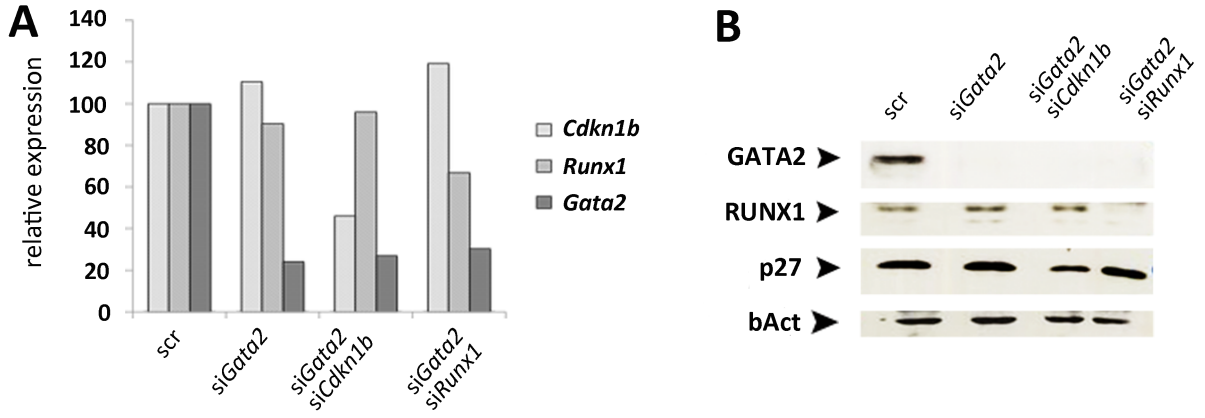

Figure 34: Expression studies of *Cdkn1b*/p27 and *Runx1*/RUNX1 in dependency of *Gata2* level modulation. (A) qRT-PCR analysis revealed no differential mRNA expression of *Cdkn1b* and *Runx1* transcripts upon *Gata2* knockdown. [n=2] **(B)** At the protein level, the modulation of Gata2 expression had no effect on the level of p27 and RUNX1 as detected by western blotting. The house keeping gene β-Actin (bAct) was used as loading control. [scr: scrambled negative transfection control; GATA2: 1:1000, 51 kDa; RUNX1: 1:1000, 49 kDa; p27: 1:500, 27 kDa; bAct: 1:1000, 42 kDa]

To check whether GATA2 co-localizes with RUNX1 or p27, co-IF experiments were performed. Unfortunately, no anti-Runx1 antibody produced in a different species compared with the available anti-Gata2 antibody (α-rabbit) could be found. Therefore, a putative co-localization could only be investigated by IF for GATA2 and p27, using primary antibodies made in different species. p27 and GATA2 are localized to the nuclei of rat adrenomedullary cells and in many of them they co-localized (Figure 35).

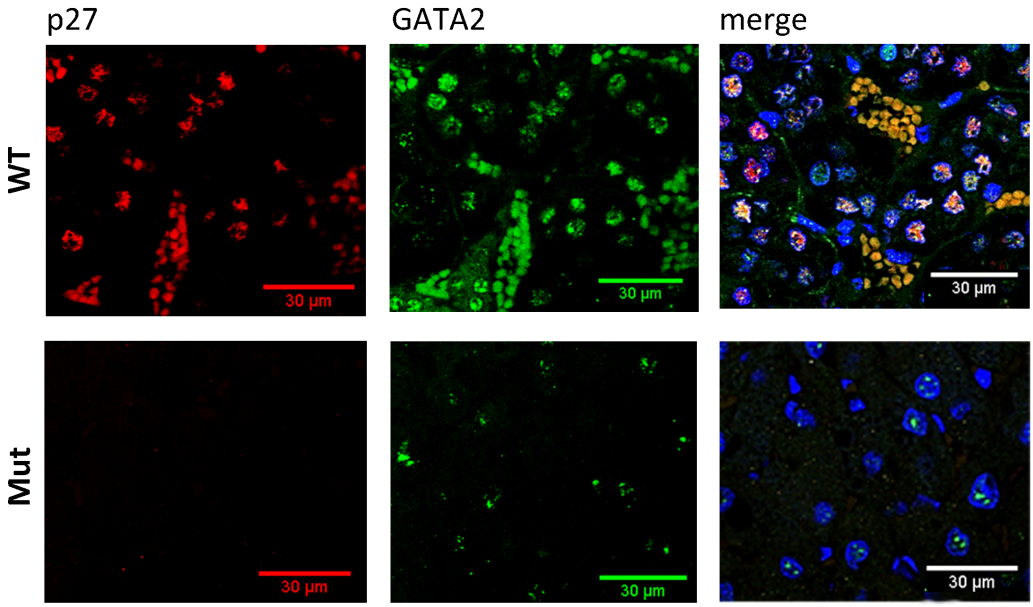

Figure 35: Co-IF of GATA2 and p27 in adrenomedullary tissues from WT and MENX mutant (Mut) rats. p27 could be shown to be expressed in the cell nuclei of adrenomedullary WT rat tissues. In rat mutant tissues, no p27 could be detected by IF, as expected. Gata2 was expressed in the nuclei of WT rat adrenal cells and co-localized with p27 (merge picture). In homozygous mutant rat tissues (Mut), GATA2 is expressed in cell nuclei but with lower level compared with WT adrenal cells. [scale bars: 30 µm; p27: 1:400; GATA2: 1:500]

GATA2 is an interaction partner of RUNX1 in AML and hematopoietic cells (Lizama *et al.*, 2015; Loke *et al.*, 2017; Pippa *et al.*, 2016). To validate a possible interaction of GATA2 with p27 or RUNX1 in PC12 cells and in WT rat adrenomedullary tissues, we conducted co-IP experiments (Figure 36). The IP was performed with a specific anti-Gata2 antibody and then p27 or RUNX1 were detected by western blotting. Figure 36 B shows the result of GATA2-IP then probed against GATA2 itself, p27 or RUNX1. In both, PC12 cells and WT rat adrenomedullary tissues, a signal could be shown for GATA2 - indicating a successful IP. In PC12 cells, a band for RUNX1 was observed, which confirmed a GATA2-RUNX1 interaction. For p27, no signal could be detected by western blotting after GATA2-IP in PC12 cells, nor in WT rat tissues. We also performed the reverse experiment: IP using an anti-p27 antibody for the pull-down and anti-Gata2 antibody for western blotting (Figure 36 B). Surprisingly, GATA2 was detected in the p27-IP sample (Figure 36 B). Based on these experiments, the co-localization of GATA2 with p27 and RUNX1 could be determined in PC12 cells, and even an interaction of GATA2 with RUNX1 could be observed in these cells as well as in WT rat adrenomedullary tissue. Unfortunately, no anti-Runx1 antibody generated in any species other than rabbit was available. Thus, we could not perform PLA for RUNX1 and GATA2.

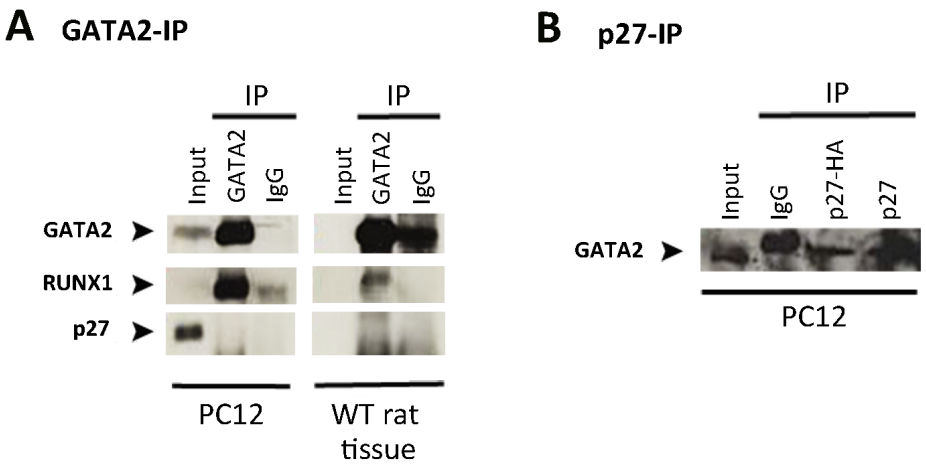

Figure 36: Interaction of GATA2 with p27 and RUNX1. (A) In GATA2-IP experiments, RUNX1 was pulled-down together with GATA2 in PC12 cells and in WT rat adrenomedullary tissues. For p27, no signal was detected in PC12 cells and rat tissues. **(B)** In p27-IP experiments performed in PC12 cells, GATA2 could be observed as interacting with endogenous p27 or with an overexpressed HA-tag p27 (p27-HA). [GATA2: 1:1000, 51 kDa; RUNX1: 1:1000, 49 kDa; p27: 1:500, 27 kDa]

4 DISCUSSION

4.1 p27 is a chromosomal binding protein

The classical role of p27 relates to its function as cell cycle inhibitor. Specifically, p27 binds to and inhibits CyclinE/CDK2 complexes thereby blocking the progression from G1 to S phase of the cell cycle (Larrea *et al*., 2009). In 2012, a novel role for p27 was identified in quiescent MEF cells having high levels of the protein, a role as an indirect transcriptional regulator of specific target genes (Pippa *et al*., 2012). In MEF cells, p27 interacts with the transcription factors p130 and E2F4 and suppresses gene expression. Several studies had previously suggested a cell cycle-independent role for nuclear p27 in quiescent cells (Muñoz-Alonso *et al*., 2005; Nguyen *et al*., 2007; Pippa *et al*., 2012). Although the molecular mechanisms still need to be elucidated, this role of p27 might involve the transcriptional repression of specific target genes.

MENX rats represent a unique animal model of multiple endocrine neoplasias available in our lab. Affected rats develop among others bilateral PCCs, which are tumors of the adrenal medulla (Fritz *et al*., 2002). MENX rats harbor an eight-bp tandem duplication in *Cdkn1b* exon 2, which causes a frameshift mutation leading to an encoded protein having a C-terminus different from the WT protein. Because of this mutation, the variant p27 protein is rapidly degraded *in vitro* and *in vivo*. Therefore, the levels of p27 in the rat tissues depend on the number of *Cdkn1b* functional alleles that varies when analyzing homozygous mutant animals (Mut (hom.)), heterozygous mutants (Mut (het.)) or WT rats in a gene-dosage-dependent manner (Figure 37). The identification of the germline *Cdkn1b* mutation in MENX rats demonstrated that p27 can act as tumor suppressor in neuroendocrine cells and that its inactivation leads to multi-tissue tumor formation in this model. Subsequently, different mutations (to date 12 different mutations are known (Lee and Pellegata, 2013)) in the human homologue *CDKN1B* were also identified and a new MEN syndrome was discovered (MEN4) caused by p27 mutation (Pellegata *et al*., 2006).

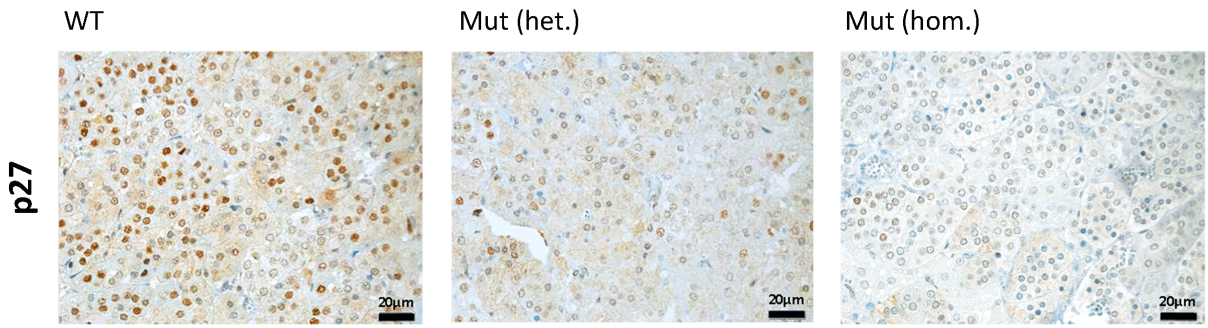

Figure 37: p27 IHC stainings of adrenal glands (medullary part) of MENX rats having different *Cdkn1b* genotypes. WT rats show a normal expression level of p27 in cell nuclei of most adrenomedullary cells. In Mut (het.) rats, p27 expression is reduced in intensity and is seen in less cells. Due to the described *Cdkn1b*-mutation, p27 is almost absent in the adrenomedullary tissues of p27 homozygous mutants (Mut (hom.)). [scale bar: 20 µm; Mut (het.): heterozygous mutant; Mut (hom.): homozygous mutant; p27: 1:500, 27 kDa]

p27's function is reduced or lost in many human cancers (Chu *et al*., 2008), including PCC (Pellegata *et al*., 2007). This, combined with the observation that mice deficient for p27 develop PCC (Fero *et al*., 1998; Kiyokawa *et al*., 1996; Nakayama *et al*., 1996) and MENX rats harboring a loss-of-function mutation in p27 also develop these tumors, point toward a role for p27 in adrenomedullary tumorigenesis. The molecular mechanisms mediating this role are still unknown.

As indicated above, p27 was discovered to be able to bind to DNA and regulate gene transcription in MEF cells (Pippa *et al*., 2012). Based on these findings, a basic question arose: Is p27 able to regulate gene transcription in adrenomedullary cells as well? And Can this mediate some of the functions of p27 in the neoplastic transformation of these cells?

To address these questions, we performed p27 ChIP-Seq experiments. Because p27 is supposed to bind DNA indirectly, it needs to interact with DNA-binding proteins, such as p130 and E2F4 in MEF cells, in order to regulate transcription (Pippa *et al*., 2012). To identify novel putative genome-wide binding sites of p27-containing complexes, ChIP-Seq experiments were carried out using an anti-p27 antibody to pull-down DNA sequences bound by the above mentioned complexes. As a first step, we needed to verify whether p27 is part of protein complexes binding to the DNA in adrenomedullary cells (the cells of interest for further p27 ChIP-Seq studies), as this was never reported. After crosslinking of proteins with DNA and separation of the different adrenomedullary cell compartments, cell nuclei were separated in euchromatin, heterochromatin and the nuclear matrix. Proteins

were then extracted from the different fractions and p27 was detected by western blotting. Indeed, p27 could be found in the nuclear matrix fraction, also known as insoluble portion of the chromatin, of adrenomedullary tissues (Figure 15). This validation allowed us to demonstrate that p27 interacts with DNA in adrenomedullary tissues, thereby making worthwhile to proceed the ChIP-Seq method with a specific anti-p27 antibody.

For p21, another member of the same family of cell cycle inhibitors like p27, an indirect binding to the DNA was reported (El-Deiry, 2016; Harper *et al*., 1993; Matsuoka *et al*., 1995; Musgrove *et al*., 1995; Polyak *et al*., 1994). Besides functional similarities between p27 and p21, such as their ability to block the kinase activity of CDKs, both proteins show structural similarities (Toyoshima and Hunter, 1994). To bind to the DNA, p21 binds to PCNA (proliferating cell nuclear antigen), an auxiliary factor for DNA polymerases δ and ε that is essential for both DNA replication and DNA repair (el-Deiry, 1997). Based on that finding, the suggestion of an indirect DNA-binding role of p27 is well conceivable.

4.2 ChIP-Seq revealed that p27-containing complexes bind DNA

4.2.1 Determination of specific transcription factor binding sites by p27 ChIP

Based on the findings that p27 can indirectly bind to the DNA in adrenomedullary cells, we wanted to investigate the binding sites of putative DNA-binding p27 interaction partners at the genomic level. Therefore, p27 ChIP-Seq experiments were conducted in rat and human adrenomedullary tissues. Figure 18 revealed p27 to be specifically pulled-down in adrenomedullary tissue lysates by the use of a monoclonal anti-p27 antibody (BD Transduction Laboratories™). Sequencing analysis confirmed the successful pull-down of DNA sequences by p27 ChIP-Seq in these cells (Table 15). The human sample was excluded from further bioinformatics´ analyses since the total number of p27 peaks was unusually high (30 695) and simultaneously of low significance. These findings indicate a lower specificity of the anti-p27 antibody in the human adrenomedullary sample compared with the rat samples (total number of p27 peaks: 1 294).

By the Genomatix Tool, significantly overrepresented TF binding sites were identified among the pulled-down sequences and sorted by their Z-scores for their promoters' overrepresentation (Table 16). The Z-score represents the degree of overrepresentation; the

higher the Z-score, the higher the overrepresentation of the TF family (significant when the Z-score is above 2). A negative Z-score means an underrepresentation of the TF, which is significant when the Z-score is below -2. The most enriched TFs identified by the MEME Suite (Znf423 and Runx1) (Figure 20, Table 15) could be also identified by Genomatix (Table 16). Nonetheless, many other TF binding sites could be observed as more overrepresented based on Z-scores in the p27 ChIP data by Genomatix: *e.g.* V$GCF2, V$NDPK, V$BEDF, V$MAZF, V$PLAG, V$CTCF and V$SP1F. All the seven TF families have Z-scores higher than thirteen over the genome background and higher than four for the Z-scores over the promoter background. The following paragraph serves to discuss correlations between the named genes with p27 as perspective for further studies.

The gene *NDPK* encodes for a nucleoside diphosphate kinase. NDPK binds to a common DNA fragment in cMYC gene promoters (Cervoni *et al*., 2003, 2006; Egistelli *et al*., 2009). Interestingly, analyses of our p27 ChIP experiments identified the motif for the Myc/MAX heterodimer as significantly enriched, indicating a binding site for p27 to Myc/MAX and potential regulation of Myc/MAX by p27 (Table 15). *MAZF* (MYC-associated zinc finger protein) promotes proliferation in breast cancer and prostate cancer and interacts with cyclinE/A/p27/SKP2 to modulate the expression of p27 (Chandramohan *et al*., 2008). Simultaneously, p27 was reported to antagonize MYC by binding and inhibiting MYC independently of CDK2, but possibly by interacting with other TFs (FBXO28, HUWEI1 and SIRT1) (Bahram *et al*., 2016; Hydbring *et al*., 2017). Based on the function of p27 as repressor of gene transcription (Pippa *et al*., 2012) and on the fact that MYC and p27 can activate each other, it is conceivable that the interaction of both proteins could create a time window where transcriptional repressor proteins are recruited by p27 to target gene promoters prior to destruction of MYC and subsequent loss of p27 from the promoter; as it is described for the MYC interaction partner SKP2 (Hydbring *et al*., 2017; Kim *et al*., 2003; von der Lehr *et al*., 2003). The crosstalk between p27 and MYC is also supported by p27 knockout mice, which develop lymphomas because of MYC activation; this strengthens the hypothesis that p27 provides a negative feedback to MYC (Amente *et al*., 2010). *CTCF* (CCCTC-binding factor) has a cell cycle regulatory role in breast cancer and endometrial carcinoma (Marshall *et al*., 2017; Oh *et al*., 2017). CTCF can associate with the Sin3-HDAC complex, which is associated with HDAC1 and HDAC2. The same interaction with the Sin3-HDAC complex was reported for p27 in MEF cells by Pippa *et al*. (2012). Furthermore, in *Ctcf* knockout mice, increased levels

of p27 and p21 could be observed (Heath *et al*., 2008; Marshall *et al*., 2017; Oh *et al*., 2017; Qi *et al*., 2003). The *SP1* TF is reported to control cell proliferation in nasopheryngeal carcinoma and breast cancer by activating p27 and p21 (Chen *et al*., 2005; Huang *et al*., 2008a; Wei *et al*., 2013; Zhang *et al*., 2014). For *GCF2* (GC-Rich Sequence DNA-Binding Factor 2), *BEDF* (*ZBED*; BED-type zinc finger putative TF) and *PLAG* (PLAG zinc finger) no direct association with p27 regulation is reported by now.

4.2.2 p27 ChIP-Seq identified significantly enriched p27-binding partners

4.2.2.1 ZNF423

ZNF423 could be identified as putative binding partner of p27 since the TF binding site for ZNF423 was specifically overrepresented after p27 ChIP-Seq experiments in adrenomedullary tissues from rats (Figure 20, Table 15). To further investigate this finding, we analyzed the expression profile and correlation of both proteins and could show that p27 and ZNF423 co-localize in adrenal cell nuclei (Figure 22, Figure 23). We could not observe a direct binding of p27 and ZNF423, but an affiliation of ZNF423 to p27-complexes cannot be ruled out.

The Krüppel-like C2H2 zinc finger factor *ZNF423* (also *ZFP423* or *OAZ*; OMIM #604557) is a transcriptional modulator that has an effect on several signaling pathways and plays an essential role in cerebellar development, olfactory neurogenesis and midline patterning of the central nervous system (Cheng *et al*., 2007; Hata *et al*., 2000; Tsai and Reed, 1997; Warming *et al*., 2006). In general, ZNF423 is expressed in lung, heart, skeletal muscles, brain, pancreas and kidneys of healthy adults, but plays no role in healthy hematopoiesis (Hata *et al*., 2000; Tsai and Reed, 1997). In contrast, in many ALL patients *ZNF423* is overexpressed, which leads to maturation arrest of B cells - a hallmark of ALL (Harder *et al*., 2013). ZNF423 is the human homolog of the transcription modulator Roaz (rat O/E-1 associated zinc finger), which was discovered in the olfactory system of the rat. Hence, its other name is: Olf1/EBF (olfactory factor-1/early B-cell factor)-associated zinc finger protein (Hata *et al*., 2000; Tsai and Reed, 1997; Turner and Crossley, 1999). ZNF423 is a multifunctional protein composed of 20 zinc finger domains divided in different clusters: zinc finger domains 2-8 act as DNA-binding domain for GC rich regions of the DNA. Zinc finger domains 9-13 are responsible for the binding to the BMP2 (bone morphogenetic protein 2)-responsive element, which is

essential for the recruitment of the ZNF423-SMAD1-SMAD4 complex to promoter sequences. Zinc finger 14-19 are responsible for the protein-protein-interaction with SMAD1 and SMAD4; zinc finger domains 28-30 mediate the protein-protein-interaction with EBF. To date, the functions of zinc finger 1 and zinc fingers 20-27 are unknown (Hata *et al*., 1997, 1998, 2000).

BMPs belong to the *TGF*β (transforming growth factor) superfamily and regulate differentiation and cellular processes such as proliferation, morphogenesis and apoptosis (Ille *et al*., 2007; Pajni-Underwood *et al*., 2007; Pan *et al*., 2013). Interestingly, in our lab, BMP7 was identified as overexpressed in rat and human PCC, which promotes cell proliferation, migration and invasion in adrenal cells (Leinhäuser *et al*., 2015). BMP7 activates the SMAD complex by binding to BMP-Receptors, and thus leads to transcription of BMP target genes, including *Znf423* (Harder *et al*., 2013). In human neuroblastoma cell lines, accumulation of p27 is associated with BMP2-induced growth arrest, differentiation and activation of the Olf-1/EBF pathway, in which ZNF423 is involved (Huang *et al*., 2009b; Nakamura *et al*., 2003). In this context, it is known that BMP2/4 stimulation induces *ZNF423* expression at the transcriptional level in cellular ALL models. In general, in human embryonic stem cells, which express substantial amounts of BMPs, remarkably high levels of ZNF423 could be observed (Harder *et al*., 2013).

Recently, ZNF423 has emerged as critical transcriptional modulator in cancer. Consistent with its multifunctional potential, *ZNF423* is involved in a variety of pathways involved in cancer development, such as retinoic acid signaling (Huang *et al*., 2009a), Notch signaling (Masserdotti *et al*., 2010), and the DNA damage response (Chaki *et al*., 2012; Ku *et al*., 2003). Low ZNF423 levels correlate with poor outcome of neuroblastoma, which indicates ZNF423 to be a marker for neuroblastoma - a tumor type that arises from the same type of cells as PCC does (Harder *et al*., 2014; Huang *et al*., 2009b). In contrast, in human and rat PCC samples (where p27 level is low), ZNF423 could be observed as overexpressed. Nonetheless, no interaction between ZNF423 and p27 has been reported so far.

4.2.2.2 RUNX1

The second most enriched TF, which could be identified as putative interaction partner of

p27 based on ChIP-Seq experiments in adrenomedullary tissues from rats, is RUNX1 (Figure 20, Table 15). Further studies revealed that p27 and RUNX1 co-localize in adrenal cells (Figure 22, Figure 23), and even interact in these cells as shown by co-IP and PLA experiments (Figure 25, Figure 26).

The runt-related transcription factor 1 (*RUNX1;* OMIM #151385), also known as acute myeloid leukemia 1 (*AML1*) or core-binding factor subunit alpha 2 (*CBFA2*), belongs to the core-binding factor (CBF) family of TFs, which is able to bind to the core site of various enhancers and promoters. RUNX1 is well known as master regulator of cell fate determination in blood, bone, and neurons (Chuang *et al*., 2013). Human *RUNX1* is located at Chr. 21q22.12, spans approximately 260 kilobases containing 12 exons and is transcribed by two alternative promoters: P1 (distal) and P2 (proximal) (Levanon *et al*., 2001). P1 and P2 generate distal and proximal *RUNX1* transcripts that differ in their 5′ untranslated regions (UTRs) and N-terminal coding sequences, which influences in-exon and alternative splicing of *RUNX1* transcripts (Fujita *et al*., 2001; Ghozi *et al*., 1996; Pozner *et al*., 2007). RUNX1 consists of three DNA-binding CBFa subunits (RUNX1, RUNX2, and RUNX3) and the non-DNA-binding subunit CBFb (Speck and Gilliland, 2002). RUNX1 harbors an N-terminal highly conserved Runt domain, which contains 128 aa and gives RUNX1 the ability to bind to the DNA of target genes (Daga *et al*., 1996; Melnikova *et al*., 1993; Meyers *et al*., 1993). CBFb is a molecular heterodimerization partner of RUNX1 carrying out its transcriptional activity through the Runt homology domain (Meyers *et al*., 1993; Ogawa *et al*., 1993; Wang *et al*., 1993). The binding of CBFb and RUNX1 is an essential feature of RUNX1 that enables it to exert its biological function in the cell, and protects RUNX1 from proteasomal degradation (Huang *et al*., 2001; Lu *et al*., 1995; Wang *et al*., 1996). Once RUNX1 and CBFb dimerize, they recognize the optimal consensus sequence “PuACCPuCA” or “TGT/cGGT” on the target DNA (Kamachi *et al*., 1990; Meyers *et al*., 1993). Therefore the characteristic of RUNX1 is to interact with other proteins to form complexes that are able to regulate gene transcription.

Key roles of the RUNX family in epithelial cells and solid tumors recently started to emerge (Chuang *et al*., 2013; Scheitz and Tumbar, 2013; Taniuchi *et al*., 2012). In general, RUNX1 has tumor suppressive or oncogenic activity (Blyth *et al*., 2009; Taniuchi *et al*., 2012). In breast cancer, whole-genome and whole-exome sequencing have identified point mutations and deletions of *RUNX1* and *CBF*β in human luminal breast cancers (Banerji *et al*., 2012; van

Bragt *et al*., 2014; Ellis *et al*., 2012). Additionally, RUNX1 was identified as regulator of the development of ER+ luminal breast cancer, oral SSC or oesophageal cancer (van Bragt *et al*., 2014; Dulak *et al*., 2012; Scheitz *et al*., 2012; Zampino *et al*., 2009) (van Bragt *et al*., 2014; Scheitz *et al*., 2012). In tumorigenesis, in the vast majority of cases the genetic changes of *RUNX1* and *CBF*β lead to a loss-of-function.

RUNX proteins show a context-dependent regulation of target gene expression. RUNX1 can activate or repress target genes depending on its interaction with co-activators or co-repressors (Blyth *et al*., 2005). For example, two well known targets of RUNX1 are CEBPa and SPI-1 (also known as PU.1) (Kanno *et al*., 1998; Petrovick *et al*., 1998). CEBPa is a TF that coordinates proliferation arrest and the differentiation of myeloid progenitors, adipocytes, hepatocytes and cells of lung and placenta (Gombart *et al*., 2002; Pabst *et al*., 2001; Zhang *et al*., 1997), whereas the TF SPI-1 is necessary for normal myeloid differentiation at the late maturation stage (Friedman, 2002; Huang *et al*., 2008b; Wang and Friedman, 2002). Among CBFb and SPI-1, known interaction partners of RUNX1 are PAX5 (Liebermann and Korf, 1999), Cyclin D3 (Bernardin-Fried *et al*., 2004), STAT5 (Ogawa *et al*., 2008), GATA1 (Elagib *et al*., 2004), GATA2 (Pippa *et al*., 2016), C/EBPb (Tahirov *et al*., 2001; Wang *et al*., 1996) or AP-1 (Frank *et al*., 1999). The number of these potential binding sites for different interaction partners indicates the complexity of the regulatory network that determines the function and activity of Runx1 (Chuang *et al*., 2013; Ito, 1999).

Since RUNX1 is a master regulator of cell fate determination in HSC and p27 limits the cell division of these cells, a correlation of RUNX1 and p27 was probable (Chuang *et al*., 2013). Down-regulation of p27 could be observed in ALL when *Runx1* was mutated (chromosomal translocation t(8;21)) (Haferlach *et al*., 2011). Runx1 is known to interact with p27 since low expression of *CDKN1B* was significantly over-represented in AML with the reciprocal t(8;21)/*RUNX1-RUNX1T1* (p=0.001), t(15;17)/*PML-RARA* (p<0.001), and 11q23/*MLL*-rearrangements (p=0.038) (Haferlach *et al*., 2011). Indeed, RUNX1 is known to repress the transcription of members of the CIP/KIP family in HFSC *in vivo*: p21, p27, p57 and p15 (Haferlach *et al*., 2012; Lee *et al*., 2013; Lutterbach *et al*., 2000; Markus *et al*., 2007). RUNX1 and p21, for example, synergistically limit the extent of HFSC quiescence, which antagonizes the role of p21 as a cell cycle inhibitor (Lee *et al*., 2013). RUNX1 is reported to be able to affect stem cell, neural progenitor cell and human neuroblastoma (arise from the same type of cells like PCC) cell proliferation (Inoue and Ito, 2011; Kim *et al*., 2014; Logan *et al*., 2015;

Theriault *et al*., 2005). RUNX1 promotes the progression of G1 to S and S to G2/M phases of the cell cycle in myeloid progenitors and hair follicle stem cells (HFSC). More precisely, CCK1/cyclin B, CCK6/cyclin D3 and extracellular-regulated kinase (ERK) mediate serine/threonine phosphorylation of RUNX1 and regulate cell proliferation (Biggs *et al*., 2006; Hoi *et al*., 2010; Osorio *et al*., 2008). Since RUNX1 promotes the cell cycle progression from G1 to S, but p27 inhibits the entry into the S phase, we checked cell proliferation in PC12 cells when both proteins are down-regulated by siRNA. Figure 30 shows that, in contrast to what was described before, PC12 cell proliferation increases two-fold following *Runx1* knockdown or *Runx1-Cdkn1b* double-knockdown. When p27 allone was silenced, the proliferation rate was even higher (almost three-fold). Since *Runx1-Cdkn1b* double-knockdown lessened the over-activation of proliferation compared with the case when p27 allone was silenced, RUNX1 is indicated to have an anti-proliferative function in PC12 cells with a probably higher ordinated proliferative function than p27.

Mutation of Runx1 at S249 or S266 prevents ERK-dependent phosphorylation, which leads to RUNX1 association with the chromatin mediated by the mSin3A corepressor. This association increases RUNX1 stability and protects it from proteosomal-mediated degradation; thereby enhancing its transcriptional activity (Imai *et al*., 2004; Zhao *et al*., 2008). Similar to other TFs, RUNX1 also modulates target gene expression through recruitment of chromatin modifiers, such as histone acetylases (HATs) or histone deacetylases (HDACs) (Cheng *et al*., 2016; Zhang *et al*., 2008). An interaction with the HDAC-mSin3A complex was also described for p27 in MEF cells (Pippa *et al*., 2012). This finding could indicate the formation of a complex containing p27 and RUNX1 with mSin3A and HDACs having transcriptional regulator function.

4.3 Validation of putative RUNX1 target genes

4.3.1 Identification of RUNX1 target genes

Since the TF RUNX1 could be confirmed as direct interaction partner of p27 likly involved in regulating gene transcription in adrenomedullary cells, we identified putative target genes of RUNX1 (and p27) and investigated their expression profiles when RUNX1 and p27 levels were modulated. Based on correlation studies of adrenal p27 ChIP-Seq data and adrenal

tissue microarrays done by Dr. Juan Higareda Almaraz from the Institute of Diabetes and Cancer (IDC, HMGU, Germany), *Tcf4* and *Gata2* were selected for further investigation since they have a *Runx1* consensus motif near their promoters and/or are differentially regulated in tissue microarrays of tumors *versus* unaffected adrenals as mentioned in 3.3.1 (Figure 27). In addition, *Runx1* and *Cdkn1b* levels were modulated in PC12 cells to identify overexpressed genes as transcriptionally regulated by a p27-RUNX1 complex (Table 17). *Znf563* and *Apoc4* were identified as overexpressed when *Cdkn1b* or *Runx1* were silenced and therefore selected for further investigation.

Znf563 was shown to be overexpressed in rat PCCs with low p27 levels. No altered expression level could be observed in human PCCs however the level of p27 was not known (Figure 31 A). Based on these findings, we expected *Znf563* to be up-regulated in PC12 cells and primary adrenal cells with silenced p27. Indeed, when p27 and RUNX1 were silenced in these cells, *Znf563* was overexpressed (Figure 32). So far, articles describing ZNF563 function are missing and only GO annotations listed in the GeneCards® Human Gene Database mention ZNF563 as having nucleic acid-binding ability. These preliminary results are promising and further studies confirming the transcriptional regulation of ZNF563 by the p27-RUNX1 complex are warranted.

Apoc4 was found not to be differentially expressed in MENX rat PCCs with low endogenous p27 levels, whereas *APOC4* was dramatically decreased in human PCCs (Figure 31 B). When p27 and RUNX1 were silenced, *Apoc4* was overexpressed in PC12 cells, but down-regulated in primary adrenal cells (Figure 32). Although, *APOC4* is reported to be overexpressed in colorectal and breast cancer patients, the controversial results in adrenal cells make it difficult to estimate the regulatory effects of p27 and RUNX1 on APOC4. So, further validation needs to be done.

Tcf4 was shown to be over-expressed in rat and human PCCs by qRT-PCR (Figure 31 C). Similar to that, Tcf4 is up-regulated in a HDAC-dependent manner in ETV6/RUNX1-positive lymphoid leukemic cells compared with RUNX1-negative cells. As already mentioned in 4.2.2.2, Runx1 is known to modulate the expression of its target genes via the recruitment of HDACs (Cheng *et al*., 2016; Zhang *et al*., 2008). In addition, TCF4 controls c-MYC transcription (Meyer *et al*., 2012; Shah *et al*., 2015). We already described in paragraph 4.2.1 the link between c-MYC and p27. TCF4 is characterized as direct target of PLAG, whose TF binding site was

overrepresented in p27 ChIP samples as well (Table 16). Despite the link between TCF4 and RUNX1, the expression of *Tcf4* was not altered in PC12 cells or adrenal primary cells with silenced *Cdkn1b* and *Runx1* (Figure 32). Therefore, we concluded no regulatory function of the putative p27-Runx1 complex in adrenal cells.

Gata2 was over-expressed at mRNA level in rat and human PCCs when compared with unaffected adrenal tissues (Figure 31 D). In addition, GATA2 is a downstream target of BMP signaling (Dalgin *et al*., 2007; Maeno *et al*., 1996; Oren *et al*., 2005; Xu *et al*., 1999b) and since BMP7 is overexpressed in MENX rat and human PCCs, an over-activation of *Gata2* might be expected in these tumors (Leinhäuser *et al*., 2015). In contrast, in adrenal medullary cells of homozygous mutant rats GATA2 was under-expressed at the protein level compared to WT rats (Figure 35). Furthermore, *Gata2* (mRNA level) was under-expressed in PC12 cells and primary adrenal cells after *Cdkn1b* and *Runx1* knockdown (Figure 32). These results indicate that the expression of *Gata2* depends on p27 and Runx1 level. Since the mRNA level of Gata2 is high in mutant rats with low p27 level (Figure 31 D), but the GATA2 protein level is down-regulated in these rats (Figure 35) and PC12 cells or adrenomedullary primary cells following *Cdkn1b* knockdown (Figure 32), a feedback loop between GATA2 and p27 is conjecturable. GATA2 is known to negatively regulate the proliferation of neuronal progenitor and urogenital cells (El Wakil *et al*., 2006; Zhou *et al*., 1998). The first hint to support this function of GATA2 is that the protein participates in the differentiation pathway of various types of neurons in the ventral hindbrain and spinal cord, namely cranial nerves (Nardelli *et al*., 2003; Pata *et al*., 1999), serotoninergic neurons (Craven *et al*., 2004; Pattyn *et al*., 2004) and V2 interneurons (Karunaratne *et al*., 2002; Zhou *et al*., 2000). Indeed, *Gata2* expression could be shown to be sufficient to force cycling neural progenitors to switch to a quiescent state and eventually differentiate *in vivo,* and to inhibit proliferation of embryonic undifferentiated neuroepithelial cells in culture (El Wakil *et al*., 2006). GATA2 is able to cause transient upregulation of cyclin D1 *in vivo* in neuronal progenitors and neuroepithelial cells. In fact, cyclin E was observed as down-regulated in these cells as consequence of the higher expression of cyclin D1 (El Wakil *et al*., 2006). This can result in the inhibition of events underlying the progression towards the S phase, in particular the upregulation of cyclin E (Meyyappan *et al*., 1998; Pagano *et al*., 1994). For the development and maintenance of proliferation of stem cells migrating liver, spleen and bone marrow, RUNX1 and GATA2 could be observed to be involved. A lack of one or both of these genes leads to a rudimentary

hematopoiesis (Lancrin *et al*., 2009; Okuda *et al*., 1996; Porcher *et al*., 1996; Shivdasani *et al*., 1995; Tsai *et al*., 1994; Wang *et al*., 1996). In addition, GATA2 is known to interact with HDAC3 and HDAC5 in hematopoietic stem cells (Ozawa *et al*., 2001). The same interaction with HDACs has been also reported for p27 and RUNX1 (Cheng *et al*., 2016; Pippa *et al*., 2012; Zhang *et al*., 2008).

4.3.2 GATA2 interacts with RUNX1

Gata2 could be identified as overexpressed in adrenal tissue microarrays when MENX rat tissues were compared with WT rat tissues and it was found as predicted p27/RUNX1 target gene (Figure 27). Lizama *et al*. (2015) showed that SOX17 directly binds RUNX1 and GATA2 for repression of hematopoietic cell fate. Interestingly, Pippa *et al*. (2016) could draft a model based on ChIP experiments where RUNX1 interacts with GATA2, MYC and SP1 to bind to the *SET* minimal promoter region in AML (-318 bp before the transcription start site). They could investigate DNA motifs for *RUNX1* and *GATA2* in the *SET* distal promoter region. More precisely, MYC activates the expression of *RUNX1*, *GATA2* and *SP1*, and RUNX1 and GATA2 increase the expression of *MYC* (Pippa *et al*., 2016).

In this work, we could show a direct interaction of GATA2 with RUNX1 (Figure 36) but whether GATA2 also binds to p27 is not clear, since GATA2 was not detectable in p27-IP lysates (Figure 36). Based on these findings, we propose the model shown in Figure 38, where p27 ChIP pull-down could identify RUNX1 as direct interaction partner of p27, which enables the binding to DNA and the regulation of target genes. GATA2 binds to RUNX1, and by doing so may broaden the function of the p27 complex in regulating transcription in rat adrenomedullary cells.

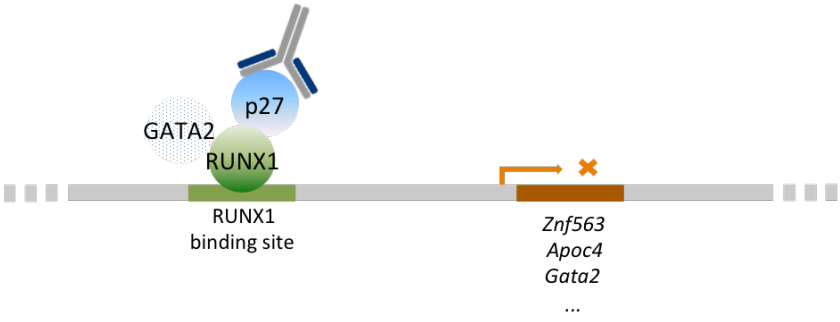

Figure 38: Scheme of the putative p27-RUNX1-GATA2 complex to regulate target gene expression in adrenal cells. By p27 ChIP-Seq experiments performed with adrenomedullary rat cells, RUNX1

binding site was found enriched. Functional studies identified RUNX1 as direct interacting partner of p27. GATA2 could be shown to interact with RUNX1. These three proteins could form a complex and recruit each other to the chromatin to regulate the expression of potential target genes (such as *Znf563, Apoc4, Gata2, Tcf4*, and other unknown genes).

4.4 Conclusions and outlook

ChIP-Seq experiments of this study revealed p27 to be a regulatory co-factor for the TF RUNX1 in adrenomedullary rat tissues (Figure 20, Table 15). We propose a model where RUNX1, bound to GATA2, associates with p27 and bind to chromatin of rat tissues of the medulla of adrenal glands (Figure 38). Furthermore, this study observed that this transcriptional complex regulates the target genes *Apoc4*, *Znf563* and *Gata2* (Figure 32).

p27 ChIP-Seq experiments could elucidate a novel role of p27 as transcriptional regulator in adrenomedullary cells. RUNX1 could be demonstrated to be a direct interaction partner of p27, which enables the association of p27-RUNX1 complexes to binding sites at target gene promoters. Although shown by co-IP and PLA on endogenous protein levels (Figure 25, Figure 26), the interaction of p27 and RUNX1 should be further verified by using GST-p27 fusion proteins for IP experiments performed with an anti-GST antibody. Furthermore, gel shift assays could help to confirm the p27-RUNX1 interaction in adrenal cells.

Since the Znf423-binding motif is highly enriched in adrenal cells, but we could not conclusively verify whether it interacts with p27, this putative binding should be further studied by using new anti-Znf423 antibodies and other molecular tools to perform ZNF423-IP experiments and IF stainings or PLAs. Additional potential p27 interacting partners identified by p27 ChIP-Seq, such as *GCF2, NDPK, BEDF, MAZF, PLAG, CTCF* and *SP1* (predicted by Genomatix (Table 16)) or *HNFA4/Rxrx/Esrrb, Spdef, Bhlhb2, Tcfe2a/Znf238, NFATC1/2* and *TBX1/5/15* (identified by the MEME Suite (Table 15) could be validated for their putative association with p27 in adrenal cells.

To broaden the study, additional interesting potential p27 target genes should be investigated for their role in tumor development. Potential p27 target genes, which could be brought into focus for further studies are *Dennd5a, Kcnj15, Irx5, Tox3, Pdlim5, Zfand6, Lnx1, Gprc5b* or *Tdc1d5* identified by correlating the p27 ChIP-Seq data and adrenal tissue gene expression microarray analyses. These genes have a p27 peak near their promoters and are

overexpressed in rat PCCs (Figure 27). Functional assays, such as luciferase assays, and ChIP-qPCR experiments should be established to validate these target genes. To clarify the transcriptional regulatory activity of p27 specifically in endocrine tissues, target genes should be analyzed for their expression levels in endocrine and non-endocrine tissues when p27 levels are altered. For that, tissues from MENX rats could be used as model since they have strongly reduced p27 levels with resulting development of neuroendocrine tumors as we already did. Furthermore, $p27^{-/-}$ mice could be used to check the tumorigenic role of putative p27 target genes in cells with p27-deficient background. Furthermore, a putative transcriptional activator or repressor function of p27 should be elucidated by investigating the expression levels of putative target genes following the modulation of p27 levels.

5 REFERENCES

Abumi, K., Anbo, H., Kaneda, K., 1996. Migration of an acupuncture needle into the medulla oblongata. Eur. Spine J. Off. Publ. Eur. Spine Soc. Eur. Spinal Deform. Soc. Eur. Sect. Cerv. Spine Res. Soc. 5, 137–139.

Acosta, J.C., Ferrándiz, N., Bretones, G., Torrano, V., Blanco, R., Richard, C., O'Connell, B., Sedivy, J., Delgado, M.D., León, J., 2008. Myc inhibits p27-induced erythroid differentiation of leukemia cells by repressing erythroid master genes without reversing p27-mediated cell cycle arrest. Mol. Cell. Biol. 28, 7286–7295. doi:10.1128/MCB.00752-08

Allen, J.A., Roddie, I.C., 1972. The role of circulating catecholamines in sweat production in man. J. Physiol. 227, 801–814.

Amente, S., Lania, L., Avvedimento, E.V., Majello, B., 2010. DNA oxidation drives Myc mediated transcription. Cell Cycle Georget. Tex 9, 3002–3004. doi:10.4161/cc.9.15.12499

Astuti, D., Agathanggelou, A., Honorio, S., Dallol, A., Martinsson, T., Kogner, P., Cummins, C., Neumann, H.P., Voutilainen, R., Dahia, P., Eng, C., Maher, E.R., Latif, F., 2001a. RASSF1A promoter region CpG island hypermethylation in phaeochromocytomas and neuroblastoma tumours. Oncogene 20, 7573–7577. doi:10.1038/sj.onc.1204968

Astuti, D., Latif, F., Dallol, A., Dahia, P.L., Douglas, F., George, E., Sköldberg, F., Husebye, E.S., Eng, C., Maher, E.R., 2001b. Gene mutations in the succinate dehydrogenase subunit SDHB cause susceptibility to familial pheochromocytoma and to familial paraganglioma. Am. J. Hum. Genet. 69, 49–54. doi:10.1086/321282

Ayer, D.E., 1999. Histone deacetylases: transcriptional repression with SINers and NuRDs. Trends Cell Biol. 9, 193–198.

Baguet, J.-P., Hammer, L., Mazzuco, T.L., Chabre, O., Mallion, J.-M., Sturm, N., Chaffanjon, P., 2004. Circumstances of discovery of phaeochromocytoma: a retrospective study of 41 consecutive patients. Eur. J. Endocrinol. 150, 681–686.

Bahram, F., Hydbring, P., Tronnersjö, S., Zakaria, S.M., Frings, O., Fahlén, S., Nilsson, H., Goodwin, J., von der Lehr, N., Su, Y., Lüscher, B., Castell, A., Larsson, L.-G., 2016. Interferon-γ-induced p27KIP1 binds to and targets MYC for proteasome-mediated degradation. Oncotarget 7, 2837–2854. doi:10.18632/oncotarget.6693

Bailey, T.L., Boden, M., Buske, F.A., Frith, M., Grant, C.E., Clementi, L., Ren, J., Li, W.W., Noble, W.S., 2009. MEME SUITE: tools for motif discovery and searching. Nucleic Acids Res. 37, W202-208. doi:10.1093/nar/gkp335

Bailey, T.L., Elkan, C., 1994. Fitting a mixture model by expectation maximization to discover motifs in biopolymers. Proc. Int. Conf. Intell. Syst. Mol. Biol. 2, 28–36.

Bailey, T.L., Machanick, P., 2012. Inferring direct DNA binding from ChIP-seq. Nucleic Acids Res. 40, e128. doi:10.1093/nar/gks433

Baldassarre, G., Belletti, B., Nicoloso, M.S., Schiappacassi, M., Vecchione, A., Spessotto, P., Morrione, A., Canzonieri, V., Colombatti, A., 2005. p27(Kip1)-stathmin interaction influences sarcoma cell migration and invasion. Cancer Cell 7, 51–63. doi:10.1016/j.ccr.2004.11.025

Bamberger, C.M., Schulte, H.M., Chrousos, G.P., 1996. Molecular determinants of glucocorticoid receptor function and tissue sensitivity to glucocorticoids. Endocr. Rev. 17, 245–261. doi:10.1210/edrv-17-3-245

Banerji, S., Cibulskis, K., Rangel-Escareno, C., Brown, K.K., Carter, S.L., Frederick, A.M., Lawrence, M.S., Sivachenko, A.Y., Sougnez, C., Zou, L., Cortes, M.L., Fernandez-Lopez, J.C., Peng, S., Ardlie, K.G., Auclair, D., Bautista-Piña, V., Duke, F., Francis, J., Jung, J., Maffuz-Aziz, A., Onofrio, R.C., Parkin, M., Pho, N.H., Quintanar-Jurado, V., Ramos, A.H., Rebollar-Vega, R., Rodriguez-Cuevas, S., Romero-Cordoba, S.L., Schumacher, S.E., Stransky, N., Thompson, K.M., Uribe-Figueroa, L., Baselga, J., Beroukhim, R., Polyak, K., Sgroi, D.C., Richardson, A.L., Jimenez-Sanchez, G., Lander, E.S., Gabriel, S.B., Garraway, L.A., Golub, T.R., Melendez-Zajgla,

J., Toker, A., Getz, G., Hidalgo-Miranda, A., Meyerson, M., 2012. Sequence analysis of mutations and translocations across breast cancer subtypes. Nature 486, 405–409. doi:10.1038/nature11154

Baysal, B.E., Ferrell, R.E., Willett-Brozick, J.E., Lawrence, E.C., Myssiorek, D., Bosch, A., van der Mey, A., Taschner, P.E., Rubinstein, W.S., Myers, E.N., Richard, C.W., Cornelisse, C.J., Devilee, P., Devlin, B., 2000. Mutations in SDHD, a mitochondrial complex II gene, in hereditary paraganglioma. Science 287, 848–851.

Bellard, M., Dretzen, G., Giangrande, A., Ramain, P., 1989. Nuclease digestion of transcriptionally active chromatin. Methods Enzymol. 170, 317–346.

Bernardin-Fried, F., Kummalue, T., Leijen, S., Collector, M.I., Ravid, K., Friedman, A.D., 2004. AML1/RUNX1 increases during G1 to S cell cycle progression independent of cytokine-dependent phosphorylation and induces cyclin D3 gene expression. J. Biol. Chem. 279, 15678–15687. doi:10.1074/jbc.M310023200

Besson, A., Gurian-West, M., Schmidt, A., Hall, A., Roberts, J.M., 2004. p27Kip1 modulates cell migration through the regulation of RhoA activation. Genes Dev. 18, 862–876. doi:10.1101/gad.1185504

Besson, A., Hwang, H.C., Cicero, S., Donovan, S.L., Gurian-West, M., Johnson, D., Clurman, B.E., Dyer, M.A., Roberts, J.M., 2007. Discovery of an oncogenic activity in p27Kip1 that causes stem cell expansion and a multiple tumor phenotype. Genes Dev. 21, 1731–1746. doi:10.1101/gad.1556607

Biggs, J.R., Peterson, L.F., Zhang, Y., Kraft, A.S., Zhang, D.-E., 2006. AML1/RUNX1 Phosphorylation by Cyclin-Dependent Kinases Regulates the Degradation of AML1/RUNX1 by the Anaphase-Promoting Complex. Mol. Cell. Biol. 26, 7420–7429. doi:10.1128/MCB.00597-06

Blagosklonny, M.V., 2002. Are p27 and p21 cytoplasmic oncoproteins? Cell Cycle Georget. Tex 1, 391–393. doi:10.4161/cc.1.6.262

Blain, S.W., 2008. Switching cyclin D-Cdk4 kinase activity on and off. Cell Cycle Georget. Tex 7, 892–898. doi:10.4161/cc.7.7.5637

Blyth, K., Cameron, E.R., Neil, J.C., 2005. The RUNX genes: gain or loss of function in cancer. Nat. Rev. Cancer 5, 376–387. doi:10.1038/nrc1607

Blyth, K., Slater, N., Hanlon, L., Bell, M., Mackay, N., Stewart, M., Neil, J.C., Cameron, E.R., 2009. Runx1 promotes B-cell survival and lymphoma development. Blood Cells. Mol. Dis. 43, 12–19. doi:10.1016/j.bcmd.2009.01.013

Borberg, A., 1951. Clinical and genetic investigations into tuberous sclerosis and Recklinghausen's neurofibromatosis; contribution to elucidation of interrelationship and eugenics of the syndromes. Acta Psychiatr. Neurol. Scand. Suppl. 71, 1–239.

Bravo, E.L., Tagle, R., 2003. Pheochromocytoma: state-of-the-art and future prospects. Endocr. Rev. 24, 539–553. doi:10.1210/er.2002-0013

Breuer, H.W., Skyschally, A., Schulz, R., Martin, C., Wehr, M., Heusch, G., 1993. Heart rate variability and circulating catecholamine concentrations during steady state exercise in healthy volunteers. Br. Heart J. 70, 144–149.

Brivanlou, A.H., Darnell, J.E., 2002. Signal transduction and the control of gene expression. Science 295, 813–818. doi:10.1126/science.1066355

Burnichon, N., Brière, J.-J., Libé, R., Vescovo, L., Rivière, J., Tissier, F., Jouanno, E., Jeunemaitre, X., Bénit, P., Tzagoloff, A., Rustin, P., Bertherat, J., Favier, J., Gimenez-Roqueplo, A.-P., 2010. SDHA is a tumor suppressor gene causing paraganglioma. Hum. Mol. Genet. 19, 3011–3020. doi:10.1093/hmg/ddq206

Burnichon, N., Vescovo, L., Amar, L., Libé, R., de Reynies, A., Venisse, A., Jouanno, E., Laurendeau, I., Parfait, B., Bertherat, J., Plouin, P.-F., Jeunemaitre, X., Favier, J., Gimenez-Roqueplo, A.-P., 2011. Integrative genomic analysis reveals somatic mutations in pheochromocytoma and paraganglioma. Hum. Mol. Genet. 20, 3974–3985. doi:10.1093/hmg/ddr324

Bywater, M.J., Pearson, R.B., McArthur, G.A., Hannan, R.D., 2013. Dysregulation of the basal RNA polymerase transcription apparatus in cancer. Nat. Rev. Cancer 13, 299–314. doi:10.1038/nrc3496

Cabrera, J.R., Bouzas-Rodriguez, J., Tauszig-Delamasure, S., Mehlen, P., 2011. RET modulates cell adhesion via its cleavage by caspase in sympathetic neurons. J. Biol. Chem. 286, 14628–14638. doi:10.1074/jbc.M110.195461

Carrano, A.C., Eytan, E., Hershko, A., Pagano, M., 1999. SKP2 is required for ubiquitin-mediated degradation of the CDK inhibitor p27. Nat. Cell Biol. 1, 193–199.

Carty, S.E., Helm, A.K., Amico, J.A., Clarke, M.R., Foley, T.P., Watson, C.G., Mulvihill, J.J., 1998. The variable penetrance and spectrum of manifestations of multiple endocrine neoplasia type 1. Surgery 124, 1106-1113; discussion 1113-1114.

Cascon, A., Ruiz-Llorente, S., Fraga, M.F., Leton, R., Telleria, D., Sastre, J., Diez, J.J., Martinez Diaz-Guerra, G., Diaz Perez, J.A., Benitez, J., Esteller, M., Robledo, M., 2004. Genetic and epigenetic profile of sporadic pheochromocytomas. J. Med. Genet. 41, e30.

Castro-Vega, L.J., Buffet, A., De Cubas, A.A., Cascón, A., Menara, M., Khalifa, E., Amar, L., Azriel, S., Bourdeau, I., Chabre, O., Currás-Freixes, M., Franco-Vidal, V., Guillaud-Bataille, M., Simian, C., Morin, A., Letón, R., Gómez-Graña, A., Pollard, P.J., Rustin, P., Robledo, M., Favier, J., Gimenez-Roqueplo, A.-P., 2014. Germline mutations in FH confer predisposition to malignant pheochromocytomas and paragangliomas. Hum. Mol. Genet. 23, 2440–2446. doi:10.1093/hmg/ddt639

Castro-Vega, L.J., Letouzé, E., Burnichon, N., Buffet, A., Disderot, P.-H., Khalifa, E., Loriot, C., Elarouci, N., Morin, A., Menara, M., Lepoutre-Lussey, C., Badoual, C., Sibony, M., Dousset, B., Libé, R., Zinzindohoue, F., Plouin, P.F., Bertherat, J., Amar, L., de Reyniès, A., Favier, J., Gimenez-Roqueplo, A.-P., 2015. Multi-omics analysis defines core genomic alterations in pheochromocytomas and paragangliomas. Nat. Commun. 6, 6044. doi:10.1038/ncomms7044

Cervoni, L., Egistelli, L., Eufemi, M., Scotto d'Abusco, A., Altieri, F., Lascu, I., Turano, C., Giartosio, A., 2006. DNA sequences acting as binding sites for NM23/NDPK proteins in melanoma M14 cells. J. Cell. Biochem. 98, 421–428. doi:10.1002/jcb.20808

Cervoni, L., Pietrangeli, P., Chichiarelli, S., Altieri, F., Egistelli, L., Turano, C., Lascu, I., Giartosio, A., 2003. In vivo cross-linking of nm23/nucleoside diphosphate kinase to the PDGF-A gene promoter. Mol. Biol. Rep. 30, 33–40.

Chaki, M., Airik, R., Ghosh, A.K., Giles, R.H., Chen, R., Slaats, G.G., Wang, H., Hurd, T.W., Zhou, W., Cluckey, A., Gee, H.Y., Ramaswami, G., Hong, C.-J., Hamilton, B.A., Cervenka, I., Ganji, R.S., Bryja, V., Arts, H.H., van Reeuwijk, J., Oud, M.M., Letteboer, S.J.F., Roepman, R., Husson, H., Ibraghimov-Beskrovnaya, O., Yasunaga, T., Walz, G., Eley, L., Sayer, J.A., Schermer, B., Liebau, M.C., Benzing, T., Le Corre, S., Drummond, I., Janssen, S., Allen, S.J., Natarajan, S., O'Toole, J.F., Attanasio, M., Saunier, S., Antignac, C., Koenekoop, R.K., Ren, H., Lopez, I., Nayir, A., Stoetzel, C., Dollfus, H., Massoudi, R., Gleeson, J.G., Andreoli, S.P., Doherty, D.G., Lindstrad, A., Golzio, C., Katsanis, N., Pape, L., Abboud, E.B., Al-Rajhi, A.A., Lewis, R.A., Omran, H., Lee, E.Y.-H.P., Wang, S., Sekiguchi, J.M., Saunders, R., Johnson, C.A., Garner, E., Vanselow, K., Andersen, J.S., Shlomai, J., Nurnberg, G., Nurnberg, P., Levy, S., Smogorzewska, A., Otto, E.A., Hildebrandt, F., 2012. Exome capture reveals ZNF423 and CEP164 mutations, linking renal ciliopathies to DNA damage response signaling. Cell 150, 533–548. doi:10.1016/j.cell.2012.06.028

Chandramohan, V., Mineva, N.D., Burke, B., Jeay, S., Wu, M., Shen, J., Yang, W., Hann, S.R., Sonenshein, G.E., 2008. c-Myc represses FOXO3a-mediated transcription of the gene encoding the p27(Kip1) cyclin dependent kinase inhibitor. J. Cell. Biochem. 104, 2091–2106. doi:10.1002/jcb.21765

Chandrasekharappa, S.C., Guru, S.C., Manickam, P., Olufemi, S.E., Collins, F.S., Emmert-Buck, M.R., Debelenko, L.V., Zhuang, Z., Lubensky, I.A., Liotta, L.A., Crabtree, J.S., Wang, Y., Roe, B.A., Weisemann, J., Boguski, M.S., Agarwal, S.K., Kester, M.B., Kim, Y.S., Heppner, C., Dong, Q., Spiegel, A.M., Burns, A.L., Marx, S.J., 1997. Positional cloning of the gene for multiple endocrine neoplasia-type 1. Science 276, 404–407.

Chen, F., Kim, E., Wang, C.-C., Harrison, L.E., 2005. Ciglitazone-induced p27 gene transcriptional activity is mediated through Sp1 and is negatively regulated by the MAPK signaling pathway. Cell. Signal. 17, 1572–1577. doi:10.1016/j.cellsig.2005.03.012

Chen, K.-B., Zhang, Y., 2010. A varying threshold method for ChIP peak-calling using multiple sources of information. Bioinforma. Oxf. Engl. 26, i504-510. doi:10.1093/bioinformatics/btq379

Cheng, C.K., Chan, N.P.H., Wan, T.S.K., Lam, L.Y., Cheung, C.H.Y., Wong, T.H.Y., Ip, R.K.L., Wong, R.S.M., Ng, M.H.L., 2016. Helicase-like transcription factor is a RUNX1 target whose downregulation promotes genomic instability and correlates with complex cytogenetic features in acute myeloid leukemia. Haematologica 101, 448–457. doi:10.3324/haematol.2015.137125

Cheng, L.E., Zhang, J., Reed, R.R., 2007. The transcription factor Zfp423/OAZ is required for cerebellar development and CNS midline patterning. Dev. Biol. 307, 43–52. doi:10.1016/j.ydbio.2007.04.005

Cheung, P.S., Thompson, N.W., Dmuchowski, C.F., Sisson, J.C., 1988. Spectrum of pheochromocytoma in the 131I-MIBG era. World J. Surg. 12, 546–551.

Chu, I., Sun, J., Arnaout, A., Kahn, H., Hanna, W., Narod, S., Sun, P., Tan, C.-K., Hengst, L., Slingerland, J., 2007. p27 phosphorylation by Src regulates inhibition of cyclin E-Cdk2. Cell 128, 281–294. doi:10.1016/j.cell.2006.11.049

Chu, I.M., Hengst, L., Slingerland, J.M., 2008. The Cdk inhibitor p27 in human cancer: prognostic potential and relevance to anticancer therapy. Nat. Rev. Cancer 8, 253–267. doi:10.1038/nrc2347

Chuang, L.S.H., Ito, K., Ito, Y., 2013. RUNX family: Regulation and diversification of roles through interacting proteins. Int. J. Cancer 132, 1260–1271. doi:10.1002/ijc.27964

Cochard, P., Goldstein, M., Black, I.B., 1978. Ontogenetic appearance and disappearance of tyrosine hydroxylase and catecholamines in the rat embryo. Proc. Natl. Acad. Sci. U. S. A. 75, 2986–2990.

Cockburn, J.G., Richardson, D.S., Gujral, T.S., Mulligan, L.M., 2010. RET-mediated cell adhesion and migration require multiple integrin subunits. J. Clin. Endocrinol. Metab. 95, E342-346. doi:10.1210/jc.2010-0771

Collard, J.G., 2004. Cancer: Kip moving. Nature 428, 705–708. doi:10.1038/428705a

Comino-Méndez, I., Gracia-Aznárez, F.J., Schiavi, F., Landa, I., Leandro-García, L.J., Letón, R., Honrado, E., Ramos-Medina, R., Caronia, D., Pita, G., Gómez-Graña, A., de Cubas, A.A., Inglada-Pérez, L., Maliszewska, A., Taschin, E., Bobisse, S., Pica, G., Loli, P., Hernández-Lavado, R., Díaz, J.A., Gómez-Morales, M., González-Neira, A., Roncador, G., Rodríguez-Antona, C., Benítez, J., Mannelli, M., Opocher, G., Robledo, M., Cascón, A., 2011. Exome sequencing identifies MAX mutations as a cause of hereditary pheochromocytoma. Nat. Genet. 43, 663–667. doi:10.1038/ng.861

Craven, S.E., Lim, K.-C., Ye, W., Engel, J.D., de Sauvage, F., Rosenthal, A., 2004. Gata2 specifies serotonergic neurons downstream of sonic hedgehog. Dev. Camb. Engl. 131, 1165–1173. doi:10.1242/dev.01024

Daga, A., Karlovich, C.A., Dumstrei, K., Banerjee, U., 1996. Patterning of cells in the Drosophila eye by Lozenge, which shares homologous domains with AML1. Genes Dev. 10, 1194–1205.

Dahia, P.L.M., 2014. Pheochromocytoma and paraganglioma pathogenesis: learning from genetic heterogeneity. Nat. Rev. Cancer 14, 108–119. doi:10.1038/nrc3648

Dalgin, G., Goldman, D.C., Donley, N., Ahmed, R., Eide, C.A., Christian, J.L., 2007. GATA-2 functions downstream of BMPs and CaM KIV in ectodermal cells during primitive hematopoiesis. Dev. Biol. 310, 454–469. doi:10.1016/j.ydbio.2007.08.012

Dannenberg, J.-H., David, G., Zhong, S., van der Torre, J., Wong, W.H., Depinho, R.A., 2005. mSin3A corepressor regulates diverse transcriptional networks governing normal and neoplastic growth and survival. Genes Dev. 19, 1581–1595. doi:10.1101/gad.1286905

Dodic, M., Wintour, E.M., Whitworth, J.A., Coghlan, J.P., 1999. Effect of steroid hormones on blood pressure. Clin. Exp. Pharmacol. Physiol. 26, 550–552.

Dulak, A.M., Schumacher, S.E., van Lieshout, J., Imamura, Y., Fox, C., Shim, B., Ramos, A.H., Saksena, G., Baca, S.C., Baselga, J., Tabernero, J., Barretina, J., Enzinger, P.C., Corso, G., Roviello, F., Lin, L., Bandla, S., Luketich, J.D., Pennathur, A., Meyerson, M., Ogino, S., Shivdasani, R.A., Beer, D.G., Godfrey, T.E., Beroukhim, R., Bass, A.J., 2012. Gastrointestinal adenocarcinomas of the

esophagus, stomach, and colon exhibit distinct patterns of genome instability and oncogenesis. Cancer Res. 72, 4383–4393. doi:10.1158/0008-5472.CAN-11-3893

Edström Elder, E., Hjelm Skog, A.-L., Höög, A., Hamberger, B., 2003. The management of benign and malignant pheochromocytoma and abdominal paraganglioma. Eur. J. Surg. Oncol. J. Eur. Soc. Surg. Oncol. Br. Assoc. Surg. Oncol. 29, 278–283.

Egistelli, L., Chichiarelli, S., Gaucci, E., Eufemi, M., Schininà, M.E., Giorgi, A., Lascu, I., Turano, C., Giartosio, A., Cervoni, L., 2009. IFI16 and NM23 bind to a common DNA fragment both in the P53 and the cMYC gene promoters. J. Cell. Biochem. 106, 666–672. doi:10.1002/jcb.22053

Eisenhofer, G., Bornstein, S.R., Brouwers, F.M., Cheung, N.-K.V., Dahia, P.L., de Krijger, R.R., Giordano, T.J., Greene, L.A., Goldstein, D.S., Lehnert, H., Manger, W.M., Maris, J.M., Neumann, H.P.H., Pacak, K., Shulkin, B.L., Smith, D.I., Tischler, A.S., Young, W.F., 2004. Malignant pheochromocytoma: current status and initiatives for future progress. Endocr. Relat. Cancer 11, 423–436.

Eisenhofer, G., Huynh, T.-T., Pacak, K., Brouwers, F.M., Walther, M.M., Linehan, W.M., Munson, P.J., Mannelli, M., Goldstein, D.S., Elkahloun, A.G., 2004. Distinct gene expression profiles in norepinephrine- and epinephrine-producing hereditary and sporadic pheochromocytomas: activation of hypoxia-driven angiogenic pathways in von Hippel-Lindau syndrome. Endocr. Relat. Cancer 11, 897–911. doi:10.1677/erc.1.00838

el-Deiry, W.S., 1997. Role of oncogenes in resistance and killing by cancer therapeutic agents. Curr. Opin. Oncol. 9, 79–87.

El Wakil, A., Francius, C., Wolff, A., Pleau-Varet, J., Nardelli, J., 2006. The GATA2 transcription factor negatively regulates the proliferation of neuronal progenitors. Dev. Camb. Engl. 133, 2155–2165. doi:10.1242/dev.02377

Elagib, K.E., Xiao, M., Hussaini, I.M., Delehanty, L.L., Palmer, L.A., Racke, F.K., Birrer, M.J., Ganapathy-Kanniappan, S., Shanmugasundaram, G., McDevitt, M.A., Goldfarb, A.N., 2004. Jun blockade of erythropoiesis: role for repression of GATA-1 by HERP2. Mol. Cell. Biol. 24, 7779–7794. doi:10.1128/MCB.24.17.7779-7794.2004

El-Deiry, W.S., 2016. p21(WAF1) Mediates Cell-Cycle Inhibition, Relevant to Cancer Suppression and Therapy. Cancer Res. 76, 5189–5191. doi:10.1158/0008-5472.CAN-16-2055

Ellis, M.J., Ding, L., Shen, D., Luo, J., Suman, V.J., Wallis, J.W., Van Tine, B.A., Hoog, J., Goiffon, R.J., Goldstein, T.C., Ng, S., Lin, L., Crowder, R., Snider, J., Ballman, K., Weber, J., Chen, K., Koboldt, D.C., Kandoth, C., Schierding, W.S., McMichael, J.F., Miller, C.A., Lu, C., Harris, C.C., McLellan, M.D., Wendl, M.C., DeSchryver, K., Allred, D.C., Esserman, L., Unzeitig, G., Margenthaler, J., Babiera, G.V., Marcom, P.K., Guenther, J.M., Leitch, M., Hunt, K., Olson, J., Tao, Y., Maher, C.A., Fulton, L.L., Fulton, R.S., Harrison, M., Oberkfell, B., Du, F., Demeter, R., Vickery, T.L., Elhammali, A., Piwnica-Worms, H., McDonald, S., Watson, M., Dooling, D.J., Ota, D., Chang, L.-W., Bose, R., Ley, T.J., Piwnica-Worms, D., Stuart, J.M., Wilson, R.K., Mardis, E.R., 2012. Whole-genome analysis informs breast cancer response to aromatase inhibition. Nature 486, 353–360. doi:10.1038/nature11143

Ernsberger, U., Patzke, H., Tissier-Seta, J.P., Reh, T., Goridis, C., Rohrer, H., 1995. The expression of tyrosine hydroxylase and the transcription factors cPhox-2 and Cash-1: evidence for distinct inductive steps in the differentiation of chick sympathetic precursor cells. Mech. Dev. 52, 125–136.

Even, J.L., Crosby, C.G., Song, Y., McGirt, M.J., Devin, C.J., 2012. Effects of epidural steroid injections on blood glucose levels in patients with diabetes mellitus. Spine 37, E46-50. doi:10.1097/BRS.0b013e31821fd21f

Fernández-Calvet, L., García-Mayor, R.V., 1994. Incidence of pheochromocytoma in South Galicia, Spain. J. Intern. Med. 236, 675–677.

Fero, M.L., Randel, E., Gurley, K.E., Roberts, J.M., Kemp, C.J., 1998. The murine gene p27Kip1 is haplo-insufficient for tumour suppression. Nature 396, 177–180. doi:10.1038/24179

Fero, M.L., Rivkin, M., Tasch, M., Porter, P., Carow, C.E., Firpo, E., Polyak, K., Tsai, L.H., Broudy, V., Perlmutter, R.M., Kaushansky, K., Roberts, J.M., 1996. A syndrome of multiorgan hyperplasia

with features of gigantism, tumorigenesis, and female sterility in p27(Kip1)-deficient mice. Cell 85, 733–744.

Frank, R.C., Sun, X., Berguido, F.J., Jakubowiak, A., Nimer, S.D., 1999. The t(8;21) fusion protein, AML1/ETO, transforms NIH3T3 cells and activates AP-1. Oncogene 18, 1701–1710. doi:10.1038/sj.onc.1202459

Friedman, A.D., 2002. Transcriptional regulation of myelopoiesis. Int. J. Hematol. 75, 466–472.

Fritz, A., Walch, A., Piotrowska, K., Rosemann, M., Schäffer, E., Weber, K., Timper, A., Wildner, G., Graw, J., Höfler, H., Atkinson, M.J., 2002. Recessive transmission of a multiple endocrine neoplasia syndrome in the rat. Cancer Res. 62, 3048–3051.

Fujita, Y., Nishimura, M., Taniwaki, M., Abe, T., Okuda, T., 2001. Identification of an alternatively spliced form of the mouse AML1/RUNX1 gene transcript AML1c and its expression in early hematopoietic development. Biochem. Biophys. Res. Commun. 281, 1248–1255. doi:10.1006/bbrc.2001.4513

Gaertner, F.C., Wiedemann, T., Yousefi, B.H., Lee, M., Repokis, I., Higuchi, T., Nekolla, S.G., Yu, M., Robinson, S., Schwaiger, M., Pellegata, N.S., 2013. Preclinical evaluation of 18F-LMI1195 for in vivo imaging of pheochromocytoma in the MENX tumor model. J. Nucl. Med. Off. Publ. Soc. Nucl. Med. 54, 2111–2117. doi:10.2967/jnumed.113.119966

Garcia-Lavandeira, M., Diaz-Rodriguez, E., Garcia-Rendueles, M.E.R., Rodrigues, J.S., Perez-Romero, S., Bravo, S.B., Alvarez, C.V., 2010. Functional role of the RET dependence receptor, GFRa co-receptors and ligands in the pituitary. Front. Horm. Res. 38, 127–138. doi:10.1159/000318502

Garvie, C.W., Wolberger, C., 2001. Recognition of specific DNA sequences. Mol. Cell 8, 937–946.

Geoghegan, J.G., Emberton, M., Bloom, S.R., Lynn, J.A., 1998. Changing trends in the management of phaeochromocytoma. Br. J. Surg. 85, 117–120. doi:10.1046/j.1365-2168.1998.02875.x

Georgitsi, M., 2010. MEN-4 and other multiple endocrine neoplasias due to cyclin-dependent kinase inhibitors (p27(Kip1) and p18(INK4C)) mutations. Best Pract. Res. Clin. Endocrinol. Metab. 24, 425–437. doi:10.1016/j.beem.2010.01.001

Ghozi, M.C., Bernstein, Y., Negreanu, V., Levanon, D., Groner, Y., 1996. Expression of the human acute myeloid leukemia gene AML1 is regulated by two promoter regions. Proc. Natl. Acad. Sci. U. S. A. 93, 1935–1940.

Giasson, B.I., Bruening, W., Durham, H.D., Mushynski, W.E., 1999. Activation of stress-activated protein kinases correlates with neurite outgrowth induced by protease inhibition in PC12 cells. J. Neurochem. 72, 1081–1087.

Gil, D., Gutiérrez, D., Alarcón, B., 2001. Intracellular redistribution of nucleolin upon interaction with the CD3epsilon chain of the T cell receptor complex. J. Biol. Chem. 276, 11174–11179. doi:10.1074/jbc.M010114200

Gimenez-Roqueplo, A.-P., Dahia, P.L., Robledo, M., 2012. An update on the genetics of paraganglioma, pheochromocytoma, and associated hereditary syndromes. Horm. Metab. Res. Horm. Stoffwechselforschung Horm. Metab. 44, 328–333. doi:10.1055/s-0031-1301302

Gimenez-Roqueplo, A.-P., Favier, J., Rustin, P., Rieubland, C., Crespin, M., Nau, V., Khau Van Kien, P., Corvol, P., Plouin, P.-F., Jeunemaitre, X., COMETE Network, 2003. Mutations in the SDHB gene are associated with extra-adrenal and/or malignant phaeochromocytomas. Cancer Res. 63, 5615–5621.

Goldstein, R.E., O'Neill, J.A., Holcomb, G.W., Morgan, W.M., Neblett, W.W., Oates, J.A., Brown, N., Nadeau, J., Smith, B., Page, D.L., Abumrad, N.N., Scott, H.W., 1999. Clinical experience over 48 years with pheochromocytoma. Ann. Surg. 229, 755-764; discussion 764-766.

Gombart, A.F., Hofmann, W.-K., Kawano, S., Takeuchi, S., Krug, U., Kwok, S.H., Larsen, R.J., Asou, H., Miller, C.W., Hoelzer, D., Koeffler, H.P., 2002. Mutations in the gene encoding the transcription factor CCAAT/enhancer binding protein alpha in myelodysplastic syndromes and acute myeloid leukemias. Blood 99, 1332–1340.

Gombos, E.A., Hulet, W.H., Bopp, P., Goldringw, null, Baldwin, D.S., Chasis, H., 1962. Reactivity of renal and systemic circulations to vasoconstrictor agents in normotensive and hypertensive subjects. J. Clin. Invest. 41, 203–217. doi:10.1172/JCI104472

Grant, C.E., Bailey, T.L., Noble, W.S., 2011. FIMO: scanning for occurrences of a given motif. Bioinforma. Oxf. Engl. 27, 1017–1018. doi:10.1093/bioinformatics/btr064

Grimmler, M., Wang, Y., Mund, T., Cilensek, Z., Keidel, E.-M., Waddell, M.B., Jäkel, H., Kullmann, M., Kriwacki, R.W., Hengst, L., 2007. Cdk-inhibitory activity and stability of p27Kip1 are directly regulated by oncogenic tyrosine kinases. Cell 128, 269–280. doi:10.1016/j.cell.2006.11.047

Haferlach, C., Bacher, U., Kohlmann, A., Schindela, S., Alpermann, T., Kern, W., Schnittger, S., Haferlach, T., 2011. CDKN1B, encoding the cyclin-dependent kinase inhibitor 1B (p27), is located in the minimally deleted region of 12p abnormalities in myeloid malignancies and its low expression is a favorable prognostic marker in acute myeloid leukemia. Haematologica 96, 829–836. doi:10.3324/haematol.2010.035584

Haferlach, C., Grossmann, V., Kohlmann, A., Schindela, S., Kern, W., Schnittger, S., Haferlach, T., 2012. Deletion of the tumor-suppressor gene NF1 occurs in 5% of myeloid malignancies and is accompanied by a mutation in the remaining allele in half of the cases. Leukemia 26, 834–839. doi:10.1038/leu.2011.296

Hansford, J.R., Mulligan, L.M., 2000. Multiple endocrine neoplasia type 2 and RET: from neoplasia to neurogenesis. J. Med. Genet. 37, 817–827.

Hao, H.-X., Khalimonchuk, O., Schraders, M., Dephoure, N., Bayley, J.-P., Kunst, H., Devilee, P., Cremers, C.W.R.J., Schiffman, J.D., Bentz, B.G., Gygi, S.P., Winge, D.R., Kremer, H., Rutter, J., 2009. SDH5, a gene required for flavination of succinate dehydrogenase, is mutated in paraganglioma. Science 325, 1139–1142. doi:10.1126/science.1175689

Harder, L., Eschenburg, G., Zech, A., Kriebitzsch, N., Otto, B., Streichert, T., Behlich, A.-S., Dierck, K., Klingler, B., Hansen, A., Stanulla, M., Zimmermann, M., Kremmer, E., Stocking, C., Horstmann, M.A., 2013. Aberrant ZNF423 impedes B cell differentiation and is linked to adverse outcome of ETV6-RUNX1 negative B precursor acute lymphoblastic leukemia. J. Exp. Med. 210, 2289–2304. doi:10.1084/jem.20130497

Harder, L., Otto, B., Horstmann, M.A., 2014. Transcriptional dysregulation of the multifunctional zinc finger factor 423 in acute lymphoblastic leukemia of childhood. Genomics Data 2, 96–98. doi:10.1016/j.gdata.2014.05.009

Harper, J.W., Adami, G.R., Wei, N., Keyomarsi, K., Elledge, S.J., 1993. The p21 Cdk-interacting protein Cip1 is a potent inhibitor of G1 cyclin-dependent kinases. Cell 75, 805–816.

Hata, A., Lagna, G., Massagué, J., Hemmati-Brivanlou, A., 1998. Smad6 inhibits BMP/Smad1 signaling by specifically competing with the Smad4 tumor suppressor. Genes Dev. 12, 186–197.

Hata, A., Lo, R.S., Wotton, D., Lagna, G., Massagué, J., 1997. Mutations increasing autoinhibition inactivate tumour suppressors Smad2 and Smad4. Nature 388, 82–87. doi:10.1038/40424

Hata, A., Seoane, J., Lagna, G., Montalvo, E., Hemmati-Brivanlou, A., Massagué, J., 2000. OAZ uses distinct DNA- and protein-binding zinc fingers in separate BMP-Smad and Olf signaling pathways. Cell 100, 229–240.

He, B.Z., Holloway, A.K., Maerkl, S.J., Kreitman, M., 2011. Does positive selection drive transcription factor binding site turnover? A test with Drosophila cis-regulatory modules. PLoS Genet. 7, e1002053. doi:10.1371/journal.pgen.1002053

Heath, H., Ribeiro de Almeida, C., Sleutels, F., Dingjan, G., van de Nobelen, S., Jonkers, I., Ling, K.-W., Gribnau, J., Renkawitz, R., Grosveld, F., Hendriks, R.W., Galjart, N., 2008. CTCF regulates cell cycle progression of alphabeta T cells in the thymus. EMBO J. 27, 2839–2850. doi:10.1038/emboj.2008.214

Heppner, C., Bilimoria, K.Y., Agarwal, S.K., Kester, M., Whitty, L.J., Guru, S.C., Chandrasekharappa, S.C., Collins, F.S., Spiegel, A.M., Marx, S.J., Burns, A.L., 2001. The tumor suppressor protein menin interacts with NF-kappaB proteins and inhibits NF-kappaB-mediated transactivation. Oncogene 20, 4917–4925. doi:10.1038/sj.onc.1204529

Hescot, S., Leboulleux, S., Amar, L., Vezzosi, D., Borget, I., Bournaud-Salinas, C., de la Fouchardiere, C., Libé, R., Do Cao, C., Niccoli, P., Tabarin, A., Raingeard, I., Chougnet, C., Giraud, S., Gimenez-Roqueplo, A.-P., Young, J., Borson-Chazot, F., Bertherat, J., Wemeau, J.-L., Bertagna, X., Plouin, P.-F., Schlumberger, M., Baudin, E., French group of Endocrine and Adrenal tumors (Groupe des Tumeurs Endocrines-REseau NAtional des Tumeurs ENdocrines and COrtico-

MEdullo Tumeurs Endocrines networks), 2013. One-year progression-free survival of therapy-naive patients with malignant pheochromocytoma and paraganglioma. J. Clin. Endocrinol. Metab. 98, 4006–4012. doi:10.1210/jc.2013-1907

Hoi, C.S.L., Lee, S.E., Lu, S.-Y., McDermitt, D.J., Osorio, K.M., Piskun, C.M., Peters, R.M., Paus, R., Tumbar, T., 2010. Runx1 directly promotes proliferation of hair follicle stem cells and epithelial tumor formation in mouse skin. Mol. Cell. Biol. 30, 2518–2536. doi:10.1128/MCB.01308-09

Huang, C.-S., Ho, W.-L., Lee, W.-S., Sheu, M.-T., Wang, Y.-J., Tu, S.-H., Chen, R.-J., Chu, J.-S., Chen, L.-C., Lee, C.-H., Tseng, H., Ho, Y.-S., Wu, C.-H., 2008. SP1-regulated p27/Kip1 gene expression is involved in terbinafine-induced human A431 cancer cell differentiation: an in vitro and in vivo study. Biochem. Pharmacol. 75, 1783–1796. doi:10.1016/j.bcp.2008.02.005

Huang, G., Shigesada, K., Ito, K., Wee, H.J., Yokomizo, T., Ito, Y., 2001. Dimerization with PEBP2beta protects RUNX1/AML1 from ubiquitin-proteasome-mediated degradation. EMBO J. 20, 723–733. doi:10.1093/emboj/20.4.723

Huang, G., Zhang, P., Hirai, H., Elf, S., Yan, X., Chen, Z., Koschmieder, S., Okuno, Y., Dayaram, T., Growney, J.D., Shivdasani, R.A., Gilliland, D.G., Speck, N.A., Nimer, S.D., Tenen, D.G., 2008. PU.1 is a major downstream target of AML1 (RUNX1) in adult mouse hematopoiesis. Nat. Genet. 40, 51–60. doi:10.1038/ng.2007.7

Huang, J., Bi, Y., Zhu, G.-H., He, Y., Su, Y., He, B.-C., Wang, Y., Kang, Q., Chen, L., Zuo, G.-W., Luo, Q., Shi, Q., Zhang, B.-Q., Huang, A., Zhou, L., Feng, T., Luu, H.H., Haydon, R.C., He, T.-C., Tang, N., 2009. Retinoic acid signalling induces the differentiation of mouse fetal liver-derived hepatic progenitor cells. Liver Int. Off. J. Int. Assoc. Study Liver 29, 1569–1581. doi:10.1111/j.1478-3231.2009.02111.x

Huang, S., Laoukili, J., Epping, M.T., Koster, J., Hölzel, M., Westerman, B.A., Nijkamp, W., Hata, A., Asgharzadeh, S., Seeger, R.C., Versteeg, R., Beijersbergen, R.L., Bernards, R., 2009. ZNF423 is critically required for retinoic acid-induced differentiation and is a marker of neuroblastoma outcome. Cancer Cell 15, 328–340. doi:10.1016/j.ccr.2009.02.023

Huber, K., 2006. The sympathoadrenal cell lineage: specification, diversification, and new perspectives. Dev. Biol. 298, 335–343. doi:10.1016/j.ydbio.2006.07.010

Hughes, C.M., Rozenblatt-Rosen, O., Milne, T.A., Copeland, T.D., Levine, S.S., Lee, J.C., Hayes, D.N., Shanmugam, K.S., Bhattacharjee, A., Biondi, C.A., Kay, G.F., Hayward, N.K., Hess, J.L., Meyerson, M., 2004. Menin associates with a trithorax family histone methyltransferase complex and with the hoxc8 locus. Mol. Cell 13, 587–597.

Hydbring, P., Castell, A., Larsson, L.-G., 2017. MYC Modulation around the CDK2/p27/SKP2 Axis. Genes 8. doi:10.3390/genes8070174

Ille, F., Atanasoski, S., Falk, S., Ittner, L.M., Märki, D., Büchmann-Møller, S., Wurdak, H., Suter, U., Taketo, M.M., Sommer, L., 2007. Wnt/BMP signal integration regulates the balance between proliferation and differentiation of neuroepithelial cells in the dorsal spinal cord. Dev. Biol. 304, 394–408. doi:10.1016/j.ydbio.2006.12.045

Imai, Y., Kurokawa, M., Yamaguchi, Y., Izutsu, K., Nitta, E., Mitani, K., Satake, M., Noda, T., Ito, Y., Hirai, H., 2004. The corepressor mSin3A regulates phosphorylation-induced activation, intranuclear location, and stability of AML1. Mol. Cell. Biol. 24, 1033–1043.

Inoue, K.-I., Ito, Y., 2011. Neuroblastoma cell proliferation is sensitive to changes in levels of RUNX1 and RUNX3 protein. Gene 487, 151–155. doi:10.1016/j.gene.2011.05.016

Ishida, N., Hara, T., Kamura, T., Yoshida, M., Nakayama, K., Nakayama, K.I., 2002. Phosphorylation of p27Kip1 on serine 10 is required for its binding to CRM1 and nuclear export. J. Biol. Chem. 277, 14355–14358. doi:10.1074/jbc.C100762200

Ito, Y., 1999. Molecular basis of tissue-specific gene expression mediated by the runt domain transcription factor PEBP2/CBF. Genes Cells Devoted Mol. Cell. Mech. 4, 685–696.

Jalil, N.D., Pattou, F.N., Combemale, F., Chapuis, Y., Henry, J.F., Peix, J.L., Proye, C.A., 1998. Effectiveness and limits of preoperative imaging studies for the localisation of pheochromocytomas and paragangliomas: a review of 282 cases. French Association of

Surgery (AFC), and The French Association of Endocrine Surgeons (AFCE). Eur. J. Surg. Acta Chir. 164, 23–28. doi:10.1080/110241598750004913

James, M.K., Ray, A., Leznova, D., Blain, S.W., 2008. Differential modification of p27Kip1 controls its cyclin D-cdk4 inhibitory activity. Mol. Cell. Biol. 28, 498–510. doi:10.1128/MCB.02171-06

Ji, H., Jiang, H., Ma, W., Johnson, D.S., Myers, R.M., Wong, W.H., 2008. An integrated software system for analyzing ChIP-chip and ChIP-seq data. Nat. Biotechnol. 26, 1293–1300. doi:10.1038/nbt.1505

Jin, S., Mao, H., Schnepp, R.W., Sykes, S.M., Silva, A.C., D'Andrea, A.D., Hua, X., 2003. Menin associates with FANCD2, a protein involved in repair of DNA damage. Cancer Res. 63, 4204–4210.

Junion, G., Spivakov, M., Girardot, C., Braun, M., Gustafson, E.H., Birney, E., Furlong, E.E.M., 2012. A transcription factor collective defines cardiac cell fate and reflects lineage history. Cell 148, 473–486. doi:10.1016/j.cell.2012.01.030

Kadonaga, J.T., 2004. Regulation of RNA polymerase II transcription by sequence-specific DNA binding factors. Cell 116, 247–257.

Kaji, H., Canaff, L., Lebrun, J.J., Goltzman, D., Hendy, G.N., 2001. Inactivation of menin, a Smad3-interacting protein, blocks transforming growth factor type beta signaling. Proc. Natl. Acad. Sci. U. S. A. 98, 3837–3842. doi:10.1073/pnas.061358098

Kaloostian, P.E., Zadnik, P.L., Kim, J.E., Groves, M.L., Wolinsky, J.-P., Gokaslan, Z.L., Witham, T.F., Bydon, A., Sciubba, D.M., 2014. High incidence of morbidity following resection of metastatic pheochromocytoma in the spine. J. Neurosurg. Spine 20, 726–733. doi:10.3171/2014.3.SPINE13535

Kamachi, Y., Ogawa, E., Asano, M., Ishida, S., Murakami, Y., Satake, M., Ito, Y., Shigesada, K., 1990. Purification of a mouse nuclear factor that binds to both the A and B cores of the polyomavirus enhancer. J. Virol. 64, 4808–4819.

Kamura, T., Hara, T., Matsumoto, M., Ishida, N., Okumura, F., Hatakeyama, S., Yoshida, M., Nakayama, K., Nakayama, K.I., 2004. Cytoplasmic ubiquitin ligase KPC regulates proteolysis of p27(Kip1) at G1 phase. Nat. Cell Biol. 6, 1229–1235. doi:10.1038/ncb1194

Kanno, Y., Kanno, T., Sakakura, C., Bae, S.C., Ito, Y., 1998. Cytoplasmic sequestration of the polyomavirus enhancer binding protein 2 (PEBP2)/core binding factor alpha (CBFalpha) subunit by the leukemia-related PEBP2/CBFbeta-SMMHC fusion protein inhibits PEBP2/CBF-mediated transactivation. Mol. Cell. Biol. 18, 4252–4261.

Kantorovich, V., Koch, C.A., Pacak, K., 2000. Pheochromocytoma and Paraganglioma, in: De Groot, L.J., Chrousos, G., Dungan, K., Feingold, K.R., Grossman, A., Hershman, J.M., Koch, C., Korbonits, M., McLachlan, R., New, M., Purnell, J., Rebar, R., Singer, F., Vinik, A. (Eds.), Endotext. MDText.com, Inc., South Dartmouth (MA).

Karagiannis, A., Mikhailidis, D.P., Athyros, V.G., Harsoulis, F., 2007. Pheochromocytoma: an update on genetics and management. Endocr. Relat. Cancer 14, 935–956. doi:10.1677/ERC-07-0142

Karunaratne, A., Hargrave, M., Poh, A., Yamada, T., 2002. GATA proteins identify a novel ventral interneuron subclass in the developing chick spinal cord. Dev. Biol. 249, 30–43.

Keller-Wood, M.E., Dallman, M.F., 1984. Corticosteroid inhibition of ACTH secretion. Endocr. Rev. 5, 1–24. doi:10.1210/edrv-5-1-1

Kheirelseid, E.A.H., Chang, K.H., Newell, J., Kerin, M.J., Miller, N., 2010. Identification of endogenous control genes for normalisation of real-time quantitative PCR data in colorectal cancer. BMC Mol. Biol. 11, 12. doi:10.1186/1471-2199-11-12

Kim, S.Y., Herbst, A., Tworkowski, K.A., Salghetti, S.E., Tansey, W.P., 2003. Skp2 regulates Myc protein stability and activity. Mol. Cell 11, 1177–1188.

Kim, W., Barron, D.A., San Martin, R., Chan, K.S., Tran, L.L., Yang, F., Ressler, S.J., Rowley, D.R., 2014. RUNX1 is essential for mesenchymal stem cell proliferation and myofibroblast differentiation. Proc. Natl. Acad. Sci. U. S. A. 111, 16389–16394. doi:10.1073/pnas.1407097111

Kiyokawa, H., Kineman, R.D., Manova-Todorova, K.O., Soares, V.C., Hoffman, E.S., Ono, M., Khanam, D., Hayday, A.C., Frohman, L.A., Koff, A., 1996. Enhanced growth of mice lacking the cyclin-dependent kinase inhibitor function of p27(Kip1). Cell 85, 721–732.

Knoepfler, P.S., Eisenman, R.N., 1999. Sin meets NuRD and other tails of repression. Cell 99, 447–450.

Knudsen, K.A., Horwitz, A.F., Buck, C.A., 1985. A monoclonal antibody identifies a glycoprotein complex involved in cell-substratum adhesion. Exp. Cell Res. 157, 218–226.

Koch, C.A., 2005. Molecular pathogenesis of MEN2-associated tumors. Fam. Cancer 4, 3–7. doi:10.1007/s10689-004-7022-3

Kodama, T., Bard-Chapeau, E.A., Newberg, J.Y., Kodama, M., Rangel, R., Yoshihara, K., Ward, J.M., Jenkins, N.A., Copeland, N.G., 2016. Two-Step Forward Genetic Screen in Mice Identifies Ral GTPase-Activating Proteins as Suppressors of Hepatocellular Carcinoma. Gastroenterology 151, 324–337.e12. doi:10.1053/j.gastro.2016.04.040

Korpershoek, E., Van Nederveen, F.H., Dannenberg, H., Petri, B.J., Komminoth, P., Perren, A., Lenders, J.W., Verhofstad, A.A., De Herder, W.W., De Krijger, R.R., Dinjens, W.N.M., 2006. Genetic analyses of apparently sporadic pheochromocytomas: the Rotterdam experience. Ann. N. Y. Acad. Sci. 1073, 138–148. doi:10.1196/annals.1353.014

Kreuz, L.E., Rose, R.M., Jennings, J.R., 1972. Suppression of plasma testosterone levels and psychological stress. A longitudinal study of young men in Officer Candidate School. Arch. Gen. Psychiatry 26, 479–482.

Krieger, E., Nabuurs, S.B., Vriend, G., 2003. Homology modeling. Methods Biochem. Anal. 44, 509–523.

Ku, S., Yoon, H., Suh, H.S., Chung, Y.-Y., 2003. Male-sterility of thermosensitive genic male-sterile rice is associated with premature programmed cell death of the tapetum. Planta 217, 559–565. doi:10.1007/s00425-003-1030-7

Kudva, Y.C., Sawka, A.M., Young, W.F., 2003. Clinical review 164: The laboratory diagnosis of adrenal pheochromocytoma: the Mayo Clinic experience. J. Clin. Endocrinol. Metab. 88, 4533–4539. doi:10.1210/jc.2003-030720

Kudva, Y.C., Young, W.F., 1997. Lightheaded spells and hypertension. Lancet Lond. Engl. 350, 1140. doi:10.1016/S0140-6736(97)08338-4

Lairmore, T.C., Piersall, L.D., DeBenedetti, M.K., Dilley, W.G., Mutch, M.G., Whelan, A.J., Zehnbauer, B., 2004. Clinical genetic testing and early surgical intervention in patients with multiple endocrine neoplasia type 1 (MEN 1). Ann. Surg. 239, 637-645; discussion 645-647.

Laity, J.H., Lee, B.M., Wright, P.E., 2001. Zinc finger proteins: new insights into structural and functional diversity. Curr. Opin. Struct. Biol. 11, 39–46.

Lancrin, C., Sroczynska, P., Stephenson, C., Allen, T., Kouskoff, V., Lacaud, G., 2009. The haemangioblast generates haematopoietic cells through a haemogenic endothelium stage. Nature 457, 892–895. doi:10.1038/nature07679

Langmead, B., Trapnell, C., Pop, M., Salzberg, S.L., 2009. Ultrafast and memory-efficient alignment of short DNA sequences to the human genome. Genome Biol. 10, R25. doi:10.1186/gb-2009-10-3-r25

Larrea, M.D., Wander, S.A., Slingerland, J.M., 2009. p27 as Jekyll and Hyde: regulation of cell cycle and cell motility. Cell Cycle Georget. Tex 8, 3455–3461. doi:10.4161/cc.8.21.9789

Latchman, D.S., 1997. Transcription factors: an overview. Int. J. Biochem. Cell Biol. 29, 1305–1312.

Lee, D.K., Duan, H.O., Chang, C., 2000. From androgen receptor to the general transcription factor TFIIH. Identification of cdk activating kinase (CAK) as an androgen receptor NH(2)-terminal associated coactivator. J. Biol. Chem. 275, 9308–9313.

Lee, J., Hoi, C.S.L., Lilja, K.C., White, B.S., Lee, S.E., Shalloway, D., Tumbar, T., 2013. Runx1 and p21 synergistically limit the extent of hair follicle stem cell quiescence in vivo. Proc. Natl. Acad. Sci. U. S. A. 110, 4634–4639. doi:10.1073/pnas.1213015110

Lee, M., Pellegata, N.S., 2013. Multiple endocrine neoplasia type 4. Front. Horm. Res. 41, 63–78. doi:10.1159/000345670

Lee, M., Theodoropoulou, M., Graw, J., Roncaroli, F., Zatelli, M.C., Pellegata, N.S., 2011. Levels of p27 sensitize to dual PI3K/mTOR inhibition. Mol. Cancer Ther. 10, 1450–1459. doi:10.1158/1535-7163.MCT-11-0188

Lee, M., Waser, B., Reubi, J.-C., Pellegata, N.S., 2012. Secretin receptor promotes the proliferation of endocrine tumor cells via the PI3K/AKT pathway. Mol. Endocrinol. Baltim. Md 26, 1394–1405. doi:10.1210/me.2012-1055

Lee, S.H., Kang, Y.J., Kim, D.H., Sung, B., Kang, J.A., Chun, P., Yoon, J.-H., Moon, H.R., Kim, H.S., Chung, H.Y., Kim, N.D., 2014. A novel oxiranylchromenone derivative, MHY336, induces apoptosis and cell cycle arrest via a p53- and p21-dependent pathway in HCT116 human colon cancer cells. Int. J. Oncol. 44, 943–949. doi:10.3892/ijo.2013.2226

Lee, S.-J., Youn, Y.C., Han, E.S., Lee, C.S., 2005. Depressant effect of mitochondrial respiratory complex inhibitors on proteasome inhibitor-induced mitochondrial dysfunction and cell death in PC12 cells. Neurochem. Res. 30, 1191–1200. doi:10.1007/s11064-005-8158-8

Lee, T.I., Johnstone, S.E., Young, R.A., 2006. Chromatin immunoprecipitation and microarray-based analysis of protein location. Nat. Protoc. 1, 729–748. doi:10.1038/nprot.2006.98

Leinhäuser, I., Richter, A., Lee, M., Höfig, I., Anastasov, N., Fend, F., Ercolino, T., Mannelli, M., Gimenez-Roqueplo, A.-P., Robledo, M., de Krijger, R., Beuschlein, F., Atkinson, M.J., Pellegata, N.S., 2015. Oncogenic features of the bone morphogenic protein 7 (BMP7) in pheochromocytoma. Oncotarget 6, 39111–39126. doi:10.18632/oncotarget.4912

Lelli, K.M., Slattery, M., Mann, R.S., 2012. Disentangling the many layers of eukaryotic transcriptional regulation. Annu. Rev. Genet. 46, 43–68. doi:10.1146/annurev-genet-110711-155437

Lenders, J.W.M., Pacak, K., Eisenhofer, G., 2002. New advances in the biochemical diagnosis of pheochromocytoma: moving beyond catecholamines. Ann. N. Y. Acad. Sci. 970, 29–40.

Lenhard, B., Sandelin, A., Carninci, P., 2012. Metazoan promoters: emerging characteristics and insights into transcriptional regulation. Nat. Rev. Genet. 13, 233–245. doi:10.1038/nrg3163

Levanon, D., Glusman, G., Bangsow, T., Ben-Asher, E., Male, D.A., Avidan, N., Bangsow, C., Hattori, M., Taylor, T.D., Taudien, S., Blechschmidt, K., Shimizu, N., Rosenthal, A., Sakaki, Y., Lancet, D., Groner, Y., 2001. Architecture and anatomy of the genomic locus encoding the human leukemia-associated transcription factor RUNX1/AML1. Gene 262, 23–33.

Liebermann, F., Korf, B.R., 1999. Emerging approaches toward the treatment of neurofibromatoses. Genet. Med. Off. J. Am. Coll. Med. Genet. 1, 158-164; quiz 165-166. doi:10.1097/00125817-199905000-00008

Lin, S.Y., Elledge, S.J., 2003. Multiple tumor suppressor pathways negatively regulate telomerase. Cell 113, 881–889.

Littlewood, T.D., Evan, G.I., 1995. Transcription factors 2: helix-loop-helix. Protein Profile 2, 621–702.

Lizama, C.O., Hawkins, J.S., Schmitt, C.E., Bos, F.L., Zape, J.P., Cautivo, K.M., Borges Pinto, H., Rhyner, A.M., Yu, H., Donohoe, M.E., Wythe, J.D., Zovein, A.C., 2015. Repression of arterial genes in hemogenic endothelium is sufficient for haematopoietic fate acquisition. Nat. Commun. 6, 7739. doi:10.1038/ncomms8739

Logan, T.T., Rusnak, M., Symes, A.J., 2015. Runx1 promotes proliferation and neuronal differentiation in adult mouse neurosphere cultures. Stem Cell Res. 15, 554–564. doi:10.1016/j.scr.2015.09.014

Loke, J., Assi, S.A., Imperato, M.R., Ptasinska, A., Cauchy, P., Grabovska, Y., Soria, N.M., Raghavan, M., Delwel, H.R., Cockerill, P.N., Heidenreich, O., Bonifer, C., 2017. RUNX1-ETO and RUNX1-EVI1 Differentially Reprogram the Chromatin Landscape in t(8;21) and t(3;21) AML. Cell Rep. 19, 1654–1668. doi:10.1016/j.celrep.2017.05.005

López-Jiménez, E., Gómez-López, G., Leandro-García, L.J., Muñoz, I., Schiavi, F., Montero-Conde, C., de Cubas, A.A., Ramires, R., Landa, I., Leskelä, S., Maliszewska, A., Inglada-Pérez, L., de la Vega, L., Rodríguez-Antona, C., Letón, R., Bernal, C., de Campos, J.M., Diez-Tascón, C., Fraga, M.F., Boullosa, C., Pisano, D.G., Opocher, G., Robledo, M., Cascón, A., 2010. Research resource: Transcriptional profiling reveals different pseudohypoxic signatures in SDHB and VHL-related pheochromocytomas. Mol. Endocrinol. Baltim. Md 24, 2382–2391. doi:10.1210/me.2010-0256

Lu, J., Maruyama, M., Satake, M., Bae, S.C., Ogawa, E., Kagoshima, H., Shigesada, K., Ito, Y., 1995. Subcellular localization of the alpha and beta subunits of the acute myeloid leukemia-linked transcription factor PEBP2/CBF. Mol. Cell. Biol. 15, 1651–1661.

Ludérus, M.E., de Graaf, A., Mattia, E., den Blaauwen, J.L., Grande, M.A., de Jong, L., van Driel, R., 1992. Binding of matrix attachment regions to lamin B1. Cell 70, 949–959.

Luscombe, N.M., Thornton, J.M., 2002. Protein-DNA interactions: amino acid conservation and the effects of mutations on binding specificity. J. Mol. Biol. 320, 991–1009.

Lutterbach, B., Westendorf, J.J., Linggi, B., Isaac, S., Seto, E., Hiebert, S.W., 2000. A mechanism of repression by acute myeloid leukemia-1, the target of multiple chromosomal translocations in acute leukemia. J. Biol. Chem. 275, 651–656.

Machens, A., Brauckhoff, M., Holzhausen, H.-J., Thanh, P.N., Lehnert, H., Dralle, H., 2005. Codon-specific development of pheochromocytoma in multiple endocrine neoplasia type 2. J. Clin. Endocrinol. Metab. 90, 3999–4003. doi:10.1210/jc.2005-0064

Maeno, M., Mead, P.E., Kelley, C., Xu, R.H., Kung, H.F., Suzuki, A., Ueno, N., Zon, L.I., 1996. The role of BMP-4 and GATA-2 in the induction and differentiation of hematopoietic mesoderm in Xenopus laevis. Blood 88, 1965–1972.

Manger, W.M., Gifford, R.W., 1980. Pheochromocytoma: diagnosis and management. N. Y. State J. Med. 80, 216–226.

Marinoni, I., Pellegata, N.S., 2011. p27kip1: a new multiple endocrine neoplasia gene? Neuroendocrinology 93, 19–28. doi:10.1159/000320366

Markus, J., Garin, M.T., Bies, J., Galili, N., Raza, A., Thirman, M.J., Le Beau, M.M., Rowley, J.D., Liu, P.P., Wolff, L., 2007. Methylation-independent silencing of the tumor suppressor INK4b (p15) by CBFbeta-SMMHC in acute myelogenous leukemia with inv(16). Cancer Res. 67, 992–1000. doi:10.1158/0008-5472.CAN-06-2964

Marshall, A.D., Bailey, C.G., Champ, K., Vellozzi, M., O'Young, P., Metierre, C., Feng, Y., Thoeng, A., Richards, A.M., Schmitz, U., Biro, M., Jayasinghe, R., Ding, L., Anderson, L., Mardis, E.R., Rasko, J.E.J., 2017. CTCF genetic alterations in endometrial carcinoma are pro-tumorigenic. Oncogene. doi:10.1038/onc.2017.25

Marx, S.J., Agarwal, S.K., Kester, M.B., Heppner, C., Kim, Y.S., Emmert-Buck, M.R., Debelenko, L.V., Lubensky, I.A., Zhuang, Z., Guru, S.C., Manickam, P., Olufemi, S.E., Skarulis, M.C., Doppman, J.L., Alexander, R.H., Liotta, L.A., Collins, F.S., Chandrasekharappa, S.C., Spiegel, A.M., Burns, A.L., 1998. Germline and somatic mutation of the gene for multiple endocrine neoplasia type 1 (MEN1). J. Intern. Med. 243, 447–453.

Masserdotti, G., Badaloni, A., Green, Y.S., Croci, L., Barili, V., Bergamini, G., Vetter, M.L., Consalez, G.G., 2010. ZFP423 coordinates Notch and bone morphogenetic protein signaling, selectively up-regulating Hes5 gene expression. J. Biol. Chem. 285, 30814–30824. doi:10.1074/jbc.M110.142869

Maston, G.A., Evans, S.K., Green, M.R., 2006. Transcriptional regulatory elements in the human genome. Annu. Rev. Genomics Hum. Genet. 7, 29–59. doi:10.1146/annurev.genom.7.080505.115623

Matsuoka, S., Edwards, M.C., Bai, C., Parker, S., Zhang, P., Baldini, A., Harper, J.W., Elledge, S.J., 1995. p57KIP2, a structurally distinct member of the p21CIP1 Cdk inhibitor family, is a candidate tumor suppressor gene. Genes Dev. 9, 650–662.

Mayol, X., Garriga, J., Graña, X., 1996. G1 cyclin/CDK-independent phosphorylation and accumulation of p130 during the transition from G1 to G0 lead to its association with E2F-4. Oncogene 13, 237–246.

Mayr, B., Apenberg, S., Rothämel, T., von zur Mühlen, A., Brabant, G., 1997. Menin mutations in patients with multiple endocrine neoplasia type 1. Eur. J. Endocrinol. 137, 684–687.

McAllister, S.S., Becker-Hapak, M., Pintucci, G., Pagano, M., Dowdy, S.F., 2003. Novel p27(kip1) C-terminal scatter domain mediates Rac-dependent cell migration independent of cell cycle arrest functions. Mol. Cell. Biol. 23, 216–228.

Melnikova, I.N., Crute, B.E., Wang, S., Speck, N.A., 1993. Sequence specificity of the core-binding factor. J. Virol. 67, 2408–2411.

Meyer, M.B., Goetsch, P.D., Pike, J.W., 2012. VDR/RXR and TCF4/β-catenin cistromes in colonic cells of colorectal tumor origin: impact on c-FOS and c-MYC gene expression. Mol. Endocrinol. Baltim. Md 26, 37–51. doi:10.1210/me.2011-1109

Meyers, S., Downing, J.R., Hiebert, S.W., 1993. Identification of AML-1 and the (8;21) translocation protein (AML-1/ETO) as sequence-specific DNA-binding proteins: the runt homology domain is required for DNA binding and protein-protein interactions. Mol. Cell. Biol. 13, 6336–6345.

Meyyappan, M., Wong, H., Hull, C., Riabowol, K.T., 1998. Increased expression of cyclin D2 during multiple states of growth arrest in primary and established cells. Mol. Cell. Biol. 18, 3163–3172.

Molatore, S., Liyanarachchi, S., Irmler, M., Perren, A., Mannelli, M., Ercolino, T., Beuschlein, F., Jarzab, B., Wloch, J., Ziaja, J., Zoubaa, S., Neff, F., Beckers, J., Höfler, H., Atkinson, M.J., Pellegata, N.S., 2010. Pheochromocytoma in rats with multiple endocrine neoplasia (MENX) shares gene expression patterns with human pheochromocytoma. Proc. Natl. Acad. Sci. U. S. A. 107, 18493–18498. doi:10.1073/pnas.1003956107

Molatore, S., Pellegata, N.S., 2010. The MENX syndrome and p27: relationships with multiple endocrine neoplasia. Prog. Brain Res. 182, 295–320. doi:10.1016/S0079-6123(10)82013-8

Mulligan, L.M., Gardner, E., Smith, B.A., Mathew, C.G., Ponder, B.A., 1993. Genetic events in tumour initiation and progression in multiple endocrine neoplasia type 2. Genes. Chromosomes Cancer 6, 166–177.

Munck, A., Guyre, P.M., Holbrook, N.J., 1984. Physiological functions of glucocorticoids in stress and their relation to pharmacological actions. Endocr. Rev. 5, 25–44. doi:10.1210/edrv-5-1-25

Muñoz-Alonso, M.J., Acosta, J.C., Richard, C., Delgado, M.D., Sedivy, J., León, J., 2005. p21Cip1 and p27Kip1 induce distinct cell cycle effects and differentiation programs in myeloid leukemia cells. J. Biol. Chem. 280, 18120–18129. doi:10.1074/jbc.M500758200

Muscarella, P., Bloomston, M., Brewer, A.R., Mahajan, A., Frankel, W.L., Ellison, E.C., Farrar, W.B., Weghorst, C.M., Li, J., 2008. Expression of the p16INK4A/Cdkn2a gene is prevalently downregulated in human pheochromocytoma tumor specimens. Gene Expr. 14, 207–216.

Musgrove, E.A., Lilischkis, R., Cornish, A.L., Lee, C.S., Setlur, V., Seshadri, R., Sutherland, R.L., 1995. Expression of the cyclin-dependent kinase inhibitors p16INK4, p15INK4B and p21WAF1/CIP1 in human breast cancer. Int. J. Cancer 63, 584–591.

Nakamura, Y., Ozaki, T., Koseki, H., Nakagawara, A., Sakiyama, S., 2003. Accumulation of p27 KIP1 is associated with BMP2-induced growth arrest and neuronal differentiation of human neuroblastoma-derived cell lines. Biochem. Biophys. Res. Commun. 307, 206–213.

Nakayama, K., Ishida, N., Shirane, M., Inomata, A., Inoue, T., Shishido, N., Horii, I., Loh, D.Y., Nakayama, K., 1996. Mice lacking p27(Kip1) display increased body size, multiple organ hyperplasia, retinal dysplasia, and pituitary tumors. Cell 85, 707–720.

Nardelli, J., Catala, M., Charnay, P., 2003. Establishment of embryonic neuroepithelial cell lines exhibiting an epiplastic expression pattern of region specific markers. J. Neurosci. Res. 73, 737–752. doi:10.1002/jnr.10716

Narlikar, G.J., Fan, H.-Y., Kingston, R.E., 2002. Cooperation between complexes that regulate chromatin structure and transcription. Cell 108, 475–487.

Neumann, H.P., Wiestler, O.D., 1991. Clustering of features of von Hippel-Lindau syndrome: evidence for a complex genetic locus. Lancet Lond. Engl. 337, 1052–1054.

Nguyen, L., Besson, A., Heng, J.I.-T., Schuurmans, C., Teboul, L., Parras, C., Philpott, A., Roberts, J.M., Guillemot, F., 2007. [p27Kip1 independently promotes neuronal differentiation and migration in the cerebral cortex]. Bull. Mem. Acad. R. Med. Belg. 162, 310–314.

Niccoli-Sire, P., Conte-Devolx, B., 2007. [Multiple endocrine neoplasia type 2]. Ann. Endocrinol. 68, 317–324. doi:10.1016/j.ando.2007.04.005

Niemann, S., Müller, U., 2000. Mutations in SDHC cause autosomal dominant paraganglioma, type 3. Nat. Genet. 26, 268–270. doi:10.1038/81551

Nikolov, D.B., Burley, S.K., 1997. RNA polymerase II transcription initiation: a structural view. Proc. Natl. Acad. Sci. U. S. A. 94, 15–22.

Nomura, K., Kimura, H., Shimizu, S., Kodama, H., Okamoto, T., Obara, T., Takano, K., 2009. Survival of patients with metastatic malignant pheochromocytoma and efficacy of combined cyclophosphamide, vincristine, and dacarbazine chemotherapy. J. Clin. Endocrinol. Metab. 94, 2850–2856. doi:10.1210/jc.2008-2697

Ogawa, E., Maruyama, M., Kagoshima, H., Inuzuka, M., Lu, J., Satake, M., Shigesada, K., Ito, Y., 1993. PEBP2/PEA2 represents a family of transcription factors homologous to the products of the Drosophila runt gene and the human AML1 gene. Proc. Natl. Acad. Sci. U. S. A. 90, 6859–6863.

Ogawa, S., Satake, M., Ikuta, K., 2008. Physical and functional interactions between STAT5 and Runx transcription factors. J. Biochem. (Tokyo) 143, 695–709. doi:10.1093/jb/mvn022

Oh, S., Oh, C., Yoo, K.H., 2017. Functional roles of CTCF in breast cancer. BMB Rep.

Okoniewski, M.J., Hey, Y., Pepper, S.D., Miller, C.J., 2007. High correspondence between Affymetrix exon and standard expression arrays. BioTechniques 42, 181–185.

Okuda, T., van Deursen, J., Hiebert, S.W., Grosveld, G., Downing, J.R., 1996. AML1, the target of multiple chromosomal translocations in human leukemia, is essential for normal fetal liver hematopoiesis. Cell 84, 321–330.

Oren, T., Torregroza, I., Evans, T., 2005. An Oct-1 binding site mediates activation of the gata2 promoter by BMP signaling. Nucleic Acids Res. 33, 4357–4367. doi:10.1093/nar/gki746

Orlando, V., Strutt, H., Paro, R., 1997. Analysis of chromatin structure by in vivo formaldehyde cross-linking. Methods San Diego Calif 11, 205–214. doi:10.1006/meth.1996.0407

Orphanides, G., Lagrange, T., Reinberg, D., 1996. The general transcription factors of RNA polymerase II. Genes Dev. 10, 2657–2683.

Osorio, K.M., Lee, S.E., McDermitt, D.J., Waghmare, S.K., Zhang, Y.V., Woo, H.N., Tumbar, T., 2008. Runx1 modulates developmental, but not injury-driven, hair follicle stem cell activation. Dev. Camb. Engl. 135, 1059–1068. doi:10.1242/dev.012799

Ozawa, Y., Towatari, M., Tsuzuki, S., Hayakawa, F., Maeda, T., Miyata, Y., Tanimoto, M., Saito, H., 2001. Histone deacetylase 3 associates with and represses the transcription factor GATA-2. Blood 98, 2116–2123.

Pabst, T., Mueller, B.U., Zhang, P., Radomska, H.S., Narravula, S., Schnittger, S., Behre, G., Hiddemann, W., Tenen, D.G., 2001. Dominant-negative mutations of CEBPA, encoding CCAAT/enhancer binding protein-alpha (C/EBPalpha), in acute myeloid leukemia. Nat. Genet. 27, 263–270. doi:10.1038/85820

Pacak, K., Eisenhofer, G., Ilias, I., 2004. Diagnostic imaging of pheochromocytoma. Front. Horm. Res. 31, 107–120.

Pagano, M., Theodoras, A.M., Tam, S.W., Draetta, G.F., 1994. Cyclin D1-mediated inhibition of repair and replicative DNA synthesis in human fibroblasts. Genes Dev. 8, 1627–1639.

Pajni-Underwood, S., Wilson, C.P., Elder, C., Mishina, Y., Lewandoski, M., 2007. BMP signals control limb bud interdigital programmed cell death by regulating FGF signaling. Dev. Camb. Engl. 134, 2359–2368. doi:10.1242/dev.001677

Pan, H., Hao, S., Zheng, Q., Li, J., Zheng, J., Hu, Z., Yang, S., Guo, X., Yang, Q., 2013. Bone induction by biomimetic PLGA copolymer loaded with a novel synthetic RADA16-P24 peptide in vivo. Mater. Sci. Eng. C Mater. Biol. Appl. 33, 3336–3345. doi:10.1016/j.msec.2013.04.019

Pata, I., Studer, M., van Doorninck, J.H., Briscoe, J., Kuuse, S., Engel, J.D., Grosveld, F., Karis, A., 1999. The transcription factor GATA3 is a downstream effector of Hoxb1 specification in rhombomere 4. Dev. Camb. Engl. 126, 5523–5531.

Pattyn, A., Simplicio, N., van Doorninck, J.H., Goridis, C., Guillemot, F., Brunet, J.-F., 2004. Ascl1/Mash1 is required for the development of central serotonergic neurons. Nat. Neurosci. 7, 589–595. doi:10.1038/nn1247

Pellegata, N.S., Quintanilla-Martinez, L., Keller, G., Liyanarachchi, S., Höfler, H., Atkinson, M.J., Fend, F., 2007. Human pheochromocytomas show reduced p27Kip1 expression that is not associated with somatic gene mutations and rarely with deletions. Virchows Arch. Int. J. Pathol. 451, 37–46. doi:10.1007/s00428-007-0431-6

Pellegata, N.S., Quintanilla-Martinez, L., Siggelkow, H., Samson, E., Bink, K., Höfler, H., Fend, F., Graw, J., Atkinson, M.J., 2006. Germ-line mutations in p27Kip1 cause a multiple endocrine neoplasia syndrome in rats and humans. Proc. Natl. Acad. Sci. U. S. A. 103, 15558–15563. doi:10.1073/pnas.0603877103

Perlman, R.L., Chalfie, M., 1977. Catecholamine release from the adrenal medulla. Clin. Endocrinol. Metab. 6, 551–576.

Petrovick, M.S., Hiebert, S.W., Friedman, A.D., Hetherington, C.J., Tenen, D.G., Zhang, D.E., 1998. Multiple functional domains of AML1: PU.1 and C/EBPalpha synergize with different regions of AML1. Mol. Cell. Biol. 18, 3915–3925.

Philipp-Staheli, J., Payne, S.R., Kemp, C.J., 2001. p27(Kip1): regulation and function of a haploinsufficient tumor suppressor and its misregulation in cancer. Exp. Cell Res. 264, 148–168. doi:10.1006/excr.2000.5143

Philley, J.V., Kannan, A., Griffith, D.E., Devine, M.S., Benwill, J.L., Wallace, R.J., Brown-Elliott, B.A., Thakkar, F., Taskar, V., Fox, J.G., Alqaid, A., Bains, H., Gupta, S., Dasgupta, S., 2017. Exosome secretome and mediated signaling in breast cancer patients with nontuberculous mycobacterial disease. Oncotarget 8, 18070–18081. doi:10.18632/oncotarget.14964

Pierce, J.V., Kumamoto, C.A., 2012. Variation in Candida albicans EFG1 expression enables host-dependent changes in colonizing fungal populations. mBio 3, e00117-00112. doi:10.1128/mBio.00117-12

Pippa, R., Dominguez, A., Malumbres, R., Endo, A., Arriazu, E., Marcotegui, N., Guruceaga, E., Odero, M.D., 2016. MYC-dependent recruitment of RUNX1 and GATA2 on the SET oncogene promoter enhances PP2A inactivation in acute myeloid leukemia. Oncotarget. doi:10.18632/oncotarget.9840

Pippa, R., Espinosa, L., Gundem, G., García-Escudero, R., Dominguez, A., Orlando, S., Gallastegui, E., Saiz, C., Besson, A., Pujol, M.J., López-Bigas, N., Paramio, J.M., Bigas, A., Bachs, O., 2012. p27Kip1 represses transcription by direct interaction with p130/E2F4 at the promoters of target genes. Oncogene 31, 4207–4220. doi:10.1038/onc.2011.582

Pogorzelski, R., Toutounchi, S., Krajewska, E., Fiszer, P., Łykowski, M., Zapała, Ł., Szostek, M., Jakuczun, W., Pachucki, J., Skórski, M., 2014. The effect of surgical treatment of phaeochromocytoma on concomitant arterial hypertension and diabetes mellitus in a single-centre retrospective study. Cent. Eur. J. Urol. 67, 361–365. doi:10.5173/ceju.2014.04.art9

Polyak, K., Kato, J.Y., Solomon, M.J., Sherr, C.J., Massague, J., Roberts, J.M., Koff, A., 1994. p27Kip1, a cyclin-Cdk inhibitor, links transforming growth factor-beta and contact inhibition to cell cycle arrest. Genes Dev. 8, 9–22.

Porcher, C., Swat, W., Rockwell, K., Fujiwara, Y., Alt, F.W., Orkin, S.H., 1996. The T cell leukemia oncoprotein SCL/tal-1 is essential for development of all hematopoietic lineages. Cell 86, 47–57.

Pozner, A., Lotem, J., Xiao, C., Goldenberg, D., Brenner, O., Negreanu, V., Levanon, D., Groner, Y., 2007. Developmentally regulated promoter-switch transcriptionally controls Runx1 function during embryonic hematopoiesis. BMC Dev. Biol. 7, 84. doi:10.1186/1471-213X-7-84

Pratt, W.A., 1951. Chromaffin cell tymor simulating malignant hypertension; report of a case with surgical cure. J. Clin. Endocrinol. Metab. 11, 630–640. doi:10.1210/jcem-11-6-630

Qi, C.-F., Martensson, A., Mattioli, M., Dalla-Favera, R., Lobanenkov, V.V., Morse, H.C., 2003. CTCF functions as a critical regulator of cell-cycle arrest and death after ligation of the B cell receptor on immature B cells. Proc. Natl. Acad. Sci. U. S. A. 100, 633–638. doi:10.1073/pnas.0237127100

Qin, Y., Yao, L., King, E.E., Buddavarapu, K., Lenci, R.E., Chocron, E.S., Lechleiter, J.D., Sass, M., Aronin, N., Schiavi, F., Boaretto, F., Opocher, G., Toledo, R.A., Toledo, S.P.A., Stiles, C., Aguiar, R.C.T., Dahia, P.L.M., 2010. Germline mutations in TMEM127 confer susceptibility to pheochromocytoma. Nat. Genet. 42, 229–233. doi:10.1038/ng.533

Ramachandran, R., Rewari, V., 2017. Current perioperative management of pheochromocytomas. Indian J. Urol. IJU J. Urol. Soc. India 33, 19–25. doi:10.4103/0970-1591.194781

Ranabir, S., Reetu, K., 2011. Stress and hormones. Indian J. Endocrinol. Metab. 15, 18–22. doi:10.4103/2230-8210.77573

Remboutsika, E., Lutz, Y., Gansmuller, A., Vonesch, J.L., Losson, R., Chambon, P., 1999. The putative nuclear receptor mediator TIF1alpha is tightly associated with euchromatin. J. Cell Sci. 112 (Pt 11), 1671–1683.

Rivier, C., Vale, W., 1983. Modulation of stress-induced ACTH release by corticotropin-releasing factor, catecholamines and vasopressin. Nature 305, 325–327.

Robinson, J.T., Thorvaldsdóttir, H., Winckler, W., Guttman, M., Lander, E.S., Getz, G., Mesirov, J.P., 2011. Integrative genomics viewer. Nat. Biotechnol. 29, 24–26. doi:10.1038/nbt.1754

Roeder, R.G., 1996. The role of general initiation factors in transcription by RNA polymerase II. Trends Biochem. Sci. 21, 327–335.

Saito, R., Shirakawa, R., Nishiyama, H., Kobayashi, T., Kawato, M., Kanno, T., Nishizawa, K., Matsui, Y., Ohbayashi, T., Horiguchi, M., Nakamura, T., Ikeda, T., Yamane, K., Nakayama, E., Nakamura, E., Toda, Y., Kimura, T., Kita, T., Ogawa, O., Horiuchi, H., 2013. Downregulation of Ral GTPase-activating protein promotes tumor invasion and metastasis of bladder cancer. Oncogene 32, 894–902. doi:10.1038/onc.2012.101

Saito, Y., Tsubuki, S., Ito, H., Ohmi-Imajo, S., Kawashima, S., 1992. Possible involvement of clathrin in neuritogenesis induced by a protease inhibitor (benzyloxycarbonyl-Leu-Leu-Leu-aldehyde) in PC12 cells. J. Biochem. (Tokyo) 112, 448–455.

Santoro, M., Melillo, R.M., Carlomagno, F., Fusco, A., Vecchio, G., 2002. Molecular mechanisms of RET activation in human cancer. Ann. N. Y. Acad. Sci. 963, 116–121.

Scheitz, C.J.F., Lee, T.S., McDermitt, D.J., Tumbar, T., 2012. Defining a tissue stem cell-driven Runx1/Stat3 signalling axis in epithelial cancer. EMBO J. 31, 4124–4139. doi:10.1038/emboj.2012.270

Scheitz, C.J.F., Tumbar, T., 2013. New insights into the role of Runx1 in epithelial stem cell biology and pathology. J. Cell. Biochem. 114, 985–993. doi:10.1002/jcb.24453

Schimke, R.N., Hartmann, W.H., 1965. Familial amyloid-producing medullary thyroid carcinoma and pheochromocytoma. A distinct genetic entity. Ann. Intern. Med. 63, 1027–1039.

Sealy, L., Burgess, R.R., Cotten, M., Chalkley, R., 1989. Purification of Xenopus egg nucleoplasmin and its use in chromatin assembly in vitro. Methods Enzymol. 170, 612–630.

Shah, M., Rennoll, S.A., Raup-Konsavage, W.M., Yochum, G.S., 2015. A dynamic exchange of TCF3 and TCF4 transcription factors controls MYC expression in colorectal cancer cells. Cell Cycle Georget. Tex 14, 323–332. doi:10.4161/15384101.2014.980643

Shi, X., Richard, J., Zirbes, K.M., Gong, W., Lin, G., Kyba, M., Thomson, J.A., Koyano-Nakagawa, N., Garry, D.J., 2014. Cooperative interaction of Etv2 and Gata2 regulates the development of endothelial and hematopoietic lineages. Dev. Biol. 389, 208–218. doi:10.1016/j.ydbio.2014.02.018

Shirane, M., Harumiya, Y., Ishida, N., Hirai, A., Miyamoto, C., Hatakeyama, S., Nakayama, K., Kitagawa, M., 1999. Down-regulation of p27(Kip1) by two mechanisms, ubiquitin-mediated degradation and proteolytic processing. J. Biol. Chem. 274, 13886–13893.

Shivdasani, R.A., Mayer, E.L., Orkin, S.H., 1995. Absence of blood formation in mice lacking the T-cell leukaemia oncoprotein tal-1/SCL. Nature 373, 432–434. doi:10.1038/373432a0

Silverstein, R.A., Ekwall, K., 2005. Sin3: a flexible regulator of global gene expression and genome stability. Curr. Genet. 47, 1–17. doi:10.1007/s00294-004-0541-5

Singer, R.H., Green, M.R., 1997. Compartmentalization of eukaryotic gene expression: causes and effects. Cell 91, 291–294.

Slingerland, J., Pagano, M., 2000. Regulation of the cdk inhibitor p27 and its deregulation in cancer. J. Cell. Physiol. 183, 10–17. doi:10.1002/(SICI)1097-4652(200004)183:1<10::AID-JCP2>3.0.CO;2-I

Speck, N.A., Gilliland, D.G., 2002. Core-binding factors in haematopoiesis and leukaemia. Nat. Rev. Cancer 2, 502–513. doi:10.1038/nrc840

Spector, S., Sjoerdsma, A., Udenfriend, S., 1965. BLOCKADE OF ENDOGENOUS NOREPINEPHRINE SYNTHESIS BY ALPHA-METHYL-TYROSINE, AN INHIBITOR OF TYROSINE HYDROXYLASE. J. Pharmacol. Exp. Ther. 147, 86–95.

Spitz, F., Furlong, E.E.M., 2012. Transcription factors: from enhancer binding to developmental control. Nat. Rev. Genet. 13, 613–626. doi:10.1038/nrg3207

Stanford, P.M., Halliday, G.M., Brooks, W.S., Kwok, J.B., Storey, C.E., Creasey, H., Morris, J.G., Fulham, M.J., Schofield, P.R., 2000. Progressive supranuclear palsy pathology caused by a novel silent mutation in exon 10 of the tau gene: expansion of the disease phenotype caused by tau gene mutations. Brain J. Neurol. 123 (Pt 5), 880–893.

Tahirov, T.H., Sasaki, M., Inoue-Bungo, T., Fujikawa, A., Sato, K., Kumasaka, T., Yamamoto, M., Ogata, K., 2001. Crystals of ternary protein-DNA complexes composed of DNA-binding domains of c-Myb or v-Myb, C/EBPalpha or C/EBPbeta and tom-1A promoter fragment. Acta Crystallogr. D Biol. Crystallogr. 57, 1655–1658.

Taniuchi, I., Osato, M., Ito, Y., 2012. Runx1: no longer just for leukemia. EMBO J. 31, 4098–4099. doi:10.1038/emboj.2012.282

Theriault, F.M., Nuthall, H.N., Dong, Z., Lo, R., Barnabe-Heider, F., Miller, F.D., Stifani, S., 2005. Role for Runx1 in the proliferation and neuronal differentiation of selected progenitor cells in the mammalian nervous system. J. Neurosci. Off. J. Soc. Neurosci. 25, 2050–2061. doi:10.1523/JNEUROSCI.5108-04.2005

Thomas, W., 2006. For catch bonds, it all hinges on the interdomain region. J. Cell Biol. 174, 911–913. doi:10.1083/jcb.200609029

Thompson, L., 2006. World Health Organization classification of tumours: pathology and genetics of head and neck tumours. Ear. Nose. Throat J. 85, 74.

Toyoshima, H., Hunter, T., 1994. p27, a novel inhibitor of G1 cyclin-Cdk protein kinase activity, is related to p21. Cell 78, 67–74.

Tsai, F.Y., Keller, G., Kuo, F.C., Weiss, M., Chen, J., Rosenblatt, M., Alt, F.W., Orkin, S.H., 1994. An early haematopoietic defect in mice lacking the transcription factor GATA-2. Nature 371, 221–226. doi:10.1038/371221a0

Tsai, R.Y., Reed, R.R., 1997. Cloning and functional characterization of Roaz, a zinc finger protein that interacts with O/E-1 to regulate gene expression: implications for olfactory neuronal development. J. Neurosci. Off. J. Soc. Neurosci. 17, 4159–4169.

Turner, J., Crossley, M., 1999. Mammalian Krüppel-like transcription factors: more than just a pretty finger. Trends Biochem. Sci. 24, 236–240.

Vale, W., Spiess, J., Rivier, C., Rivier, J., 1981. Characterization of a 41-residue ovine hypothalamic peptide that stimulates secretion of corticotropin and beta-endorphin. Science 213, 1394–1397.

van Baars, F.M., Cremers, C.W., van den Broek, P., Veldman, J.E., 1981. Familiar non-chromaffinic paragangliomas (glomus tumors). Clinical and genetic aspects (abridged). Acta Otolaryngol. (Stockh.) 91, 589–593.

van Bragt, M.P.A., Hu, X., Xie, Y., Li, Z., 2014. RUNX1, a transcription factor mutated in breast cancer, controls the fate of ER-positive mammary luminal cells. eLife 3, e03881. doi:10.7554/eLife.03881

van Duinen, N., Steenvoorden, D., Kema, I.P., Jansen, J.C., Vriends, A.H.J.T., Bayley, J.P., Smit, J.W.A., Romijn, J.A., Corssmit, E.P.M., 2010. Increased urinary excretion of 3-methoxytyramine in patients with head and neck paragangliomas. J. Clin. Endocrinol. Metab. 95, 209–214. doi:10.1210/jc.2009-1632

van Heerden, J.A., Sheps, S.G., Hamberger, B., Sheedy, P.F., Poston, J.G., ReMine, W.H., 1982. Pheochromocytoma: current status and changing trends. Surgery 91, 367–373.

Vergès, B., Boureille, F., Goudet, P., Murat, A., Beckers, A., Sassolas, G., Cougard, P., Chambe, B., Montvernay, C., Calender, A., 2002. Pituitary disease in MEN type 1 (MEN1): data from the France-Belgium MEN1 multicenter study. J. Clin. Endocrinol. Metab. 87, 457–465. doi:10.1210/jcem.87.2.8145

Vicha, A., Musil, Z., Pacak, K., 2013. Genetics of pheochromocytoma and paraganglioma syndromes: new advances and future treatment options. Curr. Opin. Endocrinol. Diabetes Obes. 20, 186–191. doi:10.1097/MED.0b013e32835fcc45

Viglietto, G., Motti, M.L., Bruni, P., Melillo, R.M., D'Alessio, A., Califano, D., Vinci, F., Chiappetta, G., Tsichlis, P., Bellacosa, A., Fusco, A., Santoro, M., 2002. Cytoplasmic relocalization and inhibition of the cyclin-dependent kinase inhibitor p27(Kip1) by PKB/Akt-mediated phosphorylation in breast cancer. Nat. Med. 8, 1136–1144. doi:10.1038/nm762

Vinson, C., Myakishev, M., Acharya, A., Mir, A.A., Moll, J.R., Bonovich, M., 2002. Classification of human B-ZIP proteins based on dimerization properties. Mol. Cell. Biol. 22, 6321–6335.

von der Lehr, N., Johansson, S., Wu, S., Bahram, F., Castell, A., Cetinkaya, C., Hydbring, P., Weidung, I., Nakayama, K., Nakayama, K.I., Söderberg, O., Kerppola, T.K., Larsson, L.-G., 2003. The F-box protein Skp2 participates in c-Myc proteosomal degradation and acts as a cofactor for c-Myc-regulated transcription. Mol. Cell 11, 1189–1200.

Wallace, M.R., Marchuk, D.A., Andersen, L.B., Letcher, R., Odeh, H.M., Saulino, A.M., Fountain, J.W., Brereton, A., Nicholson, J., Mitchell, A.L., 1990. Type 1 neurofibromatosis gene: identification of a large transcript disrupted in three NF1 patients. Science 249, 181–186.

Wander, S.A., Zhao, D., Slingerland, J.M., 2011. p27: a barometer of signaling deregulation and potential predictor of response to targeted therapies. Clin. Cancer Res. Off. J. Am. Assoc. Cancer Res. 17, 12–18. doi:10.1158/1078-0432.CCR-10-0752

Wang, J., Zhuang, J., Iyer, S., Lin, X., Whitfield, T.W., Greven, M.C., Pierce, B.G., Dong, X., Kundaje, A., Cheng, Y., Rando, O.J., Birney, E., Myers, R.M., Noble, W.S., Snyder, M., Weng, Z., 2012. Sequence features and chromatin structure around the genomic regions bound by 119 human transcription factors. Genome Res. 22, 1798–1812. doi:10.1101/gr.139105.112

Wang, Q., Friedman, A.D., 2002. CCAAT/enhancer-binding proteins are required for granulopoiesis independent of their induction of the granulocyte colony-stimulating factor receptor. Blood 99, 2776–2785.

Wang, Q., Stacy, T., Miller, J.D., Lewis, A.F., Gu, T.L., Huang, X., Bushweller, J.H., Bories, J.C., Alt, F.W., Ryan, G., Liu, P.P., Wynshaw-Boris, A., Binder, M., Marín-Padilla, M., Sharpe, A.H., Speck, N.A., 1996. The CBFbeta subunit is essential for CBFalpha2 (AML1) function in vivo. Cell 87, 697–708.

Wang, S., Wang, Q., Crute, B.E., Melnikova, I.N., Keller, S.R., Speck, N.A., 1993. Cloning and characterization of subunits of the T-cell receptor and murine leukemia virus enhancer core-binding factor. Mol. Cell. Biol. 13, 3324–3339.

Warming, S., Rachel, R.A., Jenkins, N.A., Copeland, N.G., 2006. Zfp423 is required for normal cerebellar development. Mol. Cell. Biol. 26, 6913–6922. doi:10.1128/MCB.02255-05

Warren, S., Chute, R.N., 1972. Pheochromocytoma. Cancer 29, 327–331.

Wei, M., Liu, B., Gu, Q., Su, L., Yu, Y., Zhu, Z., 2013. Stat6 cooperates with Sp1 in controlling breast cancer cell proliferation by modulating the expression of p21(Cip1/WAF1) and p27 (Kip1). Cell. Oncol. Dordr. 36, 79–93. doi:10.1007/s13402-012-0115-3

Wilbanks, E.G., Facciotti, M.T., 2010. Evaluation of algorithm performance in ChIP-seq peak detection. PloS One 5, e11471. doi:10.1371/journal.pone.0011471

Wintjens, R.T., Rooman, M.J., Wodak, S.J., 1996. Automatic classification and analysis of alpha alpha-turn motifs in proteins. J. Mol. Biol. 255, 235–253. doi:10.1006/jmbi.1996.0020

Xu, P., Jacobs, A.R., Taylor, S.I., 1999. Interaction of insulin receptor substrate 3 with insulin receptor, insulin receptor-related receptor, insulin-like growth factor-1 receptor, and downstream signaling proteins. J. Biol. Chem. 274, 15262–15270.

Xu, R.H., Ault, K.T., Kim, J., Park, M.J., Hwang, Y.S., Peng, Y., Sredni, D., Kung, H. f, 1999. Opposite effects of FGF and BMP-4 on embryonic blood formation: roles of PV.1 and GATA-2. Dev. Biol. 208, 352–361.

Yamanaka, S., Olaru, A.V., An, F., Luvsanjav, D., Jin, Z., Agarwal, R., Tomuleasa, C., Popescu, I., Alexandrescu, S., Dima, S., Chivu-Economescu, M., Montgomery, E.A., Torbenson, M., Meltzer, S.J., Selaru, F.M., 2012. MicroRNA-21 inhibits Serpini1, a gene with novel tumour

suppressive effects in gastric cancer. Dig. Liver Dis. Off. J. Ital. Soc. Gastroenterol. Ital. Assoc. Study Liver 44, 589–596. doi:10.1016/j.dld.2012.02.016

Zampino, M.G., Magni, E., Sonzogni, A., Renne, G., 2009. K-ras status in squamous cell anal carcinoma (SCC): it's time for target-oriented treatment? Cancer Chemother. Pharmacol. 65, 197–199. doi:10.1007/s00280-009-1117-3

Zarnegar, R., Brunaud, L., Clark, O.H., 2002. Multiple endocrine neoplasia type I. Curr. Treat. Options Oncol. 3, 335–348.

Zbar, B., Kishida, T., Chen, F., Schmidt, L., Maher, E.R., Richards, F.M., Crossey, P.A., Webster, A.R., Affara, N.A., Ferguson-Smith, M.A., Brauch, H., Glavac, D., Neumann, H.P., Tisherman, S., Mulvihill, J.J., Gross, D.J., Shuin, T., Whaley, J., Seizinger, B., Kley, N., Olschwang, S., Boisson, C., Richard, S., Lips, C.H., Lerman, M., 1996. Germline mutations in the Von Hippel-Lindau disease (VHL) gene in families from North America, Europe, and Japan. Hum. Mutat. 8, 348–357. doi:10.1002/(SICI)1098-1004(1996)8:4<348::AID-HUMU8>3.0.CO;2-3

Zhang, D.-E., Zhang, P., Wang, N., Hetherington, C.J., Darlington, G.J., Tenen, D.G., 1997. Absence of granulocyte colony-stimulating factor signaling and neutrophil development in CCAAT enhancer binding protein α-deficient mice. Proc. Natl. Acad. Sci. U. S. A. 94, 569–574.

Zhang, J., Liu, Z., Shao, H., Ma, Y., Tong, H., Wang, Y., 2008. Laboratory study of a complex translocation t(2;8;21) (p12;q22;q22) in a patient with acute myelogenous leukemia. Leuk. Lymphoma 49, 1925–1928. doi:10.1080/10428190802311383

Zhang, J.-P., Zhang, H., Wang, H.-B., Li, Y.-X., Liu, G.-H., Xing, S., Li, M.-Z., Zeng, M.-S., 2014. Down-regulation of Sp1 suppresses cell proliferation, clonogenicity and the expressions of stem cell markers in nasopharyngeal carcinoma. J. Transl. Med. 12, 222. doi:10.1186/s12967-014-0222-1

Zhao, X., Jankovic, V., Gural, A., Huang, G., Pardanani, A., Menendez, S., Zhang, J., Dunne, R., Xiao, A., Erdjument-Bromage, H., Allis, C.D., Tempst, P., Nimer, S.D., 2008. Methylation of RUNX1 by PRMT1 abrogates SIN3A binding and potentiates its transcriptional activity. Genes Dev. 22, 640–653. doi:10.1101/gad.1632608

Zhou, Y., Lim, K.C., Onodera, K., Takahashi, S., Ohta, J., Minegishi, N., Tsai, F.Y., Orkin, S.H., Yamamoto, M., Engel, J.D., 1998. Rescue of the embryonic lethal hematopoietic defect reveals a critical role for GATA-2 in urogenital development. EMBO J. 17, 6689–6700. doi:10.1093/emboj/17.22.6689

Zhou, Y., Yamamoto, M., Engel, J.D., 2000. GATA2 is required for the generation of V2 interneurons. Dev. Camb. Engl. 127, 3829–3838.

Zuber, S.M., Kantorovich, V., Pacak, K., 2011. Hypertension in pheochromocytoma: characteristics and treatment. Endocrinol. Metab. Clin. North Am. 40, 295–311, vii. doi:10.1016/j.ecl.2011.02.002

ACKNOWLEDGEMENTS

In erster Linie bedanke ich mich sehr herzlich bei PD **Natalia Pellegata**, für die Möglichkeit meiner Doktorarbeit in ihrer Arbeitsgruppe anfertigen zu können und für die Vergabe dieses spannenden und vielfältigen Themas. Vielen Dank für die Betreuung und Unterstützung bei der Bearbeitung des Projektes und für all die hilfreichen Diskussionen und Ratschläge.

Besonderer Dank gilt Prof. **Jochen Graw**, für die Empfehlung mich um diese Doktorandenstelle zu bemühen und vor allem für die Bereitschaft, meine Doktorarbeit als Doktorvater und Thesis Committee-Mitglied zu betreuen. Vielen Dank für das zeitaufwendige Korrekturlesen meiner Dissertation und für das Übernehmen der Erstprüferschaft in meiner Abschlussprüfung.

Herzlichen Dank an Dr. **Michael Rosemann**, für die Mitgliedschaft in meinem Thesis Committee und den hilfreichen Diskussionen meiner Teilergebnisse bei den jährlichen Thesis Committee Meetings.

Prof. **Stephan Herzig** und dem gesamten **IDC** danke ich für die Aufnahme in dieses Institut, der gelungenen Integration unserer Arbeitsgruppe und dem vielfältigen wissenschaftlichen Input während unserer Labmeetings.

Furthermore, I would like to thank **Enzo Lalli**, for his great support in working with the ChIP-Seq data and for the hospitality during my visit in Nice. **Mabrouka** and **Carmen**, thanks for the great time at the wonderful Cote d´Azur!

Many thanks to **Juan Higareda Almaraz** and **Steffen Sass**, for the bioinformatic analyses of ChIP-Seq and microarray data. **Martin Irmler** danke ich für die Durchführung und Auswertung der Microarrays und der steten Hilfsbereitschaft.

Besonderer Dank gilt **Elke Pulz**, für tolle Hilfsbereitschaft bei Labortätigkeiten und der Bewältigung und Diskussion methodischer Schwierigkeiten. Vielen Dank auch für all die Büro-Gespräche über Dies und Das. **Elenore Samson** danke ich für die Durchführung histopathologischer Arbeiten und die vielen unterhaltsamen Mittagspausen.

Bei **Eva**, **Tobi**, **Hermine** und **Nina** möchte ich mich für das sehr angenehme und freundschaftliche Arbeitsklima bedanken. Danke, für all die aufmunternden Gespräche und äußerst kurzweiligen Mittagspausen. Außerdem danke ich dir, **Sarah,** für dein immer offenes Ohr und deine Freundschaft.

Auch möchte ich mich herzlich bei meinen ehemaligen Kolleginnen und Freunden **Ines** und **Misu** bedanken, die mir die anfängliche Einarbeitung sehr erleichtert haben und von denen ich so viel gelernt habe.

Ganz besonders möchte ich denen danken, die mein Leben während der vergangenen Promotions-Jahre erfüllt und verbessert haben: meinen **Eltern**, meiner **Familie** und meinen **Freunden**. Euer familiärer Rückhalt war in den letzten Jahren unglaublich wertvoll! **Olli**, danke für deine Geduld, für deinen Zuspruch, für Camiro und Alma und für so vieles mehr ... ***Tulpen forever***